Doctoral School of Multidisciplinary Medicine

University of Szeged

Investigation of esophageal ion transport mechanisms using mouse esophageal 3D organoid cultures

Ph.D. thesis

Marietta Margaréta Korsós

Supervisor:
Viktória Venglovecz Ph.D., D.Sc.

Gastroenterology Epithelial Cell Research Group
Department of Pharmacology and Pharmacotherapy
Albert Szent-Györgyi Medical School
University of Szeged

2023

PUBLICATIONS

List of scientific papers cited in the thesis

1. Marietta Margaréta Korsós, Tamás Bellák, Eszter Becskeházi, Eleonóra Gál, Zoltán Veréb, Péter Hegyi, Viktória Venglovecz. Mouse organoid culture is a suitable model to study esophageal ion transport mechanisms. AMERICAN JOURNAL OF PHYSIOLOGY – CELL PHYSIOLOGY; 321(5):C798-C811. doi: 10.1152/ajpcell.00295.2021. PMID: 34524930. (2021)

IF$_{2021}$: 5.282 (Q1)

2. Eszter Becskeházi, **Marietta Margaréta Korsós**, Eleonóra Gál, Tiszlavicz L, Hoyk Z, Deli MA, Zoltán Márton Köhler, Anikó Keller-Pintér, Attila Horváth, Kata Csekő, Zsuzsanna Helyes, Péter Hegyi, Viktória Venglovecz. Inhibition of NHE-1 Increases Smoke-Induced Proliferative Activity of Barrett's Esophageal Cell Line. INTERNATIONAL JOURNAL OF MOLECULAR SCIENCES; 22(19):10581. doi: 10.3390/ijms221910581. PMID: 34638919; PMCID: PMC8509038. (2021)

IF$_{2021}$: 6.208 (Q2)

List of other scientific papers related to the subject of the thesis

3. Eszter Becskeházi*****, **Marietta Margaréta Korsós***, Bálint Erőss, Péter Hegyi, Viktória Venglovecz. OEsophageal Ion Transport Mechanisms and Significance Under Pathological Conditions. FRONTIERS IN PHYSIOLOGY; 11:855. doi: 10.3389/fphys.2020.00855. PMID: 32765303; PMCID: PMC7379034. (2020)

IF$_{2020}$: 4.566 (Q2)

    * contributed equally

Number of full publications: 3 (2 first author)
Cumulative impact factor: 16.056

TABLE OF CONTENTS

ABBREVIATIONS

$[Ca^{2+}]_i$	intracellular calcium ion concentration
$[Cl^-]_i$	intracellular chloride ion concentration
2D	2-dimensional
3D	3-dimensional
BCECF-AM	2',7'-bis-(2-carboxyethyl)-5-(and-6)-carboxyfluorescein, acetoxymethyl ester
BE	Barrett's esophagus
CBE	Cl^-/HCO_3^--exchanger
cDNA	complementary deoxyribonucleic acid
CFTR	cystic fibrosis transmembrane conductance regulator
CK14	cytokeratin 14
DRA	protein Down-regulated in adenoma protein (Slc26a3)
EAC	esophageal adenocarcinoma
EDTA	ethylene diamine tetra-acetic acid
EECs	esophageal epithelial cells
EGF	epidermal growth factor
EOs	esophageal organoids
FACS	Fluorescence-activated Cell Sorting
G-418	Geneticin-418 selection reagent
GERD	gastroesophageal reflux disease
HEPES	(4-2-hydroxyethyl)-1-piperazineethanesulfonic acid
Hepes	HEPES-buffered solutions (generally used in our laboratory, for the detailed compositions, see Table 1)
HOE-642	cariporide, a selective Na^+/H^+ exchange inhibitor
IHC	immunohistochemistry
iPCS	induced pluripotent stem cells
LGR5	leucine-rich repeat-containing G-protein coupled receptor 5
mEGF	mouse endothelial growth factor
MQAE	N-(ethoxycarbonylmethyl)-6-methoxyquinolinium bromide
mRNA	messenger ribonucleic acid
NAC	N-acetyl cysteine
NBC	Na^+/HCO_3^- cotransporter
NHE	Na^+/H^+ exchanger
PAT1	putative anion transporter 1 (Slc26a6)
PCR	polymerase chain reaction
PFA	paraformaldehyde
pH_i	intracellular pH
ROIs	Region of Interests
RT	room temperature
RT-PCR	reverse transcription polymerase chain reaction
SEC	squamous epithelial cells

1. INTRODUCTION

1.1. Structure of esophageal epithelium

The esophagus consists of four layers, namely the mucosa, submucosa, muscularis externa, and adventitia (Fig. 1). The esophageal epithelium is built up from squamous epithelial cells (SECs) arranged in stratified layers. In studies related to the investigation of ion transport processes in the esophageal epithelium, functional measurements are conducted using either human cell lines or primary cells and tissues isolated from various species of rodents [1–5]. Nonetheless, it is important to acknowledge that there are key differences between the structures of the esophageal epithelium of rodents and humans [6–8]. The main structure of the esophagus is similar between humans and rodents, with both having stratified squamous epithelium and similar cell types in the lamina propria and muscularis mucosa, but the cellular composition of the esophageal epithelium varies by layer and by species.
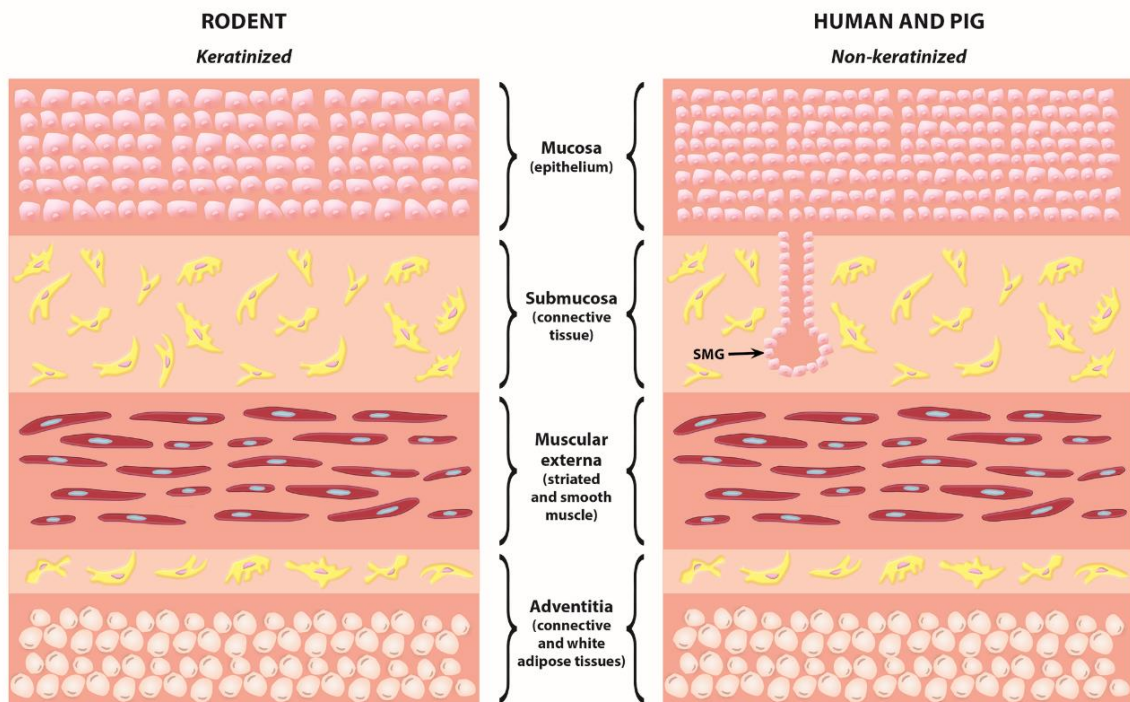

Figure 1. Schematic representation of the histological comparison of rodent and human/pig esophagus. The most common difference between rodent and human/pig esophagus is that in rodents the mucosa layer is thinner and the submucosal glands (SMG) are absent [6].

In rodents (e.g., rats and mice), the esophageal epithelium is arranged into 4 or 5 layers. The uppermost layer of the epithelium consists of cornified cells. In humans and guinea pigs, the esophageal mucosa is composed of stratified squamous epithelium as well, which in squamous cells are located in several layers, up to 10-15, and the cells are not keratinized and retain their nucleus. The submucosa layer of the esophagus contains glands that secrete mucus, HCO_3^-, and growth factors, which protect the esophagus from the harmful effects of acid reflux. Interestingly, rodents do not have glands in their esophagus, while humans and guinea pigs have numerous submucosal glands (SMGs) that secrete these substances. The submucosa layer also contains other types of cells, such as connective tissue cells, blood and lymphatic vessels, nerves, and glands. The muscular externa layer of the esophagus is composed of smooth and striated muscle, while the adventitia layer is mainly composed of connective and adipose tissue[6,9].

1.2. Defense mechanisms of esophageal epithelial barrier: focusing on the ion transporters

Esophageal epithelial cells (EECs) are crucial in preventing damage to the esophagus from stomach content reflux. Several defensive mechanisms exist in the epithelial barrier to protect against reflux-induced injuries. One of the most important is the esophageal epithelial resistance[10,11]. It consists of several physical barriers and functional components. These include 1) tight junctions, which form a barrier to prevent the backflow of stomach acid and other digestive enzymes into the esophagus; 2) surface mucus and HCO_3^- secretion, which provide an alkaline environment; 3) epithelial repair systems, which involve cell division and renewal that help to repair any damage that may have occurred; and 4) intracellular buffering systems, such as HCO_3^- or phosphate-buffering systems.

The transport proteins on the apical/luminal and basolateral membranes of EECs play an important role in the epithelial defense mechanisms [11,12] and several ion transporters have already been identified in these cells[6]. At the apical membrane of EECs, only a nonselective cation channel has been identified so far, which is equally permeable for monovalent cations (Li^+, Na^+, and K^+), but its exact function is not known. Although this channel contains all three sub-groups of the epithelial Na^+ channel (ENaC), it does not exhibit the typical characteristics of epithelial Na^+ channels and is not inhibited by amiloride[13].

In contrast, at the basolateral membrane of the esophageal epithelium, several ion transporters have been identified. The amiloride-sensitive Na^+/H^+ exchanger (NHE) plays an important role in the esophageal epithelium and has been identified in the basolateral side of EECs[14,15]. NHE is a large transporter family that contains several isoforms that show different functions and distributions in the body. NHE1 is located on the basolateral membrane of EECs and is responsible for regulating pH_i by exchanging intracellular H^+ for extracellular Na^+ in an electroneutral manner. This pH regulation is essential for the proper functioning of EECs. NHE1 is also involved in several defensive mechanisms of the esophageal epithelium, such as cell volume regulation, proliferation, and cell survival. NHE1 can help EECs maintain their volume and shape under different osmotic conditions[16]. It can also play a role in cell proliferation, allowing cells to grow and divide properly[17]. Its expression is regulated by extracellular pH, and its activity protects cells from injury and cell death by preventing intracellular acidification by extruding H^+ out of the cells[18].

Two types of Cl^-/HCO_3^- exchanger proteins (CBE) have been identified in rabbit esophageal EECs: a Na^+-independent and a Na^+-dependent CBE[19]. Although both transporters are electroneutral, their effects on pH_i are opposite. The Na^+-independent CBE mediates the exchange of Cl^- for HCO_3^- through the cell membrane in a reversible, electroneutral manner. Efflux of HCO_3^- into the lumen of the esophagus lowers the intracellular pH_i of EECs, therefore, the Na^+-independent CBE act as an acidifying transporter. In contrast, the Na^+-dependent CBE operates in a reverse mode and mediates the influx of HCO_3^- in exchange for intracellular Cl^- and therefore, along with the NHE, contributes to the alkalization of the cell.

Transepithelial Cl^- transport is a two-step process that involves the entry of Cl^- into the cell across the basolateral membrane and its secretion into the lumen through the apical membrane. In general, in most of the epithelia, this anion secretion is composed of three basic transport processes: the apical cystic fibrosis transmembrane conductance regulator (CFTR) Cl^- channel; basolateral K^+ channels of at least two types, and the basolateral Na^+-coupled Cl^- entry process with the $Na^+/K^+/2Cl^-$ cotransporter 1 (NKCC1). Transcellular Cl^- transport in SECs is not significant compared to esophageal submucosal glands (SMGs). Abdulnour-Nakhoul and his co-workers have shown the presence of a Ca^{2+}-dependent and flufenamate-sensitive Cl^- conductance on the basolateral membrane of EECs. This Cl^- current did not respond to the CBE inhibitor, 4,4′-diisothiocyano-2,2′-stilbenedisulfonic acid (DIDS) or cyclic adenosine monophosphate (cAMP), suggesting

that it may be some type of Ca^{2+}-activated Cl^- channel $(CaCC)$[20], however, this study lacks the molecular identification of the channel.

In contrast, the presence of NKCC1 was identified with indirect methods in rabbit EECs[20,21]. The NKCC mediates the electroneutral uptake of 1 Na^+, 1 K^+ and 2 Cl^- ions across the plasma membrane[22], and in EECs, the NKCC is primarily involved in cell volume regulation[21]. In most cells, NKCC interacts with the KCl cotransporter (KCC), where the effects of the two transporters are opposite. KCC is an electroneutral transporter that mediates the Cl^- and K^+ efflux, for which the energy is provided by the K^+ gradient maintained by the Na^+/K^+ ATPase pump[23,24], whereas NKCC promotes the uptake of Cl^-. In the esophagus, K^+ and Cl^- transport across the basolateral membrane of EECs seems to be a protective mechanism by which cells try to maintain the cell volume against hypoosmotic shock under an acidic pH which has a significance in reflux disease[6].

1.3. *In vitro* models for studying the ion transport process of esophageal epithelium

The activity of the main ion transporters has been less studied in the esophageal epithelium, mainly because of the lack of a suitable experimental model. Currently, there are different experimental models available for investigating ion transport processes in the esophageal epithelium that may be suitable, but most of them have several limitations that may affect the interpretation of the results toward translational application.

Several esophageal cell lines, ranging from normal cells to esophageal adenocarcinoma, are available. These cells have been cultured for many generations and can be easily propagated and manipulated in the laboratory. A major advantage of cell lines is their homogeneity, which favors experimental reproducibility. Although cell lines are easy to maintain, they also have limitations. Some esophageal cell lines are genetically modified to preserve their proliferation or derived from pre-existing cancerous tissue, making them unsuitable for studying physiological processes. In addition, because of their genetic instability, cells may undergo dedifferentiation over time[25]. Primary cell cultures are another *in vitro* model that involves culturing cells directly from esophageal epithelium. These cells are often more physiologically relevant than cell lines, but they have a limited lifespan and can be more difficult to obtain and manipulate[26].

The Ussing chamber is an old but commonly used, cost-effective apparatus for studying esophageal permeability, and it is also suitable for investigating transepithelial ion transport processes[27]. However, the application of this technique is often limited by the condition, permeability, and short lifespan of the tissue, as well as reproducibility[5].

Three-dimensional (3D) culture techniques are the most advanced models that can be used to answer fundamental biological questions. There are successful examples for most tissues and organs, and a variety of techniques have been created. These techniques are referred to as 3D culture, organotypic culture, or organoid culture. The terminology for 3D techniques can vary depending on the specific subfield and the type of cells and tissues being utilized, and it is not uniform across different disciplines[28]. Organoids are 3D models that can be derived *in vitro* from induced pluripotent stem cells (iPSC) or adult stem cells, both from human and animal tissues. Different protocols are available to induce the maturation and formation of organoids, such as matrix embedding, growing in suspension or a bioreactor, and using U-bottom cell culture plates[29].
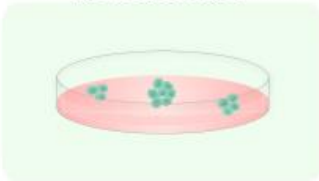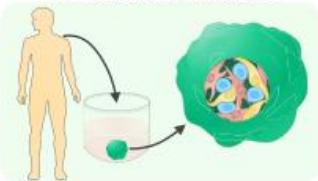

2D cell cultures

- Vascularization: Limited

- Biobanking: Feasible

- High-throughput screening: Applicable

- Modeling organogenesis: Not Applicable

- Modeling patient-derived organoids: Not Applicable

- Manipulation: Feasible

- Modeling for human physiology: Limited

- Heterogeneity: Low, more homogeneous configuration

- Reproducibility: High

- Modeling cellular/mechanical communications: Feasible

3D organoid cultures

- Vascularization: Limited

- Biobanking: Feasible

- High-throughput screening: Applicable

- Modeling organogenesis: Suitable, especially for the generation of iso-genic tissues and transplantation

- Modeling patient-derived organoids: Feasible

- Manipulation: Feasible

- Modeling for human physiology: Feasible

- Heterogeneity: High

- Reproducibility: Low

- Modeling cellular/mechanical communications: Feasible

Figure 2. Comparison of 2D cell cultures and 3D organoids. Organoids offer numerous benefits over 2D cultures and despite their limitations, they have emerged as a significant resource in scientific investigations, tissue engineering and preclinical disease modeling. Modified figure[29].

Organoids offer several advantages over traditional 2D cell culture models and animal models[29,30] (Fig. 2). First of all, they can recapitulate the complex tissue architecture and cellular diversity of the organ from which they are derived, allowing for a more physiologically relevant model. Organoids can also be generated from patient samples, enabling personalized medicine approaches and the study of disease heterogeneity[31], and

they may offer a high-throughput platform for drug screening and toxicity testing, reducing the reliance on animal models[32]. Furthermore, organoids can be expanded long-term, genetically modified, and cryopreserved, maintaining their phenotypic characteristics[33]. It is important to note that, there are also limitations to use esophageal organoid cultures (EOs)[29] (Fig. 2). They can be difficult and time-consuming to generate, and their use is limited by the cost of maintenance. In general, EOs have low reproducibility compared to 2D cell cultures. Additionally, organoids by themselves lack the immune system and vasculature present *in vivo*, which can limit their ability to fully recapitulate disease pathology[34]. There are also ethical considerations when using patient-derived organoids generated from human embryos or fetal tissues[35]. Despite these limitations, organoids have become an important tool in basic science research, allowing the study of complex organ systems in a controlled environment. As techniques for generating and manipulating organoids continue to improve, they will likely play an increasingly important role in the field of pre-clinical research, among others in drug discovery and personalized medicine as well[36].

1.4. Esophageal epithelial organoids (EOs)

Recently, a three-dimensional organoid system containing the physiologic and pathologic processes of organs has sparked a lot of interest in the field of stem cell biology and diseases. In 2014, mouse EOs were initially established by DeWard and colleagues, from the mucosa of the esophagus. They demonstrated that basal cells in the mouse esophagus contained a heterogeneous population of epithelial cells, which were separated into distinct cell populations based on cell-surface markers and differences in stem cell potential. Based on their results, a non-quiescent stem cell population is believed to reside in the basal epithelium of the mouse esophagus[37]. Similarly to the mouse, the stem cell population of the human esophagus is located in the basal layers of the esophagus[38], however, despite extensive research, it remains unclear what proportion of basal cells are stem cells, and the identification and determination of stem cells in human esophageal epithelia has remained controversial as well[39]. Although there is currently insufficient knowledge about stem cells in the adult human esophagus, it is known that the pathophysiology of esophageal disorders is frequently accompanied or characterized by stem/progenitor cell abnormalities[39,40].

The generation of EOs from tissue-resident stem cells typically involves several key steps (Fig. 3), and the stem cells can be isolated from human biopsy samples or murine

esophageal epithelial sheets. Several elaborate protocols are available for the production of both human and mouse EOs, however, the culture methods for EOs vary from study to study[41–44].
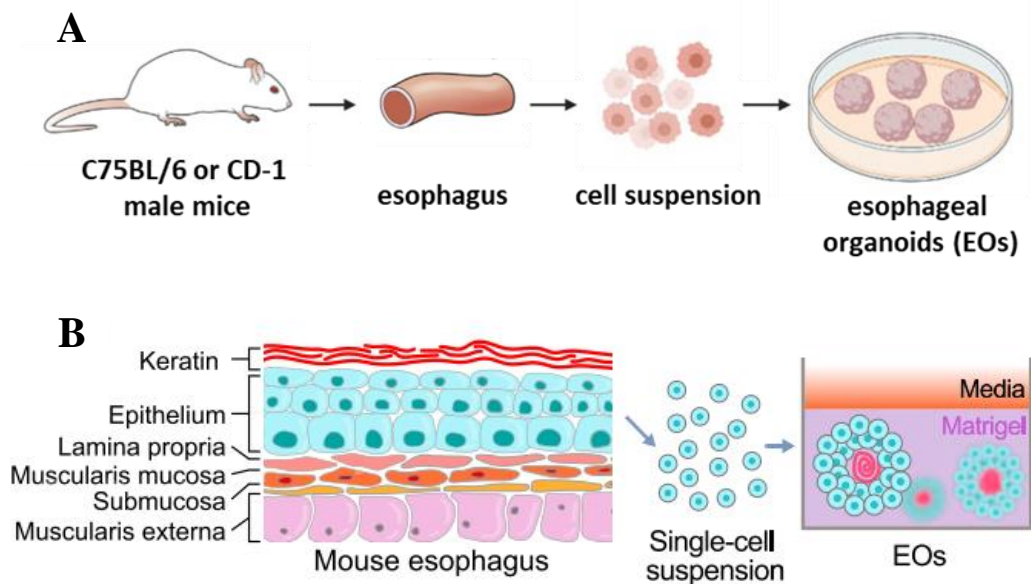

Figure 3. A schematic workflow of recapitulation of squamous esophageal epithelium in 3D organoids. (A) Esophageal epithelial cells are dissociated from tissues via enzymatic digestion. EECs are mixed into Matrigel™ at a low density and allowed to grow as single-cell-derived spherical 3D structures with a proliferation-differentiation gradient. **(B)** The 3D structure of the organoids allows for the formation of complex cell-cell and cell-matrix interactions, which are similar to those in the native tissue. However, no consensus on EO culture methods has been reached[44]. Modified figure[44]

So far, human EOs have been successfully used to investigate the molecular mechanisms involved in the pathophysiology of the esophagus. Research using human EOs includes development, differentiation/proliferation, and therapeutic approaches to Barrett's esophagus (BE)[32,45], esophageal adenocarcinoma (EADC)[32] and esophageal squamous cell carcinoma (ESCC)[42,46], esophageal signaling pathways in gastroesophageal reflux disease (GERD)[47] and eosinophilic esophagitis[41]. Moreover, studying host-microbiome interactions in esophageal disease is a relatively new field where EOs can also be used[48].

Relatively little literature is available on the use of mouse EOs compared to human EOs due to inherent species differences, and findings from mouse studies need to be carefully translated to human physiology and disease. Nonetheless, mouse EOs provide a well-usable platform for carrying out basic research-type experiments. Mouse EOs are

characterized by a fast growth rate and a short period of time, their cultivation does not require expensive reagents, and they are excellent for protocol optimization[44]. Furthermore, due to the availability of genetically engineered mouse strains, it becomes possible to set up specific experimental conditions in which esophageal diseases can be studied directly, such ESCC[49,50], and BE[51].

As is known, ion and water transport play a crucial role in the development of gastrointestinal diseases (GI)[52]. Therefore, numerous studies have utilized GI organoids to investigate the underlying mechanisms, such as pancreatic ductal organoids[53,54], gallbladder organoids[55], intestinal organoids[56], and colon organoids[57]. Although the esophageal epithelium is not a typical secretory epithelium, knowledge of its ion transport system is important for understanding the pathophysiology of esophageal diseases. However, no study has used EOs specifically to investigate ion transport processes so far.

2. AIMS OF THE STUDY

Publication No.1.:

While epithelial organoids have been generated from many regions of the gastrointestinal tract, research on EOs is still relatively new and limited. Although there have been some studies using EOs to investigate other aspects of esophageal biology and pathophysiology, no study has specifically used EOs to investigate ion transport processes in the esophageal epithelium. Our objectives were based on the hypothesis that EOs are suitable *in vitro* models for investigating the ion transport processes of the EECs from a molecular and functional perspective.

Our primary goal was to generate EOs from the esophagus of two, different strains of mice (wild type C57BL/6 and CD-1), and then to compare the organoids based on different aspects, with particular regard to ion transport processes. Our specific goals were:

I. Characterization of EOs both morphologically and by proving that they are derived from stem cells of the primary tissue.

II. Investigation of the mRNA and protein expression of the major acid-base transporters in EOs.

III. Examination of functional interactions between ion transporters.

Publication No.2.:

Primary cell cultures are another *in vitro* model that involves culturing cells directly from the esophageal epithelium. While a large number of epithelial cells can be isolated from the esophageal epithelium of the guinea pig, which is excellent for conducting functional measurements *in vitro*, it is important to note that these cells exhibit limited growth potential in a two-dimensional (2D) environment and have a restricted lifespan. Additionally, acquiring and manipulating these cells can also present certain difficulties.

In this study, as part of our research, we used guinea pig EECs for functional measurements; therefore, our aim was:

I. To investigate the viability of guinea pig EECs.

3. MATERIALS AND METHODS

3.1. Solutions and chemicals

General laboratory chemicals and amiloride hydrochloride hydrate were obtained from Sigma-Aldrich (Budapest, Hungary). 2,7-Bis-(2-carboxyethyl)-5(6)-carboxyfluorescein acetoxymethyl ester (BCECF-AM) and N-(ethoxycarbonylmethyl)-6-methoxyquinolinium bromide (MQAE) were purchased from Molecular Probes Inc. (Eugene, OR, USA). Stock solutions of BCECF-AM (2 μM) and MQAE (5 μM) were prepared in dimethyl sulfoxide (DMSO) and stored at $-20°C$. Nigericin (10 mM) was dissolved in absolute ethanol and stored at $-20°C$. 4-Isopropyl-3-methylsulfonyl benzoyl-guanidin methanesulfonate (Cariporide or HOE-642), forskolin, and CFTR inhibitor-172 were provided by Tocris (Bristol, UK). HOE-642 (1 and 50 μM); forskolin (10 μM); amiloride (0,2 mM) and CFTR inhibitor-172 (10 μM) were dissolved in DMSO and stored at 4°C, and forskolin stored at -20°C.

The solutions used for the microfluorimetric measurements were freshly prepared before the measurements. The pH of HEPES-buffered solutions was manually adjusted to 7.5 with NaOH. Standard HCO_3^-/CO_2-buffered solutions were gassed with 95% O_2/5% CO_2 to adjust their pH to 7.5. All experiments were performed at 37°C. The compositions of the solutions are presented in Table 1.

	Standard Hepes	Standard HCO_3^-	NH_4Cl Hepes	High-K^+ Hepes	NH_4Cl HCO_3^-	Na^+-free Hepes	Na^+-free HCO_3^-	Cl^--free Hepes	Cl^--free HCO_3^-
NaCl	140	115	110	5	95				
KCl	5	5	5	130	5	5	5		
$MgCl_2$	1	1	1	1	1	1	1		
$CaCl_2$	1	1	1	1	1	1	1		
HEPES acid	10		10			10		10	
Glucose	10	10	10	10	10	10	10	10	10
$NaHCO_3$		25			25				25
NH_4Cl			20		20				
Na-HEPES				10					
NMDG-Cl						140	115		
Na-gluconate								140	115
Mg-gluconate								1	1
Ca-gluconate								6	6
K_2-sulfate								2.5	2.5
Choline HCO_3^-							25		
Atropine							0.01		

Table 1. Composition of solutions. Values are in mM.

3.2. Animals

All animal experiments were performed according to national (1998. XXVIII; 40/2013) and European (2010/63/EU) animal welfare guidelines. The experimental protocols were approved by the National Scientific Ethical Committee on Animal Experimentation and by the Ethics Committee for Animal Research of the University of Szeged (approval ID: XIII./1667/2020.). Animals (wild type C57BL/6 and CD-1 mice; guinea pigs) were bred and housed under controlled conditions in the conventional animal house of the Department of Pharmacology and Pharmacotherapy, University of Szeged.

3.3. Isolation of esophageal epithelial cells (EECs)

8-12-week-old male mice were terminated by intraperitoneal injection of pentobarbital sodium (80-100 mg/kg) and used for tissue removal. After removal and longitudinal opening of the esophagus, the intact tissue was placed into dispase II solution (PluriSTEM™ 1mg/ml) and incubated at 37°C for 40 min. Then, the mucosa was peeled from the submucosa using forceps, and the mucosa was incubated at 37°C in 1x trypsin–EDTA solution for 2x15 min, during which time the tissue was vortexed every 2 min. To inactivate the trypsin, the trypsin–EDTA solution (with floating cells) was pipetted into the soybean trypsin inhibitor (STI 250 µg/ml) solution, and cells were then centrifuged for 10 min at 2000 rpm at RT. After the cell pellet was suspended in 300 µl of complete organoid culture medium, the total number of cells was counted using a Neubauer chamber. The isolation method was largely similar to that described above in the case of the guinea pig EECs. Adjusting the digestion time to the thickness of the esophageal tissue, the duration of the trypsin stage was enhanced to 20 minutes.

3.4. Evaluation of the viability of esophageal epithelial cells (EECs)

The freshly isolated guinea pig EECs were suspended in 300 µl KSFM medium and plated on poly-l-lizin treated (0.01 %) coverslips (Ø24 mm) and investigated by using Trypan Blue reagent (0.4 % solution, prepared in 0.85% NaCl; Lonza, Switzerland) hourly. After the incubation at 37°C, bright field images were taken under 10× magnification, and captures were analyzed using Fiji ImageJ software, where stained cells were counted and considered not viable.

3.5. Generation of mouse esophageal organoids (EOs)

Using cold pipette tips, the required volume of the cell suspension (target cc.: 7500 cells/well on a 24-well tissue culture plate) was mixed with Matrigel® extracellular matrix at a 40:60 ratio and portioned in the wells, followed by incubation at 37°C for 20 min to allow solidification of the gel. 1000 µl/well complete organoid culture medium was added to cover the Matrigel® and incubated at 37°C. After 3–4 days, the organoid formation was visible. They reach their maximum size on days 8–12. The growth medium consisted of Advanced Dulbecco's modified Eagle's medium/F12, 1× N2 and 1× B27 Supplements, 1× Glutamax (Gibco), 10 mM HEPES (Biosera), 2% penicillin/streptomycin (Gibco), 1 mM N-acetyl-L-cysteine (Sigma), 100 ng/mL R-spondin 1, 100 ng/mL Noggin (both from Peprotech), 50 ng/mL mouse epidermal growth factor (R&D Systems), 10 µM Y27632 ROCK-kinase inhibitor (ChemCruz), and 5 % WNT3A-conditioned medium. Wnt3A conditioned medium was prepared by collecting the supernatant from L-Wnt3A cells (ATCC CRL-2647™) according to the manufacturer's protocol.

3.6. Flow cytometry analysis

The freshly isolated mouse EECs were incubated for 30 min on ice while labeling with LGR5-PE (Origene, TA400001) and CK14-FITC (Novusbio, NBP2-47720F) fluorochrome-conjugated primary antibodies and their matching isotype controls (PE Mouse IgG1, κ Isotype Ctrl Antibody #400111 and FITC Mouse IgG3, κ Isotype Ctrl Antibody #401317, both from BioLegend). The expression of leucine-rich repeat-containing G-protein coupled receptor 5 (LGR5) and cytokeratin 14 (CK14) proteins was measured by flow cytometry on a FACSCalibur flow cytometer (BD Biosciences Immunocytometry Systems, Franklin Lakes, NJ, USA). The data were analyzed using Flowing Software (Cell Imaging Core, Turku Center for Biotechnology, Finland), and the percentage of positive cells was expressed as the mean ± SD.

3.7. Immunofluorescence staining and histology

To recover whole mouse EOs, the culturing media was removed, and the Matrigel® domes were washed with cold PBS three times to dissolve Matrigel. The EOs were then centrifuged for 10 min at 2000 rpm at RT, fixed with 4% PFA for 1 hour at room temperature (RT), and then washed three times with PBS. The fixed samples were cryoprotected in 30% sucrose solution (in PBS) containing 0.01% sodium-azide at 4°C until embedding in Cryomatrix™ frozen embedding medium (Thermo Scientific™). The

16-µm-thick multiple serial sections were cut using a cryostat (Leica CM 1850, Leica), collected on gelatin-coated slides, and stored at -20°C until use. After air-drying for 10 min, the sections were incubated for 1 hour at RT with 5% BSA in PBS. (The permeabilization step was not used, because frozen sectioning is sufficient in the case of EOs.) The sections were then incubated with primary antibodies (overnight, 4°C, Table 2). On the next day, sections were washed in 1X PBS three times and then incubated with isotype-specific secondary antibodies (Table 2) for 1 hour at RT. After the incubation, sections were washed with 1X PBS and covered using Vectashield® mounting medium containing DAPI (1.5 µg/mL, Vector Laboratories), which labeled the nuclei of the cells. Immunoreactive sections were analyzed using a BX-41 epifluorescence microscope (Olympus) equipped with a DP-74 digital camera and CellSens software (V1.18, Olympus) or an Olympus Fv-10i-W compact confocal microscope system (Olympus) with Fluoview Fv10i software (V2.1, Olympus).

For hematoxylin and eosin (HE) staining, sections were incubated with Mayer's Hematoxylin solution (Sigma) for 5 min. Sections were washed with tap water and incubated in distilled water twice for 3 min each. Sections were then incubated in 1% eosin solution in distilled water (Sigma) for 2 min. Stained sections were dehydrated through 96 and 100% ethanol, cleared in xylene, and mounted in DPX mounting media (Sigma).

Microphotographs were taken using a DP-74 digital camera with a light microscope (BX-41) and CellSens software (V1.18). All images were further processed using the GNU Image Manipulation Program (GIMP 2.10.0) and NIH ImageJ analysis software (imagej.nih.gov/ij). Details of the primary and secondary antibodies are presented in Table 2.

Type	Reactivity (isotype)	Host	Dilution for IHC	Manufacturer
Primary polyclonal	anti-Slc9a1	rabbit	1:100	Alomone
Primary polyclonal	anti-Slc9a2	rabbit	1:100	Alomone
Primary polyclonal	anti-Slc26a3	rabbit	1:600	Invitrogen
Primary monoclonal	anti-Slc26a6	rabbit	1:200	Santa Cruz Biotechnology
Primary polyclonal	anti-Slc4a4	rabbit	1:100	Abcam
Primary polyclonal	anti-CFTR	rabbit	1:200	Alomone
Primary polyclonal	anti-ANO1	rabbit	1:200	Alomone
Secondary polyclonal	Alexa Fluor 488 anti-rabbit	goat	1:600	Thermo Fisher Scientific
Secondary polyclonal	Alexa Fluor 594 anti-mouse	goat	1:600	Thermo Fisher Scientific

Table 2. List of primary and secondary antibodies used in the study

3.8. Gene expression analysis using RT-PCR

Total RNA was isolated from the recovered mouse EOs using a NucleoSpin RNA Kit (Macherey–Nagel, Düren, Germany). Two micrograms of total RNA were reverse-transcribed using a High-Capacity cDNA Reverse Transcription Kit (Applied Biosystems, Foster City, CA, USA). Conventional PCR was performed using DreamTaq DNA polymerase enzyme (5U/ µl; Thermo Scientific™) in a final volume of 20 µl. All reactions were performed under the following conditions: 94°C for 5 min; 30 cycles of 94°C for 30 s, 60°C for 30 s, and 72°C for 1 min; and final elongation at 72°C for 10 min. The PCR products (15 µl) were separated by electrophoresis on a 2 % agarose gel and visualized using an AlphaImager EC Gel Documentation System. As a positive control, mouse kidney cDNA was used in the cases of Slc9a1, Slc9a2, Slc26a6, Slc4a4, and CFTR, and mouse pancreatic cDNA was used in the cases of Slc26a3 and anoctamin-1 (ANO-1). The sequences of the individually designed primers are presented in Table 3.

Gene	Reverse primer	Forward primer	Product size (bp)
Slc9a1	TGGCTCTACTGTCCTTTGGG	GAGGAGGAAGATGAGGACGG	194
Slc9a2	GAAATCAGGCTGCCGAAGAG	CTACTTCATGCCAACTCGCC	183
Slc26a3	ACCCTTTGAGATGGTCCAGG	TTCCTTCCCACTAGCCACTG	161
Slc26a6	AGCTCCTGGTTACTGTCCAC	TCATTGGGGCCACTGGTATT	235
Slc4a4	CAGCCACATACCAGGGAAGA	CGGCTTTGCTAGTCACCATC	171
CFTR	TCTGCATGGGTTCTGGGAAT	GAGCAATGTCTGGCAGTACG	249
ANO1	GGGGCTGTGGTTGTTACAAG	ATCCCCAAAGACATCAGCCA	150

Table 3. Primer sequences used in the study

3.9. Measurement of pH$_i$ and [Cl$^-$]$_i$ with microfluorimetry

For all microfluorimetry measurements, the recovered EOs were placed on glass coverslips (Ø24 mm) covered with poly-l-lizin (0.09 %) for attachment. Then they were placed in a chamber, which formed the base of a perfusion chamber mounted on an inverted fluorescence microscope (Olympus IX71, Budapest, Hungary).

To determine intracellular pH (pH$_i$), EOs were loaded with the pH-sensitive fluorescent dye BCECF-AM (2 µM, 60 min, 37°C) in standard Hepes solution. After loading, the samples were perfused with solutions at a rate of 5-6 ml/min, and 7-10 region of interests (ROIs) were marked out. The size of the designated areas always depended on the given sample, but in each case, several organoids were captured in the same field. The fluorescence emission is measured ratiometrically at 535 nm when the sample is excited at 440 nm and 490 nm, respectively. The calibration of the fluorescence emission

ratio to pH_i and determination of the initial pH of the EOs were performed using the high-K^+/nigericin technique, as previously described[58,59].

$[Cl^-]_i$ was estimated using the fluorescent, Cl^--sensitive dye MQAE (5 μM) and the CFTR activator forskolin (10 μM). Specifically, after adhesion onto the coverslips, the recovered EOs were incubated with MQAE (5 μM) for 2–3 h at 37°C in Hepes solution, and changes in $[Cl^-]_i$ were determined by exciting the EOs at 340 nm with emitted light monitored at 380 nm. Fluorescence signals were normalized to the initial fluorescence intensity (F/F_0) and expressed as relative fluorescence. The administration of forskolin started when the baseline straightened up, and it lasted for 3 minutes.

Measurements were performed using an inverted, fluorescence microscope (Olympus IX71, Budapest, Hungary), and the real-time activity of the different ion channels was measured using xCellence imaging software (Olympus, Budapest, Hungary).

3.10. Determination buffering capacity and base efflux

The intrinsic buffering capacity (β_i) and base flux of the EOs were estimated according to the NH_4Cl-prepulse technique [60,61]. After the incubation with the dye BCECF-AM (2 μM, 60 min, 37°C), EOs were exposed to various concentrations of Na^+ and HCO_3^--free NH_4Cl-solutions to block the Na^+-dependent pH-regulatory mechanisms in the cells. The total buffering capacity (β_{total}) was calculated as follows: $\beta_{total} = \beta_i + \beta_{HCO3-} = \beta_i + 2.3$ x [$HCO_3^-]_i$, where β_{HCO3-} is the buffering capacity of the HCO_3^-/CO_2 system, and β_i refers to the ability of intrinsic cellular components (excluding HCO_3^-/CO_2) to buffer changes of pH_i. The β_i was estimated by the Henderson-Hasselbach equation.

Converting the results of the pH_i changes obtained from the measurements into transmembrane base flux $J(B^-)$ the following equation was used: $J(B^-)= \Delta pH/\Delta t$ x β_{total}, where $\Delta pH/\Delta t$ was calculated by linear regression analysis. We denoted base influx as $J(B)$ and base efflux (secretion) as $-J(B^-)$.

3.11. Functional measurements of the acid-base transporters

3.11.1. Measurement of the activity of Na^+/H^+ exchanger (NHE) and Na^+/HCO_3^- (NBC) cotransporter

To estimate the activity of NHE and NBC, the NH_4Cl pre-pulse technique was used. Briefly, exposure of EOs to 20 mM NH_4Cl for 3 min induced an immediate rise in pH_i because of the rapid entry of lipophilic, basic NH_3 into the cells. After the removal of NH_4Cl from the external perfusion solution, pH_i rapidly decreased. The diffusion of NH_3

from the cells followed by the dissociation of intracellular NH_4^+ to H^+ and NH_3 is what causes this acidification. In standard Hepes solution, the initial rate of pH_i ($\Delta pH/\Delta t$) recovery from the acid load (over the first 60 s) reflects the activities of NHEs, whereas, in HCO_3^-/CO_2-buffered solutions, this rate represents the activities of both NHEs and NBC[60]. To block the activity of NHEs and NBC, a Na^+-free external solution was applied.

A separate investigation of NHE isoforms was carried out with the NHE-specific inhibitor, cariporide (HOE-642). This inhibitor blocks NHE-1 and NHE-2 isoforms in a concentration-dependent manner. At a concentration of 1 µM, only the NHE-1 isoform is inhibited, whereas 50 µM HOE-642 inhibits both isoforms [1,62]. We chose this inhibitor because our previous studies on human esophageal cell lines indicated that these two isoforms are responsible for the majority of NHE activity[1]. The NBC-dependent pH_i changes were detected in the presence of an NHE inhibitor, amiloride (0.2 mM).

3.11.2. Measurement of the activity of Cl^-/HCO_3^- exchanger (CBE)

Two independent methods were used to estimate CBE activity. Using the NH_4Cl pre-pulse technique, the initial rate of pH_i recovery (30 sec) from alkalosis in HCO_3^-/CO_2-buffered solutions was analyzed. Previous data indicated that under these conditions, the recovery over the first 30 s reflects the activity of CBE [60]. The Cl^- withdrawal technique was also applied, in which removal of Cl^- from the external solution causes immediate and reversible alkalization of the pH_i because of the reverse operation of CBE under these conditions. Previous data illustrated that the initial rate of alkalization over the first 60 s reflects the activity of CBE [63].

3.12. Statistical analysis

Results are expressed as the mean ± SD. In the case of microfluorimetric measurements, statistical analyses were performed using the analysis of variance followed by the Bonferroni multiple comparison post hoc test. In the guinea pig EEC viability experiments, the cell viability was defined as the ratio of living cells to the total number of cells. A repeated measures ANOVA with Holm correction was used for multiple comparisons. $p \leq 0.05$ was accepted as significant.

4. RESULTS

4.1. Generation and characterization of mouse EOs

Isolated mouse EECs were plated with Matrigel® supplemented with organoid culture medium at a final concentration of 40%. On the 3rd day, organoid formation was observed, and the size of the organoids increased steadily in the following days, peaking between days 7 and 9 (Fig. 4A). According to the relevant literature, those spheres larger than 50 µm are called organoids[37]. Organoids between 50 and 150 µm in size were used for our experiments. HE staining of the organoids illustrated that cells are arranged in several layers inside the organoids, matching the structure of normal esophageal tissue (Fig. 4B). The inner cell mass consisted of differentiated cells that moved from the periphery to the inside of the organoids during their maturation. In addition, the centers of some organoids were empty or contained keratinized materials, formed by cornified epithelial cells.
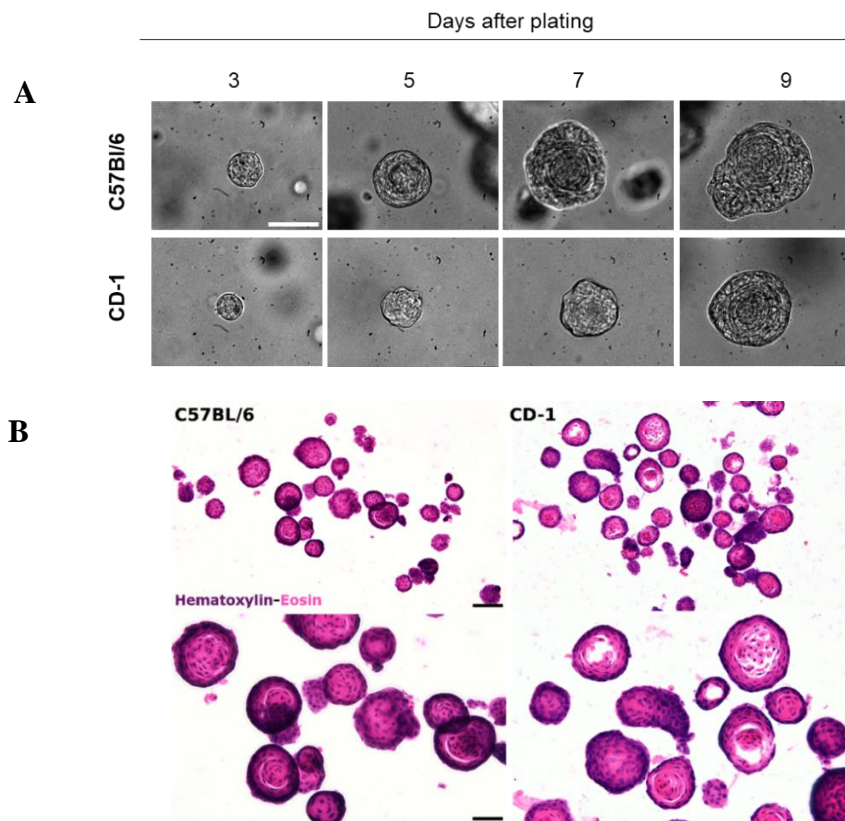

Figure 4. Characterization of esophageal organoids (EOs). (A) Representative bright field images of EOs grown for 9 days from freshly isolated esophageal mucosa. Images were taken using an Olympus IX71 inverted microscope. The scale bar represents 100 µm. **(B)** Hematoxylin and eosin staining of EOs developed from C57BL/6 and CD-1 mouse esophageal tissue. The scale bar represents 100 µm (upper line) and 50 µm (bottom line), respectively.

4.2. Three-dimensional EOs generated from stem cells and epithelial cells *in vitro*

To prove that EOs are generated from epithelial stem cells *in vitro*, we performed FACS analysis using the stem cell marker leucine-rich repeat-containing G-protein coupled receptor 5 (LGR5) and the epithelial marker cytokeratin 14 (CK14).
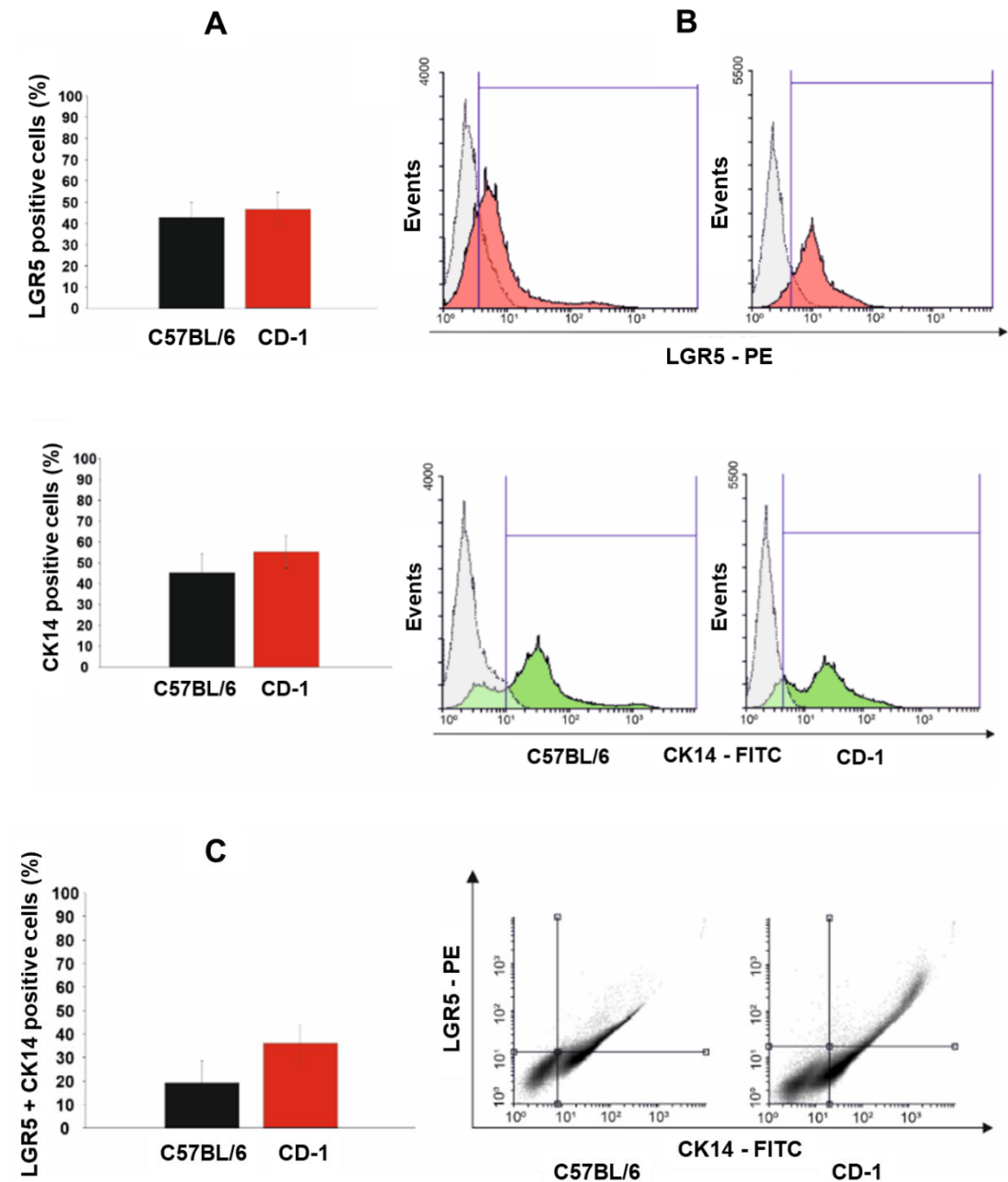

Figure 5. Flow cytometry analysis of leucine-rich repeat-containing G-protein coupled receptor 5 (LGR5) and cytokeratin 14 (CK14) expression on freshly isolated mouse esophageal epithelial cells (EECs). (A) Percentage of LGR5- and CK14-positive cells in the cell suspension of esophageal mucosa obtained from CD-1 and C57BL/6 mice. **(B)** Representative histograms of the FACS analysis with the respective isotype controls (grey color). **(C)** Representative dot plots present CK14 and LGR5 double-positive cells. n = 3

FACS analysis demonstrated that $42.70 \pm 7.27\%$ of the isolated C57BL/6 EECs and $46.46 \pm 7.81\%$ of the isolated CD-1 EECs were LGR5-positive (the upper line of Fig. 5A and 8B). In the next step, we verified that the organoids were derived from single EECs. FACS analysis indicated that $45.29 \pm 9.25\%$ of the isolated C57BL/6 EECs and $55.32 \pm 7.80\%$ of the isolated CD-1 EECs were CK14-positive (the bottom line of Fig. 5A and 5B). Interestingly, there was a slight difference in the double-positive (LGR5 and CK14) fraction. The proportion of double-positive cells was higher in CD-1 EECs ($35.37 \pm 1.24\%$) than in C57BL/6 EECs ($19.34 \pm 2.03\%$, Fig. 5C).

To complement our results obtained from FACS analysis, we used LGR5 and CK14 immunostaining of EOs. Immunofluorescence staining revealed strong LGR5 expression in both C57BL/6 and CD-1 organoids (Fig. 6). CK14 is a cytoplasmic keratin and epithelial marker that plays a crucial role in the differentiation of the basal SECs [64]. As presented in Fig. 6, the outer cell layer of the organoids was CK14-positive, indicating that the organoids originate from the mucosa and display a morphologically similar structure to normal esophageal tissue.
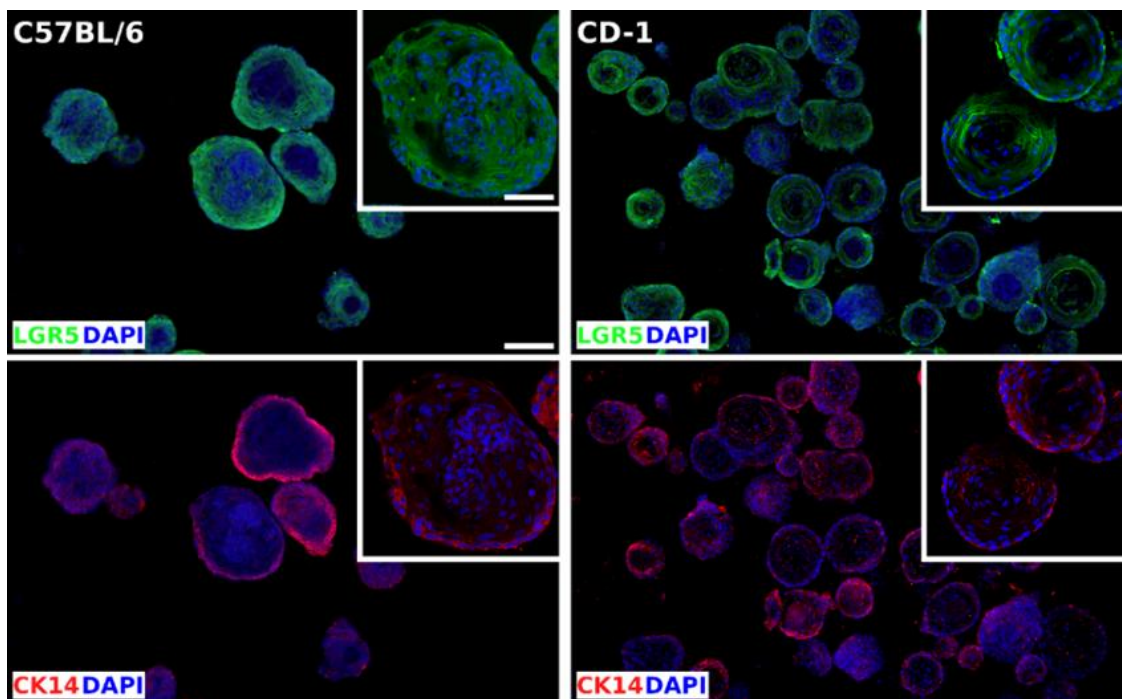

Figure 6. Immunohistochemistry staining of leucine-rich repeat-containing G-protein coupled receptor (LGR) and cytokeratin 14 (CK14) on EOs. Confocal images of EOs stained for LGR5, (green), and CK14 (red), counterstained with DAPI (blue). The scale bar represents 100 µm (main photo) and 50 µm (inset photo), respectively.

4.3. Evaluation of mRNA and protein expression of the main epithelial ion transporters on EOs

The mRNA expression of ion transporters was investigated using conventional RT-PCR. We revealed the presence of *Slc9A1* (NHE-1), *Slc9A2* (NHE-2), *Slc26a6* (PAT1), *CFTR*, *Slc4a4* (NBCe1B), and *ANO1* in both the C57BL/6 and CD-1 organoids (Fig. 7). The presence of these transporters was also confirmed at the protein level using immunohistochemistry (Fig. 8). The expression of *Slc26a3* (DRA) anion exchanger either at the mRNA or protein level was weak and nonspecific in both EOs.
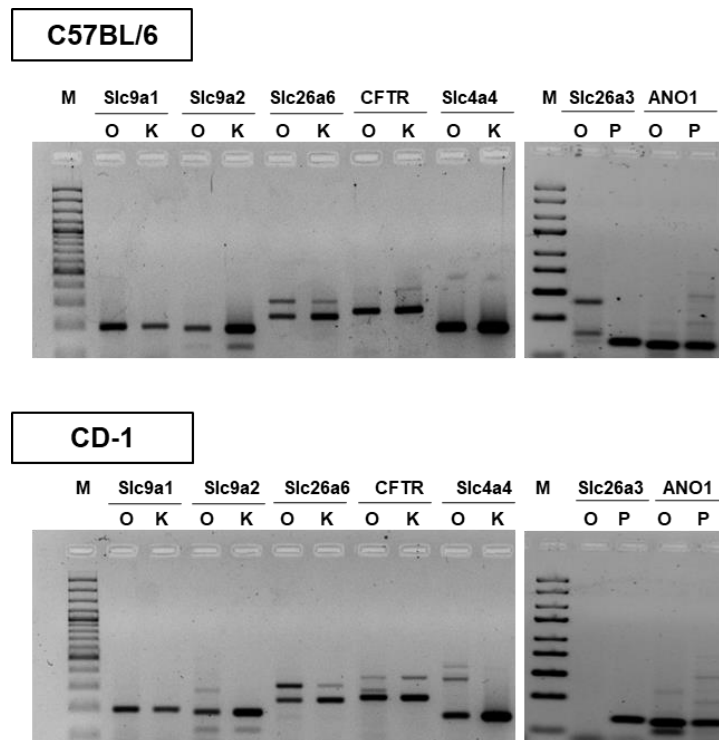

Figure 7. Expression of ion transporters in esophageal organoids (EOs). Mature EOs were collected 9 days after plating, and RNA was prepared from the organoids. Gene expression of ion transporters was investigated with traditional RT-PCR analysis.
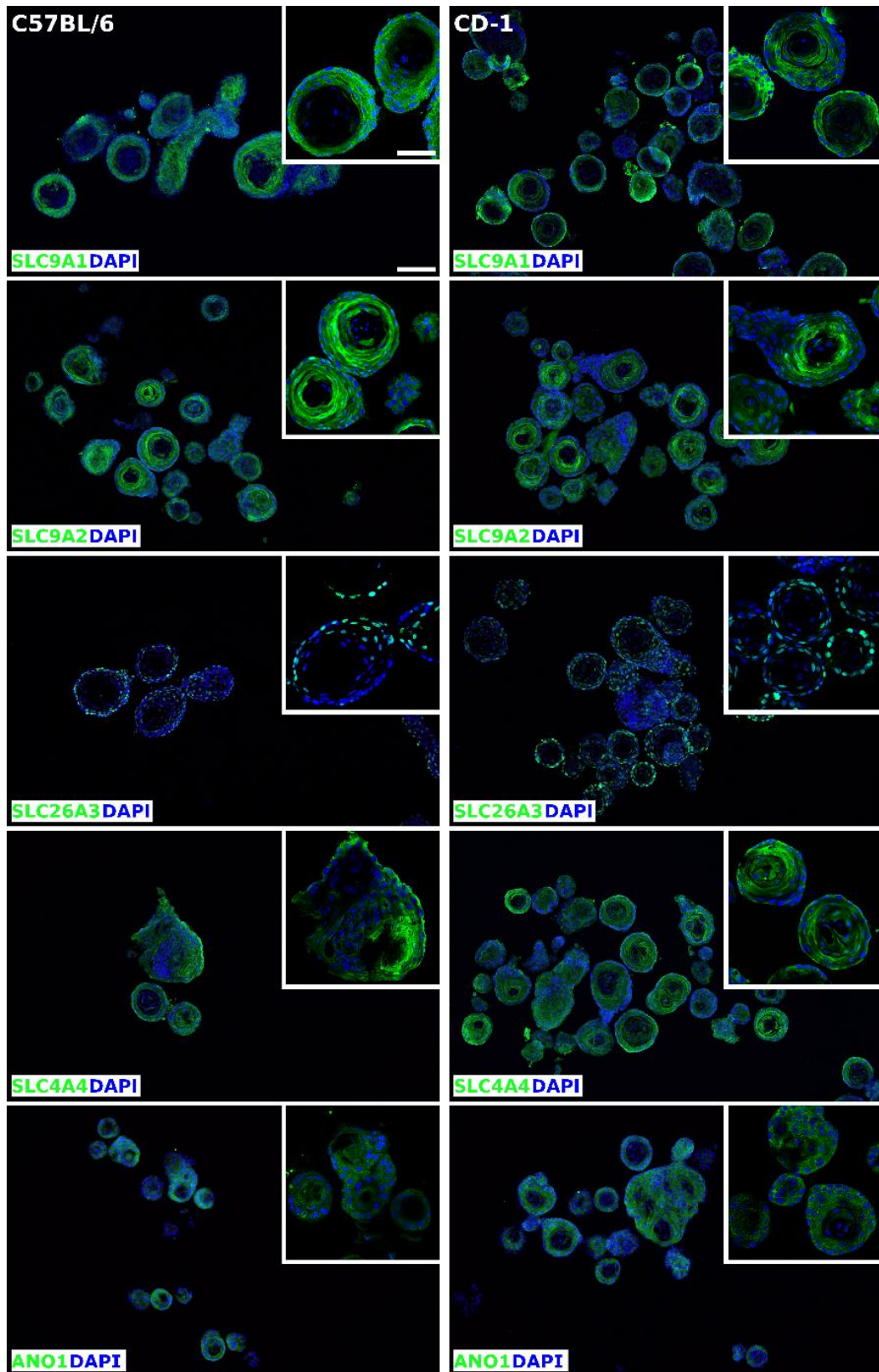
Figure 8. Immunohistochemistry staining of ion transporters on esophageal organoids (EOs). Immunostaining of EOs for Slc9a1 (first line), Slc9a2 (second line), Slc26a3 (third line), Slc4a4 (fourth line), and ANO1 (fifth line). The scale bar represents 100 μm (main photo) and 50 μm (inset photo), respectively.

Because the CFTR Cl⁻ channel and Slc26a6 interact with each other in several secretory epithelia[65], we examined the co-localization of these two transporters on the organoids. CFTR and Slc26a6 exhibited diffuse staining throughout cells without special localization to the apical or basal membrane. Interestingly, Slc26a6 staining was more detectable in cells on the periphery, whereas in the case of CFTR, central cells also displayed positive staining (Fig. 9).
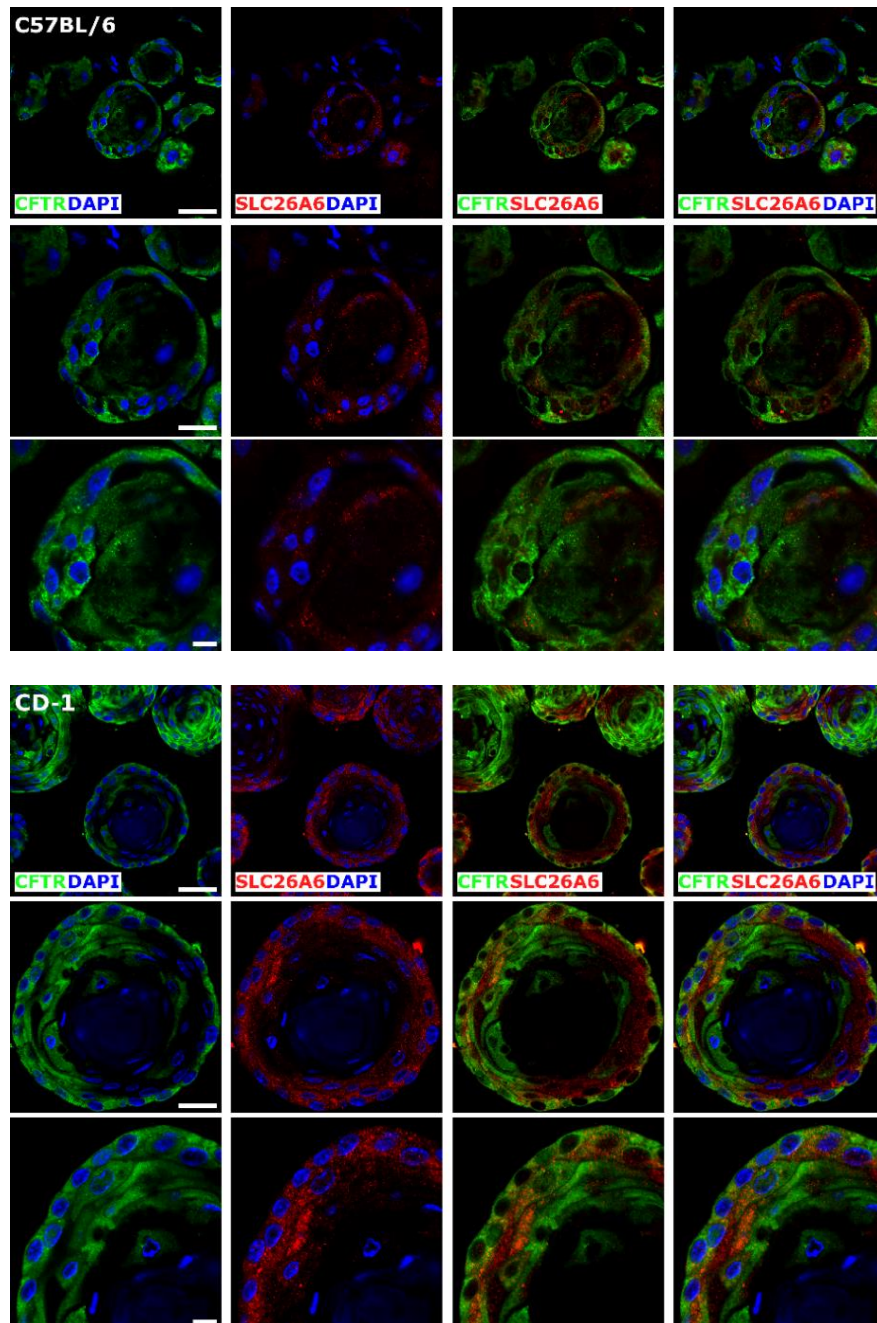

Figure 9. Colocalization of the CFTR Cl⁻-channel and Slc26a6 on esophageal organoids (EOs). Co-staining of Slc26a6 (red) and CFTR (green). The scale bar represents 50 μm (upper line), 25 μm (middle line,) and 10 μm (bottom line), for both mice strains.

4.4. Resting pH_i of EOs and determination of buffering capacity

To investigate the pH regulatory mechanisms of EO cultures, we initially determined the resting pH_i of the cells. EOs were exposed to a standard Hepes solution (pH 7.4), followed by a 5-min exposure to a high-K^+/nigericin–Hepes solution at pH 7.2, 7.4, and 7.6 (Fig. 10A and B). The resting pH_i of the organoids was determined using the classical linear model [58,59]. The resting pH_i of C57BL/6 organoids was 7.61 ± 0.03, whereas that of CD-1 organoids was 7.58 ± 0.03.
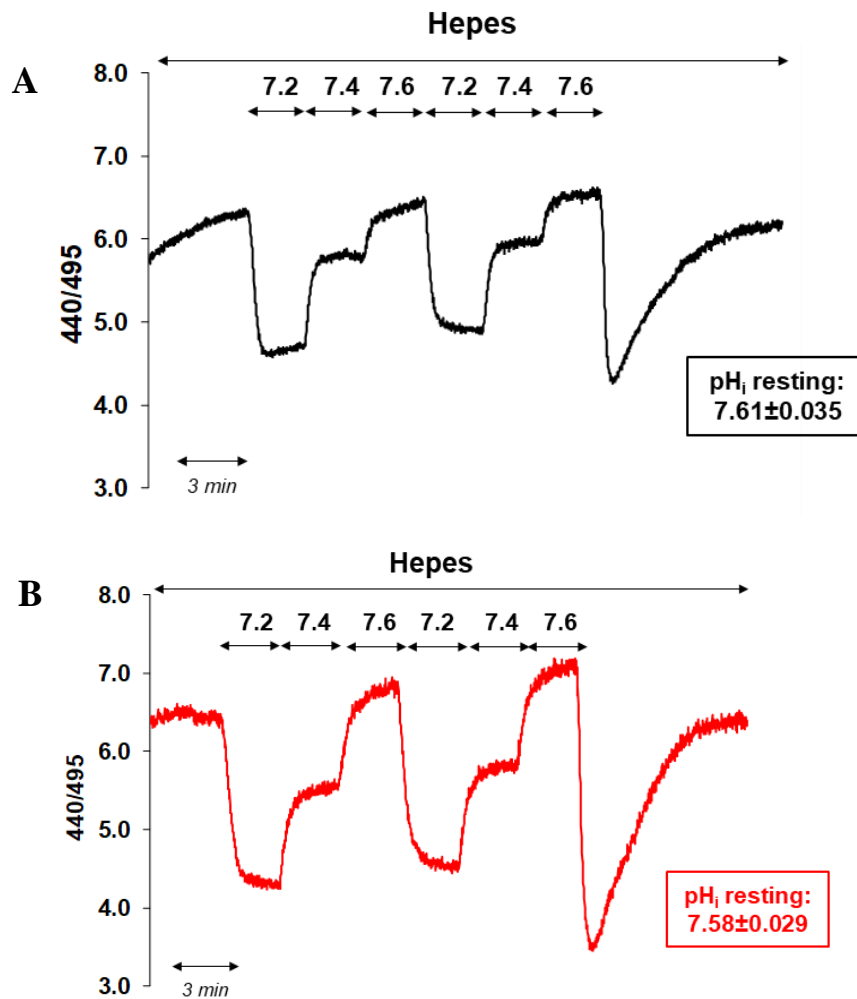

Figure 10. Determination of the resting pH of the esophageal organoids (EOs). Organoids were exposed to high-K^+/nigericin–Hepes solution at pH 7.2, 7.4, and 7.6. The resting intracellular pH (pH_i) was calculated from this three-point calibration using the classic linear model. **(A)** The black line shows the response of EOs generated from C57BL/6 mice whereas **(B)** the red line shows the response of EOs generated from CD-1 mice.

The total buffering capacity (β_{total}) of the EOs is their ability to maintain a relatively constant pH_i value in response to the alteration of the intracellular acid or base

concentration. Its value consists of several components and changes depending on the value of the extracellular pH. To study the different aspects of the pH regulatory mechanism in EOs, the total buffering capacity of EOs was estimated using the NH4Cl pre-pulse technique, as previously described (Fig. 11A and B) [60,61,66].
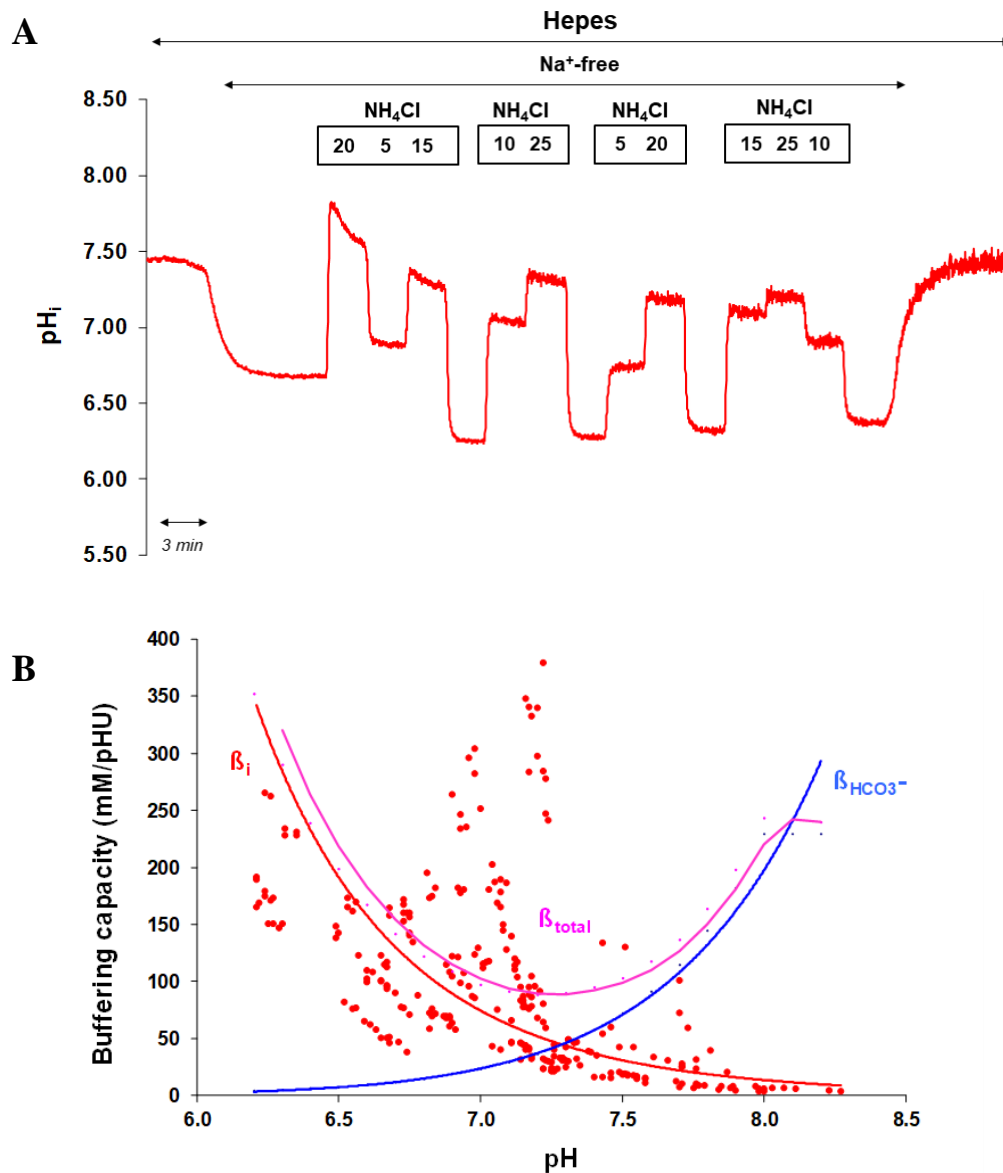

Figure 11. Assessment of the buffering capacity of the esophageal organoids (EOs). Organoids were exposed to various concentrations of NH4Cl in nominally Na$^+$- and HCO$_3^-$-free solutions, and the total buffering capacity (β_{total}) of the cells was calculated using the following equation: $\beta_{total} = \beta_i + \beta_{HCO3-} = \beta_i + 2.3 \times [HCO_3^-]_i$, where β_i refers to the ability of intrinsic cellular components to buffer changes of pH$_i$ and β_{HCO3-} is the buffering capacity of the HCO$_3^-$/CO$_2$ system. The black line shows the response of the EOs generated from C57BL/6 mice, whereas the red line shows the response of EOs generated from CD-1 mice. n = 17-19

4.5. Activity of Na$^+$/H$^+$ exchanger (NHE)

NHE is a transmembrane protein that regulates the electroneutral exchange of extracellular Na$^+$ and intracellular H$^+$, thereby playing a central role in pH$_i$ and cell volume homeostasis. NHE activity was investigated by removing extracellular Na$^+$ from the external solution. As presented in Figure 13A, Na$^+$ removal induced a rapid and sharp decrease in pH$_i$, suggesting that EOs express functionally active NHE. There was no significant difference in the rate [$-J(B^-)$] and extent (ΔpH_{max}) of the pH$_i$-decrease between the two mouse strains (Fig. 12B and C).
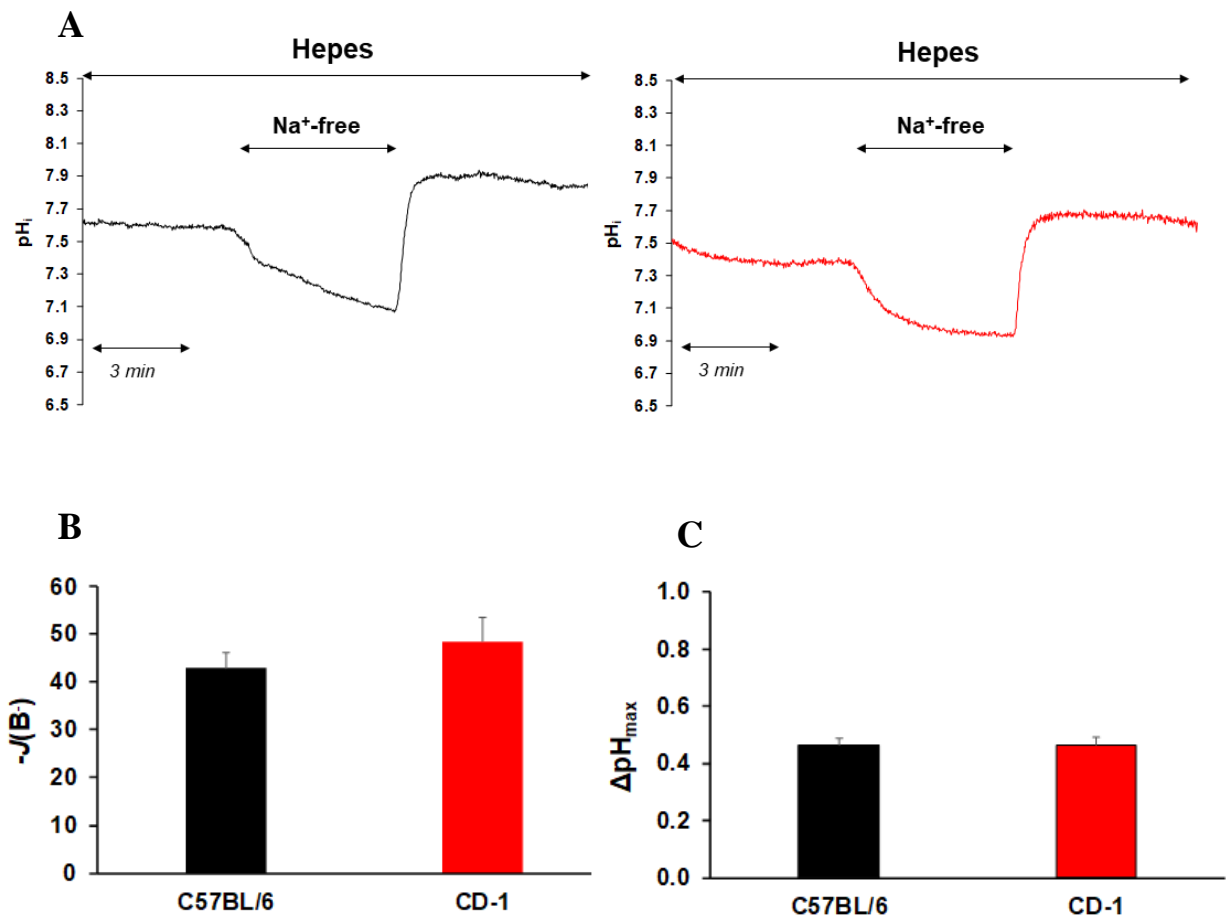

Figure 12. Investigation of Na$^+$/H$^+$ exchanger (NHE) activity on esophageal organoids (EOs). (A) Removal of Na$^+$ from standard Hepes solution caused rapid intracellular acidosis in EOs generated from C57BL/6 (black line) and CD-1 (red line) mice confirming the presence of a Na$^+$-dependent H$^+$ efflux mechanism. **(B)** Summary data for the calculated base flux [$-J(B^-)$], **(C)** and the maximal pH$_i$-change (ΔpH_{max}) induced by Na$^+$ removal.

The presence of NHE was also confirmed using the NH$_4$Cl-prepulse technique (Fig. 13A). EOs were exposed to 20 mM NH$_4$Cl (3 min) in a standard Hepes solution, which induced a high degree of intracellular alkalization because of the rapid influx of NH$_3$ into cells. After removing NH$_4$Cl from the external solution, pH$_i$ dramatically decreased and then returned to baseline. Since NHE is activated by acidic pH$_i$, recovery from acidosis reflects the activity of NHE. In the absence of Na$^+$, recovery from acidosis was negligible, indicating that in the absence of HCO$_3^-$, NHE is mainly responsible for the alkalization of cells (Fig. 13B).
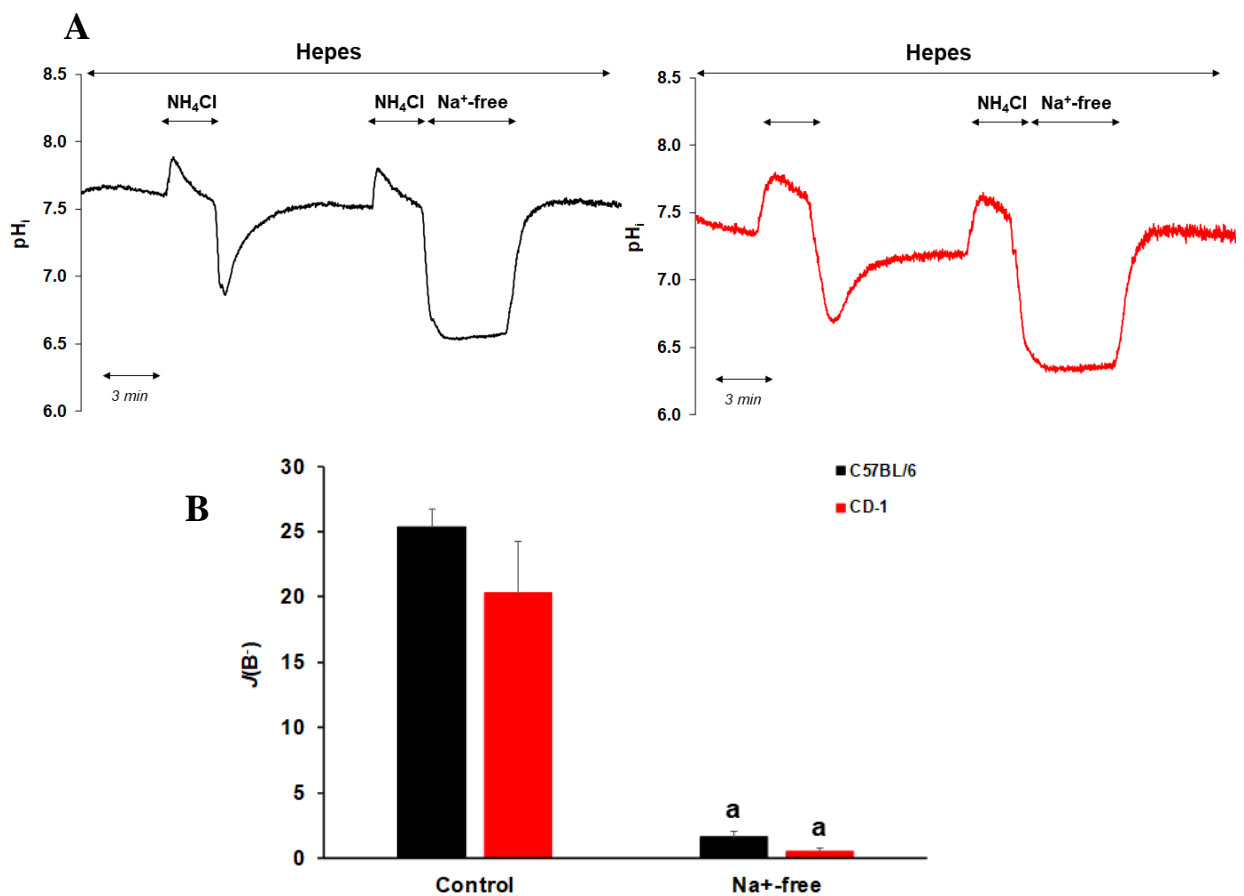

Figure 13. Investigation of Na$^+$/H$^+$ exchanger (NHE) activity on esophageal organoids (EOs) with NH$_4$Cl-prepulse technique. (A) Recovery from acid load reflects the activity of NHE in a standard Hepes solution. After the second NH$_4$Cl pulse, Na$^+$ was removed from the external solution to investigate the activity of NHE. **(B)** Summary bar chart presents the initial rate of pH$_i$ recovery [$J(B^-)$] from an acid load. $J(B^-)$ was calculated from the $\Delta pH/\Delta t$ obtained by linear regression analysis of pH$_i$ measurements made over the first 60 s after Na$^+$ removal (one pH$_i$ measurement was made per second). The buffering capacity at the initial pH$_i$ was used for the calculation of $J(B^-)$ (see Methods). Data are presented as the mean $\pm$ SD. a: $p \leq$ 0.05 vs. Control. n = 19-23

The SLC9/NHE gene family encodes the NHE proteins. Currently, 13 isoforms are known in mammals with different functions and expression patterns [67,68]. To identify the most active isoform on EOs, the NHE isoform selective inhibitor HOE-642 was used.
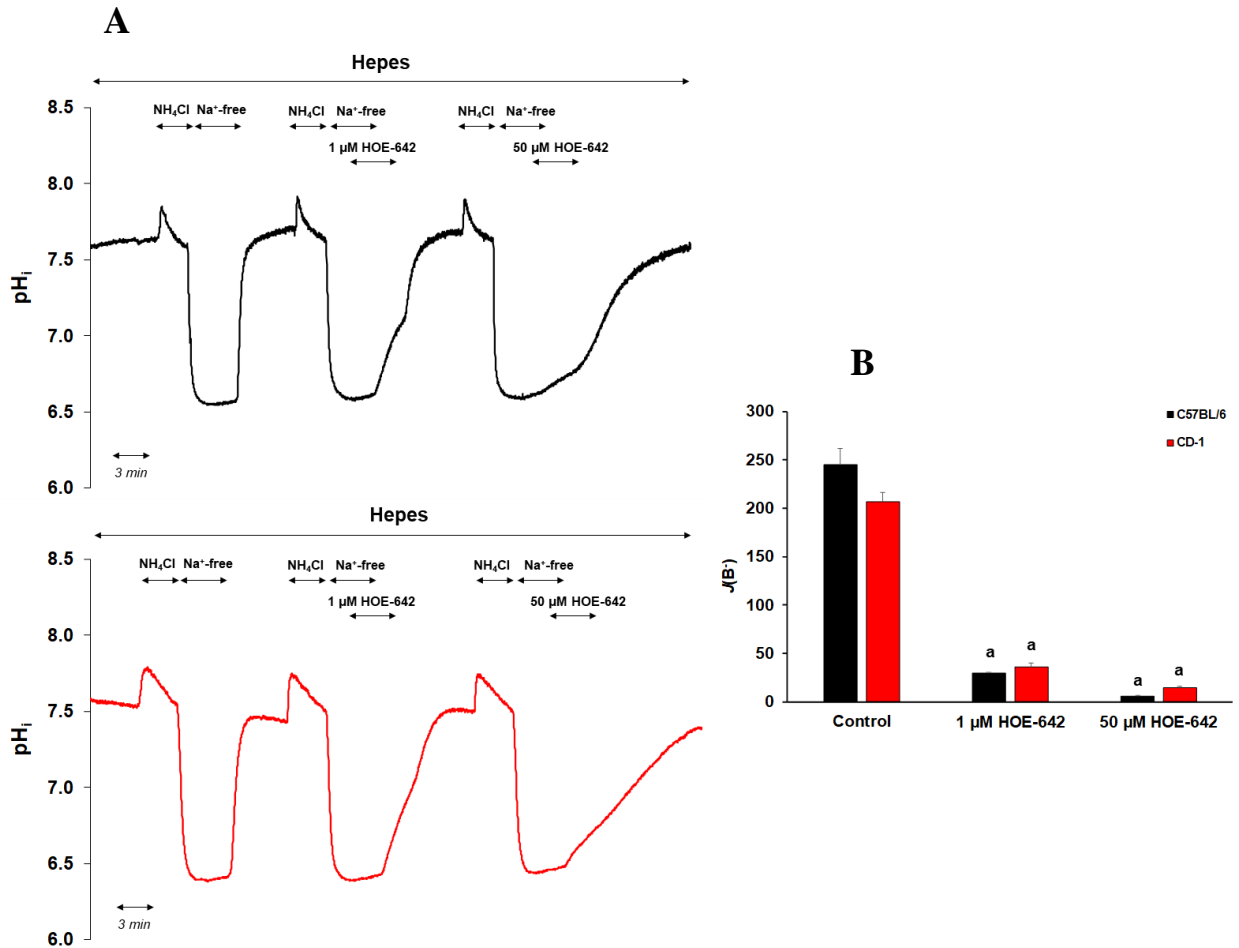

Figure 14. Investigation of Na$^+$/H$^+$ exchanger (NHE) isoforms on esophageal organoids (EOs). (A) (B) Representative intracellular pH (pH$_i$) curves (black line, C57BL/6; red line, CD-1) present the recovery from acidosis in the presence of 1 and 50 μM HOE-642. **(C)** Summary data of the calculated activities of the different NHE isoforms in the presence of the isoform-selective NHE inhibitor HOE-642. The rate of pH recovery [J(B$^-$)]was calculated from the ΔpH/Δt obtained via linear regression analysis of the pH$_i$ measurement performed over the first 60 s of recovery from the lowest pH$_i$ level (initial pH$_i$). The buffering capacity at the initial pH$_i$ was used to calculate J(B$^-$). Data are presented as the mean ± SD. a: p ≤ 0.05 vs. Control. b: p ≤ 0.05 vs. 1 μM HOE-642. n = 5–11

EOs were acid-loaded with 20 mM NH$_4$Cl followed by a 3-min incubation in a Na$^+$-free Hepes solution. In the absence of Na$^+$, the NHE is blocked, hence pH$_i$ is not regenerated. Upon the re-administration of extracellular Na$^+$, NHE regained its function, and its activity could be estimated from the initial rate of pH$_i$ recovery over the first 60 s.

As presented in Fig. 14A, 1 μM HOE-642 decreased pH_i recovery by $87.81 \pm 1.17\%$ in C57BL/6 EOs and $82.37 \pm 7.32\%$ in CD-1 EOs, whereas the administration of 50 μM HOE-642 resulted in further decreases ($97.54 \pm 0.52\%$ in C57BL/6 EOs and $92.91 \pm 3.76\%$ in CD-1 EOs, Fig. 14B). These data indicate that although NHE-1 has higher activity, NHE-2 is also active on EOs. The fact that some activity remained even in the presence of 50 μM HOE-642 suggests the presence of other Na^+-dependent acid-extruding mechanisms.

4.6. Activity of Na^+/HCO_3^- (NBC) cotransporter

NBC is an electrogenic transporter that mainly localizes to the basolateral membrane in most epithelia, where it mediates the cotransport of Na^+ and HCO_3^- into cells. Inside cells, HCO_3^- binds H^+ and causes an increase in the pH_i. Therefore, in a standard HCO_3^-/CO_2-buffered external solution, NBC together with NHE, participates in maintaining pH homeostasis.

NBC activity was investigated by the NH_4Cl-pre-pulse technique (Fig. 15A). Administration of HCO_3^-/CO_2 rapidly and largely decreased pH_i because of the quick diffusion of CO_2 into the cytoplasm. Significant pH_i recovery was observed after acidification, suggesting the important role of HCO_3^- efflux into EOs through NBC (Fig. 15A). After the NH_4Cl pulse, recovery from alkalosis was more rapid than observed in the presence of standard Hepes solution, indicating that in addition to NHE, NBC is also active in the presence of HCO_3^-. Withdrawing the Na^+ from the external solution almost completely abolished the recovery from acidosis. To determine NBC activity, NHE function was blocked by the non-selective NHE inhibitor amiloride, which was added 1 min before and during the re-administration of Na^+.

As presented in Fig.15B, the recovery from acidosis was decreased by $61.88 \pm 5.3\%$ in C57BL/6 organoids and $62.18 \pm 7.3\%$ in CD-1 organoids in the presence of amiloride, indicating that NHE is responsible for much of the recovery from acidosis. There was some remaining recovery from acidosis, for which the NBC is responsible; hence, the functionally active NBC is located on EOs. Interestingly, we found a significant difference in recovery following Na^+-withdrawal between the C57BL/6 and CD-1 EOs, suggesting greater NBC activity in C57BL/6 mice.
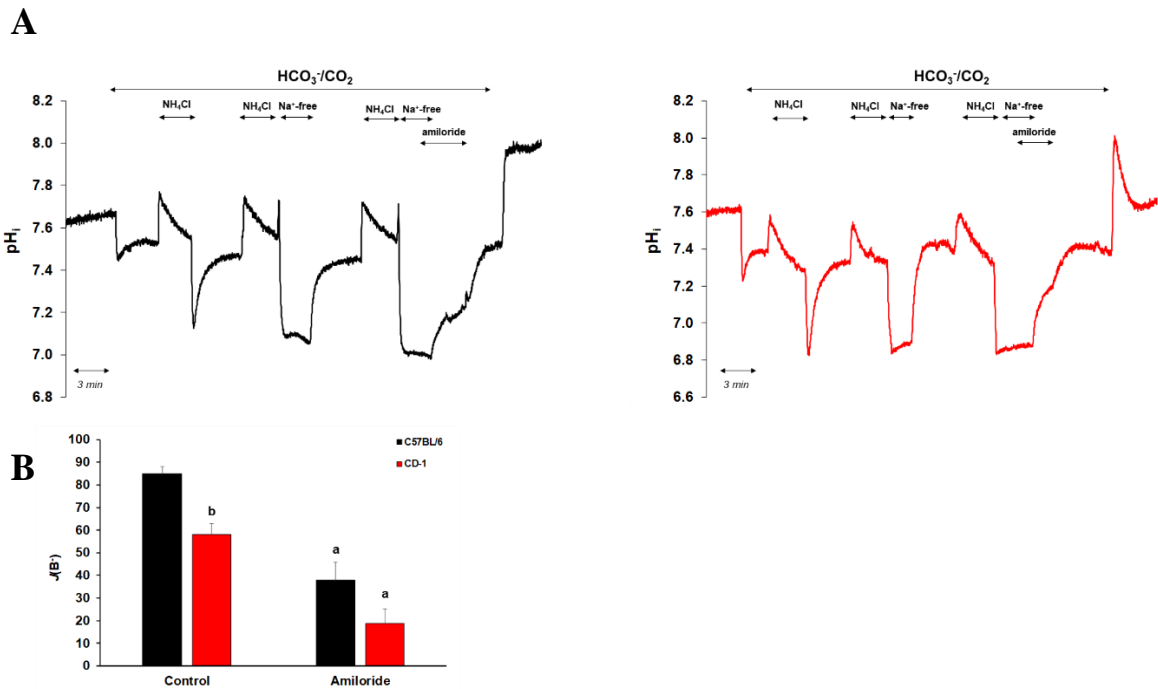
Figure 15. Investigation of Na$^+$/HCO$_3^-$ cotransporter (NBC) activity on esophageal organoids (EOs).

(A) Representative intracellular pH (pH$_i$) curves (black line, C57BL/6; red line, CD-1) present the recovery from acidosis in the presence of 0.2 mM amiloride. **(B)** Summary data present the calculated activity of NBC in the presence of the Na$^+$/H$^+$ exchanger (NHE) inhibitor amiloride. The rate of acid recovery [J(B$^-$)] was calculated from the ΔpH/Δt obtained via linear regression analysis of the pH$_i$ measurement performed over the first 60 s of recovery from the lowest pH$_i$. The buffering capacity at the initial pH$_i$ was used to calculate J(B$^-$). Data are presented as the mean ± SD. a: p ≤ 0.05 vs. Control. b: p ≤ 0.05 vs. C57BL/6. n = 15–17

4.7. Activity of the Cl$^-$/HCO$_3^-$ exchanger (CBE)

The HCO$_3^-$ transporter family (also named the anion exchanger family) includes several transport proteins, of which Slc26 proteins function as an electroneutral Cl$^-$/HCO$_3^-$ exchanger expressed in the apical membrane of the epithelium. Among the Slc26 exchangers, the presence of Slc26a6 (PAT1) was detected at both the mRNA and protein levels in the C57BL/6 and CD-1 EOs. Slc26a6 mediates Cl$^-$ and HCO$_3^-$ exchange with a 1Cl$^-$/2HCO$_3^-$ stoichiometry through the cell membrane[69].

To determine whether this Cl$^-$/HCO$_3^-$ exchanger is functionally active on the organoids, the Cl$^-$-withdrawal technique was used (Fig. 16A–C). In the presence of external Cl$^-$, Slc26a6 mediates the efflux of HCO$_3^-$ and the uptake of Cl$^-$, therefore playing a role in the acidification of cells. Removal of Cl$^-$ from standard HCO$_3^-$/CO$_2$-buffered solution induced strong alkalization because of the reverse mode of the

exchanger, when it mediates HCO_3^- reabsorption rather than secretion (Fig. 16A). By contrast, in the absence of HCO_3^-, Cl^- removal caused minimal, reversible alkalization (Fig. 16B).
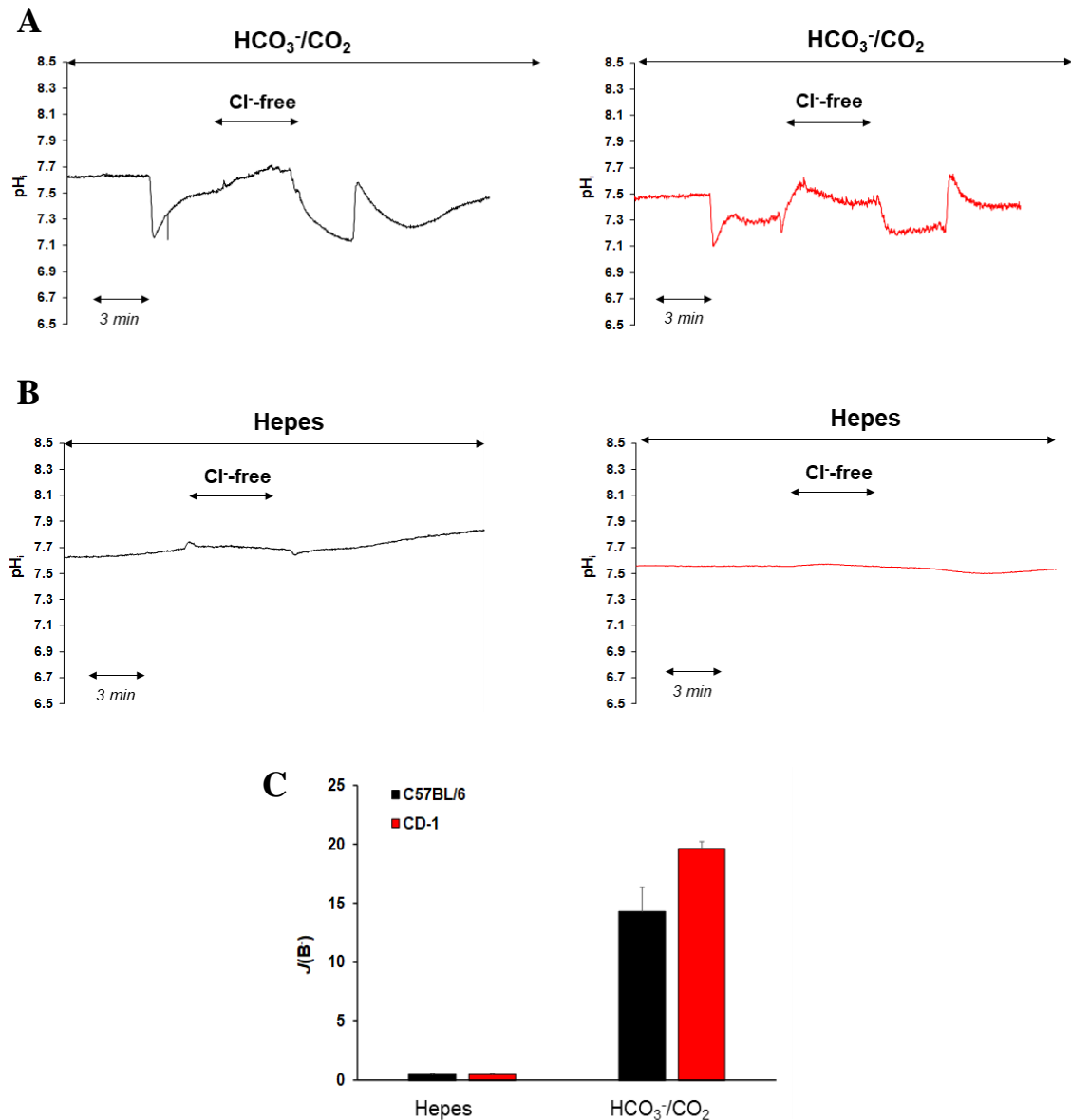
Figure 16. Investigation of Cl^-/HCO_3^- exchanger activity on esophageal organoids (EOs). Cl^-/HCO_3^- exchanger activity was investigated by the Cl^--removal technique in the presence **(A)** and absence **(B)** of HCO_3^-/CO_2 (black line, C57BL/6; red line, CD-1) **(C)** The rate of acid recovery $J(B^-)$ was calculated from the $\Delta pH/\Delta t$ obtained via linear regression analysis of pH_i-measurements performed over the first 60 s after exposure to the Cl^--free solution. The buffering capacity at the initial pH_i was used to calculate $J(B^-)$. n = 4-15

The presence of functionally active CBE has also been confirmed by the NH_4Cl-prepulse technique (Fig. 17A and B). We previously illustrated that in the presence of HCO_3^-, the initial rate of recovery (30 s) from alkalosis reflects the activity of CBEs[63,70]. As presented in Fig. 17B, there was no significant difference in CBE activity between the two mouse EOs.
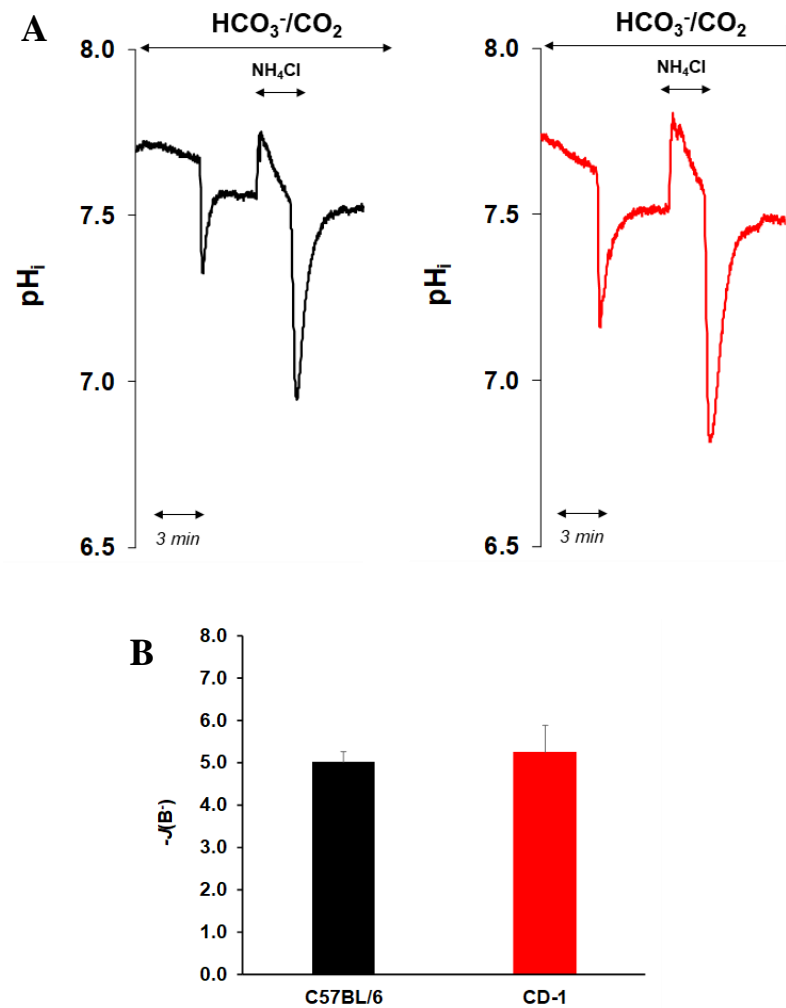
Figure 17. Investigation of the Cl^-/HCO_3^- exchanger activity on esophageal organoids (EOs) with NH_4Cl-pre-pulse technique. (A) The activity of the Cl^-/HCO_3^--exchanger was also measured using the alkali-loading method and **(B)** expressed as calculated $J(B^-)$, which was calculated from the $\Delta pH/\Delta t$ obtained via linear regression analysis of pH_i measurements performed over the first 30 s of recovery from the highest pH_i-level achieved in the presence of NH_4Cl. The buffering capacity at the start point pH_i was used for the calculation of $J(B^-)$. Data are presented as the mean $\pm$ SD. n = 25-37

4.8. Activity of cystic fibrosis transmembrane conductance regulator (CFTR) Cl⁻ channel

The CFTR Cl⁻ channel, which is present in most epithelial cells, mediates the efflux of Cl⁻ from cells. The presence of this ion channel has been detected at both the mRNA and protein levels in EOs; therefore, we also investigated its activity using the Cl⁻-sensitive fluorescent dye, MQAE combined with the CFTR activator, forskolin. As presented in Fig. 18A and B, the administration of 10 µM forskolin caused a small increase in the initial rate of Cl⁻ efflux ($19.61 \pm 4.52\%$ in C57BL/6 organoids and $21.83 \pm 9.72\%$ in CD-1 organoids), and Cl⁻ loss reached a steady state after approximately 10 min. The effect of 5 µM forskolin was negligible.
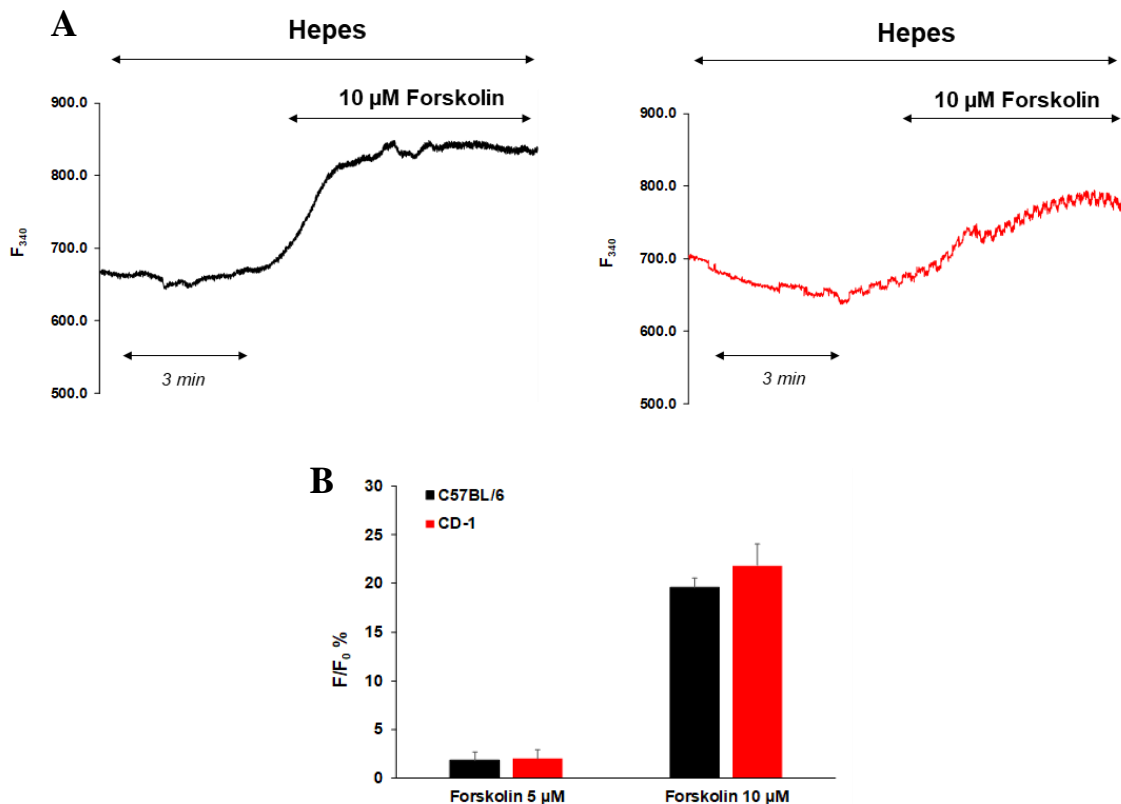
Figure 18. Investigation of cystic fibrosis transmembrane conductance regulator (CFTR) activity on esophageal organoids (EOs). (A) Representative intracellular pH (pHi) curves (black line, C57BL/6; red line, CD-1) present the effect of forskolin on Cl⁻-efflux. **(B)** Summary data for the maximal fluorescence intensity changes. n = 19-22

To investigate the presumed functional relationship between CFTR and the acid-base transporters, the activity of the ion transporters was also examined in the presence of the CFTR inhibitor, CFTRinh-172 (10 mM; Fig. 19A-C). Using the NH_4Cl-prepulse

technique, we found that the recovery from alkalosis, which reflects the activity of the CBE, was significantly decreased by CFTR inhibition ($18.60 \pm 3.34\%$ in C57BL/6 organoids and $35.71 \pm 11.77\%$ in CD-1 organoids, Fig. 19B), whereas recovery from acidosis was only inhibited in C57BL/6 organoids (Fig. 19C).
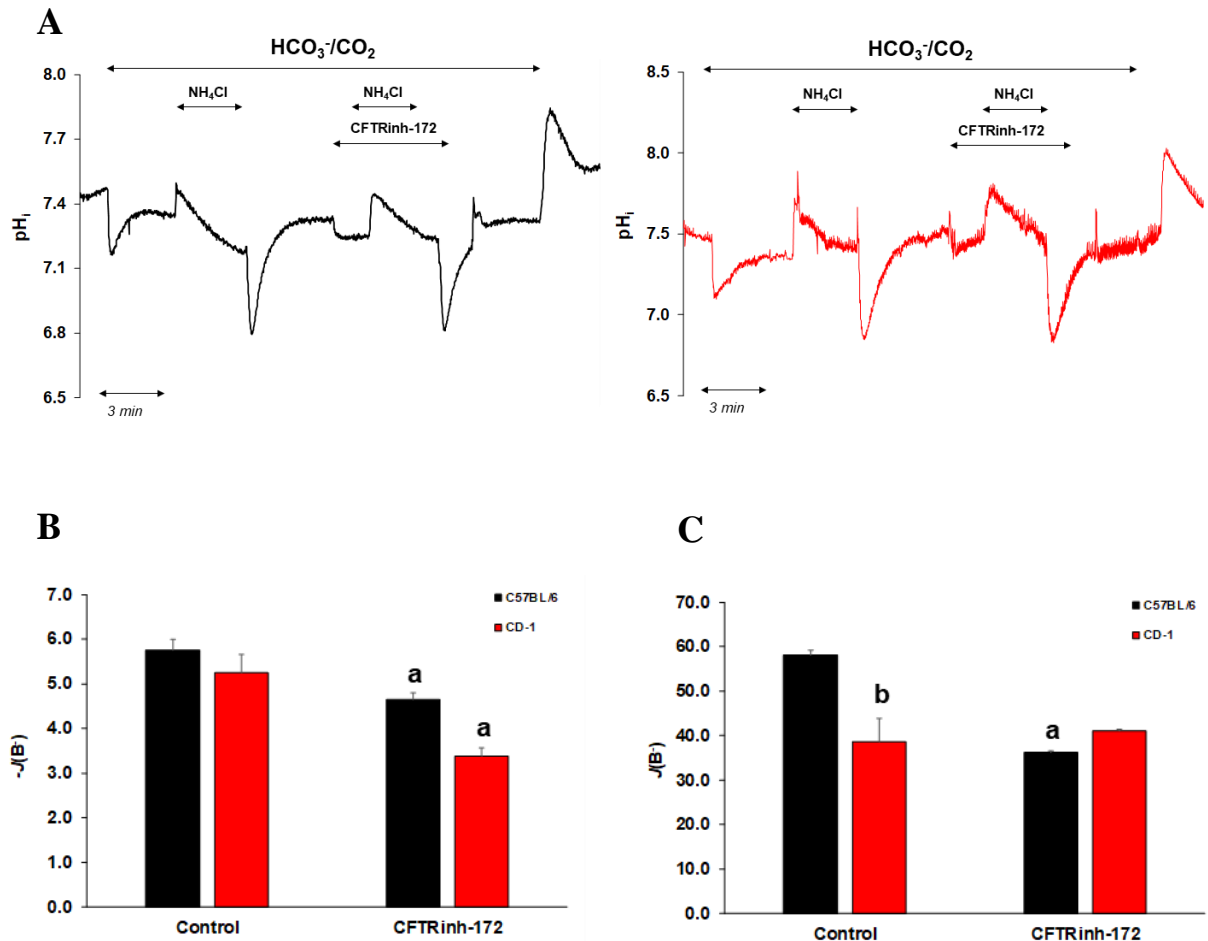
Figure 19. Investigation of the functional relationship between cystic fibrosis transmembrane conductance regulator (CFTR) and the acid-base transporters on esophageal organoids (EOs). (A) Representative pH_i curves present the recovery from acid- and alkali-loading in the presence of 10 μM CFTRinh-172. The rates of alkali recovery [-$J(B^-)$] **(B)** and acid recovery [$J(B^-)$] **(C)** were calculated from the $\Delta pH/\Delta t$ obtained via linear regression analysis of pH_i measurements performed over the first 30 and 60 s of recovery from the highest and lowest pH_i (initial pH_i), respectively. The buffering capacity at the initial pH_i was used to calculate $J(B^-)$ and $-J(B^-)$. Data are presented as the mean $\pm$ SD. a: $p \leq 0.05$ vs. Control. b: $p \leq 0.05$ vs. C57BL/6. n = 3–6

4.9. Evaluation of the viability of primary EECs

A large number of epithelial cells can be isolated from the esophageal epithelium of the guinea pig, which is excellent for conducting functional measurements *in vitro* [2]. To determine how long the primary cells are viable after the isolation, the freshly isolated and plated guinea pigs' EECs were investigated every hour after the isolation using the Trypan Blue exclusion test. After isolation, the cell viability was $88.72 \pm 3.41\%$, which we considered the control value. The cell viability significantly decreased until the third hours ($62.96 \pm 9.75\%$ and $39.01 \pm 6.87\%$). No significant difference was observed between the results measured in the third and fourth hour ($39.01 \pm 6.87\%$ vs. $30.67 \pm 3.98\%$). Then the cell viability decreased significantly from the fourth hour on, and at the fifth hour, there were barely detectable living cells in the sample ($7.41 \pm 9.43\%$). (Fig. 20)

We concluded that 4 hours is the maximum period during which the primary EECs can still be used for functional measurements after isolation.
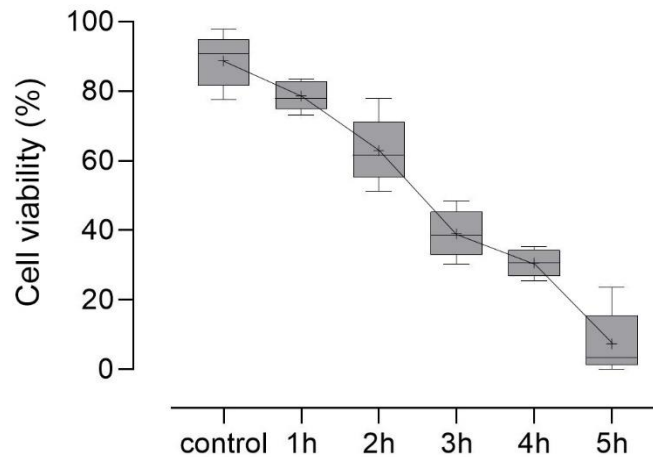
Figure 20. Cell viability of primary EECs. The cell viability of the freshly isolated cell suspension was investigated using the Trypan Blue exclusion test. Brightfield captures were taken every hour, and the number of cells was counted using ImageJ Fiji software. Cell viability decreases continuously and significantly as time progresses. A plateau phase can be observed between hours 3 and 4, when the cell viability does not decrease significantly. From the 4th hour on, the cell viability decreases continuously; eventually, in the 5th hour, almost no viable cells can be detected in the sample. The total number of cells was 1439-2800/coverslip.

5. DISCUSSION

The ion transport systems in EECs are crucial for maintaining the proper pH balance in the epithelial barrier. In addition, these transporters play an important role in the regulation of osmotic balance and are involved in the production and secretion of mucus, which helps lubricate the esophagus and protect it from mechanical and chemical damage. Alterations in pH_i have the potential to have a major influence on a wide variety of biological processes. Disruption of the ion transport systems in the esophagus can result in esophageal disorders such as GERD and esophagitis[71]. The exact role of esophageal ion transport processes is not fully understood, especially in pathological conditions, the main reason for which is the lack of a suitable experimental system reflecting the primary disease[32]. Numerous studies have been conducted on the regulation of pH_i using 2D esophageal cell cultures or primary esophageal tissue samples[6]. These studies investigated the basic acid-base transporters and evaluated how the presence of acid and bile affected the function of these transporters. Although extremely essential information was obtained from these studies, the majority of the findings are now obsolete, and the *in vitro* model used in these investigations did not permit the investigation of a particular transporter.

The development of organoid cultures was a significant breakthrough in the examination of individual organs and tissues. Organoids are three-dimensional cell cultures that show some of the key features of the represented organ. They can be derived from adult, embryonic, or induced pluripotent stem cells, which can self-organize in three-dimensional culture and have a self-renewing capability. The stem cell population of the esophageal epithelium is found in the basal layer of the epithelium, both in rodents and in the human esophagus[39]. Under appropriate culturing conditions, organoids grown from stem cells develop a similar structure to the organ of origin, including the presence of several cell layers, so they can provide a suitable model for performing functional assays. As stated in the introduction, mouse EOs can be a good platform for fundamental research experiments and protocol optimization, which is why they were chosen as an experimental model for our studies. Initially, we adopted and optimized the protocol of DeWard and colleagues for the generation of EOs from mouse tissue using two frequently used laboratory mouse strains (C57BL/6 and CD-1)[37]. On the 3rd day after isolating and plating the mouse primer EECs, organoid formation was observed, and the size of the organoids increased steadily in the following days, peaking between days 7 and 9.

According to the relevant literature, spheres larger than 50 μm were considered organoids in our study[37,41]. Organoids between 50 and 150 μm in size were used for our upcoming experiments. Demonstrating that mature EOs are derived from epithelial stem cells was a crucial step in establishing the protocol. For this reason, we determined the composition of the freshly isolated cell suspension based on cell surface markers. To prove that the organoids arise from epithelial stem cells, we used the stem cell marker Lgr5 and the epithelial marker CK14 on the freshly isolated cells. FACS analysis revealed that over half of the primary epithelial cells were Lgr5- and CK14-positive in both cases, indicating that the resultant organoids were produced from epithelial stem cells. Immunostaining showed similar results in both cases: a strong LGR5 expression was detected in both organoids, indicating that the organoids contain non-quiescent stem cells[72]. Interestingly, CK14 expression shows the strongest signal in the outer layer of organoids, as can be seen in the basal cells of the primary esophageal tissue[73].

According to our current knowledge, no study has specifically used EOs to investigate ion transport processes. As detailed in the relevant methods section, our laboratory's conventional pH microfluorometry methodology was adjusted to accommodate the EOs. To investigate the ion transport mechanisms of EOs, we initially determined their resting pH and total buffering capacity. We discovered that the initial pH of the organoids was close to 7.6 for CD-1 organoids and marginally above 7.6 for C57BL/6 organoids. Several studies have reported that the resting pH of rabbit and human esophageal cells is exceptionally high as well[15,74]. The cause of the elevated resting pH_i is unknown. This observation is most likely explained by the increased activity of alkalizing transporters, which work to neutralize acidosis.

Using functional and molecular biological techniques, we identified the major ion transporters on mouse EOs. Our findings revealed the presence of a functionally active Na^+-dependent H^+ efflux mechanism on EOs, most likely NHE. NHE-1 was previously shown to be present in rat and rabbit EECs[14]. NHE-1 and NHE-2 expression, on the other hand, is extremely low in normal human esophageal tissue but high in Barrett's and esophageal cancer[1,75,76]. HOE-642 significantly decreased NHE function, implying that NHE-1 and NHE-2 account for more than 90% of functionally active NHEs in EOs. According to our assumption, other NHE isoforms or a proton pump are likely to be responsible for the residual activity. NHE-1 and NHE-2 immunolocalization revealed that NHE-1 expression was predominantly found in the peripherial, basal layer of the EOs, but NHE-2 staining was more prominent in the inner cell layers, which are mainly

composed of differentiated keratinocytes. The fact that organoids are made up of epithelial cells with varied degrees of differentiation explains why NHE-1 and NHE-2 are found in distinct places. Our finding that NHE-1 is mainly located in basal cells is consistent with the observation that NHE-1 expression is pronounced in the basolateral membrane of the esophageal epithelium[14].

Another transporter that can protect cells from acidosis and is vital in pH_i regulation is NBC. Based on our prior findings, the presence of NBC in human EECs has been demonstrated, and its expression is elevated in BE[1]. The function of NBC in EECs is unknown, however, it is thought to be important in the regulation of pH_i and transcellular transfer of HCO_3^-[77]. CO_2-induced acidosis in EOs was nearly fully reversed in our experiment, which can be explained by the input of HCO_3 via NBC. Furthermore, we discovered a substantial difference in acidosis recovery in the presence and absence of HCO_3^-, as well as a pretty considerable recovery in the presence of amiloride. These findings strongly suggest that EOs express functionally active NBC.

Because NBC mediates HCO_3^- uptake, its presence also presupposes the presence of CBEs on EOs[78], accordingly, we successfully detected a Cl^--dependent HCO_3^- efflux mechanism on EOs. Removal of Cl^- from the external solution in the presence of HCO_3^- induced strong alkalosis via the reverse mode of the CBE. In addition, the presence of HCO_3^- significantly increased the rate of recovery from alkalosis. Previous studies by our laboratory demonstrated that recovery from alkalosis in the presence of HCO_3^- is the result of HCO_3^- efflux through the CBE[63,70]. RT-PCR and immunohistochemistry revealed that the Slc26a6 CBE was significantly expressed in EOs, whereas Slc26a3 expression was moderate and non-specific. Furthermore, Slc26a6 expression was higher towards the EO periphery, indicating that basal cells had some HCO_3^- secreting potential. The Slc26a6 transporter is primarily located on the apical membrane of secretory epithelial cells, where it plays an essential role in HCO_3^- secretion[79]. Because the esophageal epithelium is not a typical secretory epithelium, the presence of this transporter on EOs is unusual.

The role of the CFTR Cl^- channel in the esophageal epithelium is a relatively rarely researched area. Some studies on esophageal cell lines have reported the presence of CFTR in human ESCC and EA[80,81], where the protective role of the channel was demonstrated. It has also been detected in the basal epithelia of porcine esophageal mucosa, where CFTR mediates Cl^- transport together with the voltage-gated Cl^- channel ClC-2. The ClC-2 agonist lubiprostone reduced acid-related injury and improved

epithelial barrier repair. Since lubiprostone has been shown to activate CFTR in parallel[82,83], a protective role for CFTR has been hypothesized in this study[84]. In sum, these experiments demonstrated that CFTR may play a protective role against EA, and overexpression of this channel is associated with a good prognosis in ESCC. Furthermore, it is worth noting that Slc26 CBE and the CFTR Cl⁻ channel are functionally coupled in the apical membrane of many anion-secreting epithelia, such as pancreatic ductal epithelial cells, to mediate fluid and HCO_3^- secretion[85,86]. In the last part of our study, in order to investigate the presence of CFTR and its co-expression with the Slc26a6 transporter, we examined the co-localization of these transporters by immunostaining and by several microfluorimetric experiments.

An interesting result of our study is that the CFTR Cl⁻ channel is expressed on mouse EOs, which was demonstrated by immunohistochemistry, which showed that both peripheral and central cells strongly express CFTR. Co-staining of CFTR and Slc26a6 revealed some co-localization, mainly in cells on the periphery of the EOs, indicating that the two transporters interact with each other in the basal layers. The microfluorimetric approach was utilized to study the functional relationship between CFTR and Slc26a6. The specific CFTR activator, forskolin, increased CFTR activity concentration-dependently, but the response to forskolin was relatively low, even at supramaximal concentrations, indicating that CFTR channel activity is lower than typically observed in secretory epithelia, such as those in the pancreas or the lungs[87]. The presence of the CFTR inhibitor, CFTRinh-172, decreased the rate of recovery from alkalosis in both C57BL/6 and CD-1 EOs, demonstrating that the channel interacts with the Slc26a6. Interestingly, we found that CFTR inhibition also significantly reduced recovery from acidosis in C57BL/6 EOs. Because both NBC and NHE are involved in recovery from acidosis in the presence of HCO_3^-, CFTR may interact with one of these transporters, although this type of interaction has never been described before.

In addition, we also revealed the presence of the Ca^{2+}-activated Cl⁻ channel ANO1 or TMEM16A in EOs. So far, one study has examined the presence of ANO1 in the esophageal epithelium, and it was detected in the basal zone. This study indicated that its expression is increased in eosinophilic esophagitis and correlated with the severity of the disease. Furthermore, ANO1 has been reported to play a central role in the proliferation of basal zone hyperplasia via an IL-13–mediated pathway[88].

In our research group, we work with several experimental models, including primary EECs isolated from different animal models. A large number of epithelial cells can be

isolated from the esophageal epithelium of the guinea pig as well, which is excellent for conducting functional measurements *in vitro*[2]. To test how long a primary EEC is viable, we performed a cell viability test, and we found that 4 hours is the maximum period during which the primary EECs can still be used for functional measurements after isolation. Despite the fact that guinea pig EECs can be isolated easily and in large numbers, working with them is limited by their maximum viability *in vitro*.

Taken together, we successfully characterized for the first time the presence and activity of the main epithelial ion transporters using mouse EOs. This 3D cell culture model system can be used as a near-physiological experimental platform to study esophageal ion transport mechanisms not only under physiological but also under pathologic conditions. We can conclude that mouse EOs provide a relevant and suitable model system for studying the ion transport mechanisms of esophageal epithelial cells, and they can also be used as preclinical tools to examine the effects of different compounds on the ion transport system of the esophagus.

6. NOVEL FINDINGS

In summary, this is the first study to examine the ion transport system using mouse EOs, and our major findings are:

I.   We successfully generated EOs from two different, widely used laboratory mouse strains, and we described that mouse EOs are generated from tissue-resident epithelial stem cells. According to our results, there is no significant difference between the EOs from the two strains of mice in terms of culture conditions, ion transports, or usability.

II. We identified both the presence and function of the major acid-base transporters on EOs. These are the NHE, NBC, and CBE.

III. We first identified a functionally active CFTR chloride channel on mouse EOs, and we found that CFTR may interact with CBE in the alkali recovery process and may interact with NBC or NHE in the acid recovery process.

IV. We found that the primary EECs of guinea pigs are viable for up to 4 hours after isolation, so their use *in vitro* is only possible for a limited time.

SUMMARY

Altered esophageal ion transport mechanisms play a key role in inflammatory and cancerous diseases of the esophagus, but epithelial ion processes have been less studied because of the lack of a suitable experimental model. Therefore, our aim was to generate an *in vitro* organoid culture system that mimics well the key features of the esophageal epithelia and, on the other hand, is suitable for functional measurements. Organoids are three-dimensional cell culture systems that can be derived from adult, embryonic, or induced pluripotent stem cells, can self-organize in three-dimensional culture, and have a self-renewing capability. Organoids show a similar structure to the organ of origin, and cells retain their viability, so they can provide a suitable model for performing morphological and functional analysis *in vitro*.

In this study, we have adopted and optimized the protocol for the generation of esophageal organoids from mouse tissue then conducted a comprehensive analysis using functional and molecular biological approaches. EOs generated from EECs, as shown by FACS analysis, form a cell-filled structure with a diameter of 250–300 µm. The presence of Slc26a6 Cl^-/HCO_3^- exchanger (CBE), Na^+/H^+ exchanger (NHE), Na^+/HCO_3^- cotransporter (NBC), cystic fibrosis transmembrane conductance regulator (CFTR), and anoctamin 1 (ANO1) was detected in EOs using conventional PCR and immunostaining. Microfluorimetric techniques revealed high NHE, CBE, and NBC activities, whereas that of CFTR was relatively low. In addition, the inhibition of CFTR showed functional interactions between the major acid-base transporters and CFTR. We also tested how long a primary EEC is viable, and we found that 4 hours is the maximum period during which the primary EECs can still be used for functional measurements after isolation.

Summing up our results, the present study is the first to describe and functionally characterize the most common ion transport processes on EOs using two frequently used laboratory mouse strains (C57BL/6 and CD-1). We demonstrated that the major acid-base transporters are present on EOs and that they are functionally active. There was no significant difference in the expression or activity of the ion transporters between the two mouse strains. We conclude that EOs provide a relevant and suitable model system for studying the ion transport mechanisms of EECs, and they can also be used as preclinical tools to assess the effectiveness of novel therapeutic compounds in esophageal diseases associated with altered ion transport processes.

ÖSSZEFOGLALÓ

A nyelőcső epitélium iontranszport rendszere kulcsfontosságú a megfelelő intracelluláris pH-egyensúly fenntartásában. A nyelőcső epitélium iontranszport folyamatainak pontos szerepe még nem teljesen tisztázott, melynek fő oka feltételezhetően az élettanilag releváns kísérleti rendszer hiánya. Ezért fő célunk volt az organoid szövetkultúra modell létrehozása, amely *in vitro* mutatja a nyelőcső epitéliumának legfontosabb jellemzőit, másrészt alkalmas lehet funkcionális mérésekre. Az organoidok olyan háromdimenziós sejttenyésztő modellrendszerek, amelyek szöveti, embrionális vagy indukált pluripotens őssejtekből származhatnak, képesek önszerveződni háromdimenziós kultúrában, és önmegújító képességgel rendelkeznek. Az organoidok az eredeti szervhez hasonló szerkezetet mutatnak és a sejtek megőrzik életképességüket, így megfelelő modellt nyújthatnak *in vitro* morfológiai és funkcionális elemzések elvégzéséhez.

Ebben a tanulmányban optimalizáltuk a nyelőcső organoidok egérszövetből történő előállításának protokollját, majd átfogó elemzést végeztünk funkcionális és molekuláris biológiai technikák felhasználásával. Az egér nyelőcső epitélsejtekből előállított organoidok 250-300 µm átmérőjű sejttel teli szerkezetet alkotnak. Kimutattuk az Slc26a6 Cl^-/HCO_3^- kicserélő (CBE), Na^+/H^+ kicserélő (NHE), Na^+/HCO_3^- kotranszporter (NBC), cisztás fibrózis transzmembrán konduktancia szabályozó (CFTR) és anoktamin 1 (ANO1) jelenlétét az organoidokban konvencionális PCR és immunfestés alkalmazásával. A mikrofluorimetriás méréseink magas NHE, CBE és NBC aktivitást mutattak ki, míg a CFTR aktivitása viszonylag alacsony volt. Ezenkívül a CFTR gátlása funkcionális kölcsönhatást feltételez a fő sav-bázis transzporterek és a CFTR között. Továbbá megvizsgáltuk a primer tengerimalac nyelőcső epitélsejtek viabilitását, és azt találtuk, hogy 4 óra az a maximális időtartam, amely alatt a prímér epitélsejtek izolálás után felhasználhatók funkcionális mérésekre.

Összefoglalva eredményeinket, elmondható, hogy első alkalommal jellemeztük sikeresen a fő epiteliális iontranszporterek jelenlétét és aktivitását egér nyelőcső organoidok használatával. Megállapítottuk, hogy az egér nyelőcső organoidok fiziológiailag releváns és megfelelő modellrendszerek a nyelőcső epitélsejtek iontranszport mechanizmusainak tanulmányozására, valamint preklinikai eszközként is felhasználhatók különböző vegyületek nyelőcső iontranszport rendszerére gyakorolt hatásának vizsgálatára.

ACKNOWLEDGEMENTS

In addition, I am very grateful to **Katalin Jósvay** and **Dr. Csaba Vizler,** the colleagues of the Institute of Biochemistry in the Biological Research Centre. Their scientific guidance and attitude contributed to my development in the field of molecular biology and biochemistry at the beginning of my research career. I truly appreciate the advice they gave me and their valuable insights about the academic career pathway.

Last but not least, I owe a lot of thanks and gratitude to my partner, **Dr. Szabolcs Zahorán,** and my friends: **Mátyás Bukva, Gréta Elekes, Dr. Lea Avarka Szentgyörgyi,** and **Dr. Krisztina Tóth**, without whom it wouldn't have been possible.

REFERENCES

1. Laczkó, D. *et al.* Role of ion transporters in the bile acid-induced esophageal injury. *Am. J. Physiol.-Gastrointest. Liver Physiol.* **311**, G16–G31 (2016).

2. Becskeházi, E. *et al.* Inhibition of NHE-1 Increases Smoke-Induced Proliferative Activity of Barrett's Esophageal Cell Line. *Int. J. Mol. Sci.* **22**, 10581 (2021).

3. Bor, S. & Capanoglu, D. The additive effect of ethanol and extract of cigarette smoke on rabbit esophagus epithelium. *J. Gastroenterol. Hepatol.* **24**, 316–321 (2009).

4. Lin, B. R. *et al.* Luminal hydrochloric acid stimulates rapid transepithelial ion fluxes in rodent esophageal stratified squamous epithelium. *J. Physiol. Pharmacol. Off. J. Pol. Physiol. Soc.* **59**, 525–542 (2008).

5. Abdulnour-Nakhoul, S. M. & Nakhoul, N. L. Ussing Chamber Methods to Study the Esophageal Epithelial Barrier. *Methods Mol. Biol. Clifton NJ* **2367**, 215–233 (2021).

6. Becskeházi, E., Korsós, M. M., Erőss, B., Hegyi, P. & Venglovecz, V. OEsophageal Ion Transport Mechanisms and Significance Under Pathological Conditions. *Front. Physiol.* **11**, (2020).

7. Rosekrans, S. L., Baan, B., Muncan, V. & van den Brink, G. R. Esophageal development and epithelial homeostasis. *Am. J. Physiol.-Gastrointest. Liver Physiol.* **309**, G216–G228 (2015).

8. Kapoor, H., Lohani, K. R., Lee, T. H., Agrawal, D. K. & Mittal, S. K. Animal Models of Barrett's Esophagus and Esophageal Adenocarcinoma–Past, Present, and Future. *Clin. Transl. Sci.* **8**, 841–847 (2015).

9. Kuo, B. & Urma, D. Esophagus - anatomy and development. *GI Motil. Online* (2006) doi:10.1038/gimo6.

10. Hopwood, D. Oesophageal Defence Mechanisms. *Digestion* **56**, 5–8 (1995).

11. Orlando, R. C. Esophageal epithelial defense against acid injury. *J. Clin. Gastroenterol.* **13 Suppl 2**, S1-5 (1991).

12. Günther, C., Neumann, H. & Vieth, M. Esophageal Epithelial Resistance. *Dig. Dis.* **32**, 6–10 (2014).

13. Awayda, M. S., Bengrine, A., Tobey, N. A., Stockand, J. D. & Orlando, R. C. Nonselective cation transport in native esophageal epithelia. *Am. J. Physiol.-Cell Physiol.* **287**, C395–C402 (2004).

14. Shallat, S. *et al.* NHE-1 isoform of the Na+H+ antiport is expressed in the rat and rabbit esophagus. *Gastroenterology* **109**, 1421–1428 (1995).

15. Tobey, N. A., Koves, G. & Orlando, R. C. Human esophageal epithelial cells possess an Na+/H+ exchanger for H+ extrusion. *Off. J. Am. Coll. Gastroenterol. ACG* **93**, 2075 (1998).

16. Pedersen, S., Hoffmann, E. & Novak, I. Cell volume regulation in epithelial physiology and cancer. *Front. Physiol.* **4**, (2013).

17. Kooiker, A. J. & Wallert, M. A. Regulation of Cellular Proliferation and Migration by Palmitoylation of the Na+-H+ Exchanger Isoform 1 (NHE1). *FASEB J.* **34**, 1–1 (2020).

18. Fujiwara, Y. *et al.* Roles of epidermal growth factor and Na+/H+ exchanger-1 in esophageal epithelial defense against acid-induced injury. *Am. J. Physiol. Gastrointest. Liver Physiol.* **290**, G665-673 (2006).

19. Tobey, N. A. *et al.* Na+-Dependent and -Independent Cl-/HC03- Exchangers in Cultured Rabbit Esophageal Epithelial Cells. (1993).

20. Abdulnour-Nakhoul, S., Nakhoul, N. L., Caymaz-Bor, C. & Orlando, R. C. Chloride transport in rabbit esophageal epithelial cells. *Am. J. Physiol. Gastrointest. Liver Physiol.* **282**, G663-675 (2002).

21. Tobey, N. A., Cragoe, E. J. & Orlando, R. C. HCl-induced cell edema in rabbit esophageal epithelium: A bumetanide-sensitive process. *Gastroenterology* **109**, 414–421 (1995).

22. Russell, J. M. Sodium-potassium-chloride cotransport. *Physiol. Rev.* **80**, 211–276 (2000).

23. Haas, M. & Forbush, B. The Na-K-Cl cotransporters. *J. Bioenerg. Biomembr.* **30**, 161–172 (1998).

24. Haas, M. & Forbush III, B. The Na-K-Cl Cotransporter of Secretory Epithelia. *Annu. Rev. Physiol.* **62**, 515–534 (2000).

25. Bus, P., Siersema, P. D. & van Baal, J. W. P. M. Cell culture models for studying the development of Barrett's esophagus: a systematic review. *Cell. Oncol.* **35**, 149–161 (2012).

26. Underwood, T. J. *et al.* A comparison of primary oesophageal squamous epithelial cells with HET-1A in organotypic culture. *Biol. Cell* **102**, 635–644 (2010).

27. Poenar, D. P., Yang, G., Wan, W. K. & Feng, S. Low-Cost Method and Biochip for Measuring the Trans-Epithelial Electrical Resistance (TEER) of Esophageal Epithelium. *Materials* **13**, 2354 (2020).

28. Shamir, E. R. & Ewald, A. J. Three-dimensional organotypic culture: experimental models of mammalian biology and disease. *Nat. Rev. Mol. Cell Biol.* **15**, 647–664 (2014).

29. Heydari, Z. *et al.* Organoids: a novel modality in disease modeling. *Bio-Des. Manuf.* **4**, 689–716 (2021).

30. Kim, J., Koo, B.-K. & Knoblich, J. A. Human organoids: model systems for human biology and medicine. *Nat. Rev. Mol. Cell Biol.* **21**, 571–584 (2020).

31. Whelan, K. A., Muir, A. B. & Nakagawa, H. Esophageal 3D Culture Systems as Modeling Tools in Esophageal Epithelial Pathobiology and Personalized Medicine. *Cell. Mol. Gastroenterol. Hepatol.* **5**, 461–478 (2018).

32. Li, X. *et al.* Organoid cultures recapitulate esophageal adenocarcinoma heterogeneity providing a model for clonality studies and precision therapeutics. *Nat. Commun.* **9**, 2983 (2018).

33. Suarez-Martinez, E., Suazo-Sanchez, I., Celis-Romero, M. & Carnero, A. 3D and organoid culture in research: physiology, hereditary genetic diseases and cancer. *Cell Biosci.* **12**, 39 (2022).

34. Andrews, M. G. & Kriegstein, A. R. Challenges of Organoid Research. *Annu. Rev. Neurosci.* **45**, 23–39 (2022).

35. de Wert, G. & Mummery, C. Human embryonic stem cells: research, ethics and policy. *Hum. Reprod. Oxf. Engl.* **18**, 672–682 (2003).

36. Wensink, G. E. *et al.* Patient-derived organoids as a predictive biomarker for treatment response in cancer patients. *Npj Precis. Oncol.* **5**, 1–13 (2021).

37. DeWard, A. D., Cramer, J. & Lagasse, E. Cellular Heterogeneity in the Mouse Esophagus Implicates the Presence of a Nonquiescent Epithelial Stem Cell Population. *Cell Rep.* **9**, 701–711 (2014).

38. Seery, J. P. & Watt, F. M. Asymmetric stem-cell divisions define the architecture of human oesophageal epithelium. *Curr. Biol.* **10**, 1447–1450 (2000).

39. Zhang, Y., Bailey, D., Yang, P., Kim, E. & Que, J. The development and stem cells of the esophagus. *Dev. Camb. Engl.* **148**, dev193839 (2021).

40. Frountzas, M., Schizas, D., Kapelouzou, A. & Liakakos, T. The Truth Behind Esophagus: The Stem Cells' Significance. in *Digestive System Diseases: Stem Cell Mechanisms and Therapies* (eds. Gazouli, M. & Theodoropoulos, G. E.) 21–48 (Springer International Publishing, 2019). doi:10.1007/978-3-030-11965-2_3.

41. Kasagi, Y. *et al.* The Esophageal Organoid System Reveals Functional Interplay Between Notch and Cytokines in Reactive Epithelial Changes. *Cell. Mol. Gastroenterol. Hepatol.* **5**, 333–352 (2018).

42. Kijima, T. *et al.* Three-Dimensional Organoids Reveal Therapy Resistance of Esophageal and Oropharyngeal Squamous Cell Carcinoma Cells. *Cell. Mol. Gastroenterol. Hepatol.* **7**, 73–91 (2019).

43. Sachdeva, U. M. *et al.* Understanding the cellular origin and progression of esophageal cancer using esophageal organoids. *Cancer Lett.* **509**, 39–52 (2021).

44. Zheng, B. *et al.* A new murine esophageal organoid culture method and organoid-based model of esophageal squamous cell neoplasia. *iScience* **24**, 103440 (2021).

45. Zhang, Q. *et al.* A human Barrett's esophagus organoid system reveals epithelial-mesenchymal plasticity induced by acid and bile salts. *Am. J. Physiol.-Gastrointest. Liver Physiol.* **322**, G598–G614 (2022).

46. Imai, T. *et al.* KIF11 Is Required for Spheroid Formation by Oesophageal and Colorectal Cancer Cells. *Anticancer Res.* **37**, 47–55 (2017).

47. Zhao, H. *et al.* Generation and multiomic profiling of a TP53/CDKN2A double-knockout gastroesophageal junction organoid model. *Sci. Transl. Med.* **14**, eabq6146 (2022).

48. Flashner, S., Yan, K. S. & Nakagawa, H. 3D Organoids: An Untapped Platform for Studying Host–Microbiome Interactions in Esophageal Cancers. *Microorganisms* **9**, 2182 (2021).

49. Guha, M. *et al.* Esophageal 3D organoids of MPV17-/- mouse model of mitochondrial DNA depletion show epithelial cell plasticity and telomere attrition. *Oncotarget* **10**, 6245–6259 (2019).

50. Wu, Z. *et al.* Reprogramming of the esophageal squamous carcinoma epigenome by SOX2 promotes ADAR1 dependence. *Nat. Genet.* **53**, 881–894 (2021).

51. Münch, N. S. *et al.* High-fat Diet Accelerates Carcinogenesis in a Mouse Model of Barrett's Esophagus via IL8 and Alterations to the Gut Microbiome. *Gastroenterology* **157**, 492-506.e2 (2019).

52. Rao, M. C. Physiology of Electrolyte Transport in the Gut: Implications for Disease. in *Comprehensive Physiology* 947–1023 (John Wiley & Sons, Ltd, 2019). doi:10.1002/cphy.c180011.

53. Molnár, R. *et al.* Mouse pancreatic ductal organoid culture as a relevant model to study exocrine pancreatic ion secretion. *Lab. Invest.* **100**, 84–97 (2020).

54. Breunig, M. *et al.* Modeling plasticity and dysplasia of pancreatic ductal organoids derived from human pluripotent stem cells. *Cell Stem Cell* **28**, 1105-1124.e19 (2021).

55. Zarei, K., Thornell, I. M. & Stoltz, D. A. Anion Transport Across Human Gallbladder Organoids and Monolayers. *Front. Physiol.* **13**, 882525 (2022).

56. Xia, S. *et al.* High-Throughput Functional Analysis of CFTR and Other Apically Localized Proteins in iPSC-Derived Human Intestinal Organoids. *Cells* **10**, 3419 (2021).

57. Salari, A., Zhou, K., Nikolovska, K., Seidler, U. & Amiri, M. Human Colonoid–Myofibroblast Coculture for Study of Apical Na+/H+ Exchangers of the Lower Cryptal Neck Region. *Int. J. Mol. Sci.* **24**, 4266 (2023).

58. Hegyi, P., Rakonczay, Z. J., Gray, M. A. & Argent, B. E. Measurement of Intracellular pH in Pancreatic Duct Cells: A New Method for Calibrating the Fluorescence Data. *Pancreas* **28**, 427–434 (2004).

59. Thomas, J. A., Buchsbaum, R. N., Zimniak, A. & Racker, E. Intracellular pH measurements in Ehrlich ascites tumor cells utilizing spectroscopic probes generated in situ. *Biochemistry* **18**, 2210–2218 (1979).

60. Hegyi, P., Gray, M. A. & Argent, B. E. Substance P inhibits bicarbonate secretion from guinea pig pancreatic ducts by modulating an anion exchanger. *Am. J. Physiol.-Cell Physiol.* **285**, C268–C276 (2003).

61. Weintraub, W. H. & Machen, T. E. pH regulation in hepatoma cells: roles for Na-H exchange, Cl-HCO3 exchange, and Na-HCO3 cotransport. *Am. J. Physiol.-Gastrointest. Liver Physiol.* (1989) doi:10.1152/ajpgi.1989.257.3.G317.

62. Pallagi-Kunstár, É. *et al.* Bile acids inhibit Na+/H+ exchanger and Cl−/HCO3− exchanger activities via cellular energy breakdown and Ca2+ overload in human colonic crypts. *Pflüg. Arch. - Eur. J. Physiol.* **467**, 1277–1290 (2015).

63. Venglovecz, V. *et al.* Effects of bile acids on pancreatic ductal bicarbonate secretion in guinea pig. *Gut* **57**, 1102–1112 (2008).

64. Hu, L., Zhang, C., Yang, K., Li, M. & Shaker, A. Human esophageal myofibroblasts increase squamous epithelial thickness via paracrine mechanisms in an in vitro model of gastroesophageal reflux disease. *PLOS ONE* **15**, e0238852 (2020).

65. Fong, P. CFTR–SLC26 transporter interactions in epithelia. *Biophys. Rev.* **4**, 107–116 (2012).

66. Michl, J., Park, K. C. & Swietach, P. Evidence-based guidelines for controlling pH in mammalian live-cell culture systems. *Commun. Biol.* **2**, 1–12 (2019).

67. Fuster, D. G. & Alexander, R. T. Traditional and emerging roles for the SLC9 Na+/H+ exchangers. *Pflüg. Arch. - Eur. J. Physiol.* **466**, 61–76 (2014).

68. Donowitz, M., Tse, C. M. & Fuster, D. SLC9/NHE gene family, a plasma membrane and organellar family of Na+/H+ exchangers. *Mol. Aspects Med.* **34**, 236–251 (2013).

69. Bonar, P. T. & Casey, J. R. Plasma membrane Cl$^-$/HCO$_3$$^-$ exchangers: structure, mechanism and physiology. *Channels Austin Tex* **2**, 337–345 (2008).

70. Venglovecz, V. *et al.* Pathophysiological relevance of apical large-conductance Ca2+-activated potassium channels in pancreatic duct epithelial cells. *Gut* **60**, 361–369 (2011).

71. Orlando, R. C. The Integrity of the Esophageal Mucosa. Balance Between Offensive and Defensive Mechanisms. *Best Pract. Res. Clin. Gastroenterol.* **24**, 873–882 (2010).

72. Barker, N. *et al.* Identification of stem cells in small intestine and colon by marker gene Lgr5. *Nature* **449**, 1003–1007 (2007).

73. Singh, A. *et al.* Cytokeratin immunoexpression in esophageal squamous cell carcinoma of high-risk population in Northeast India. *Appl. Immunohistochem. Mol. Morphol. AIMM Off. Publ. Soc. Appl. Immunohistochem.* **17**, 419–424 (2009).

74. Tobey, N. A., Reddy, S. P., Keku, T. O., Cragoe, E. J. & Orlando, R. C. Studies of pHi in rabbit esophageal basal and squamous epithelial cells in culture. *Gastroenterology* **103**, 830–839 (1992).

75. Ariyoshi, Y. *et al.* Na+/H+ exchanger 1 has tumor suppressive activity and prognostic value in esophageal squamous cell carcinoma. *Oncotarget* **8**, 2209–2223 (2016).

76. Guan, B., Hoque, A. & Xu, X. Amiloride and guggulsterone suppression of esophageal cancer cell growth in vitro and in nude mouse xenografts. *Front. Biol.* **9**, 75–81 (2014).

77. Bernardo, A. A., Bernardo, C. M., Espiritu, D. J. & Arruda, J. A. L. The Sodium Bicarbonate Cotransporter: Structure, Function, and Regulation. *Semin. Nephrol.* **26**, 352–360 (2006).

78. Li, Y., Zhou, X. & Sun, S. X. Hydrogen, Bicarbonate, and Their Associated Exchangers in Cell Volume Regulation. *Front. Cell Dev. Biol.* **9**, (2021).

79. Wang, J., Wang, W., Wang, H. & Tuo, B. Physiological and Pathological Functions of SLC26A6. *Front. Med.* **7**, (2021).

80. Matsumoto, Y. *et al.* Expression and Role of CFTR in Human Esophageal Squamous Cell Carcinoma. *Ann. Surg. Oncol.* **28**, 6424–6436 (2021).

81. Li, W. *et al.* CFTR inhibits the invasion and growth of esophageal cancer cells by inhibiting the expression of NF-κB. *Cell Biol. Int.* **42**, 1680–1687 (2018).

82. Ao, M. *et al.* Lubiprostone activates Cl- secretion via cAMP signaling and increases membrane CFTR in the human colon carcinoma cell line, T84. *Dig. Dis. Sci.* **56**, 339–351 (2011).

83. Norimatsu, Y., Moran, A. R. & MacDonald, K. D. Lubiprostone activates CFTR, but not ClC-2, via the prostaglandin receptor (EP(4)). *Biochem. Biophys. Res. Commun.* **426**, 374–379 (2012).

84. Krüger, L., Pridgen, T. A., Taylor, E. R., Garman, K. S. & Blikslager, A. T. Lubiprostone protects esophageal mucosa from acid injury in porcine esophagus. *Am. J. Physiol. Gastrointest. Liver Physiol.* **318**, G613–G623 (2020).

85. Stewart, A. K. *et al.* Functional coupling of apical Cl−/HCO3− exchange with CFTR in stimulated HCO3− secretion by guinea pig interlobular pancreatic duct. *Am. J. Physiol. - Gastrointest. Liver Physiol.* **296**, G1307–G1317 (2009).

86. Wang, Y. *et al.* Slc26a6 regulates CFTR activity in vivo to determine pancreatic duct HCO3− secretion: relevance to cystic fibrosis. *EMBO J.* **25**, 5049–5057 (2006).

87. Saint-Criq, V. & Gray, M. A. Role of CFTR in epithelial physiology. *Cell. Mol. Life Sci. CMLS* **74**, 93–115 (2017).

88. Vanoni, S. *et al.* Identification of anoctamin 1 (ANO1) as a key driver of esophageal epithelial proliferation in eosinophilic esophagitis. *J. Allergy Clin. Immunol.* **145**, 239-254.e2 (2020).

ANNEX

PUBLICATION No.1.

AMERICAN JOURNAL OF PHYSIOLOGY

CELL PHYSIOLOGY®

RESEARCH ARTICLE

Making Cell Culture More Physiological

Mouse organoid culture is a suitable model to study esophageal ion transport mechanisms

Marietta Margaréta Korsós,[1] Tamás Bellák,[2,3] Eszter Becskeházi,[1] Eleonóra Gál,[1] Zoltán Veréb,[4] Péter Hegyi,[5,6,7] and 🟢 Viktória Venglovecz[1]

[1]*Department of Pharmacology and Pharmacotherapy, University of Szeged, Szeged, Hungary;* [2]*Department of Anatomy, Histology and Embryology, University of Szeged, Szeged, Hungary;* [3]*BioTalentum Ltd., Gödöllő, Hungary;* [4]*Regenerative Medicine and Cellular Pharmacology Research Laboratory, Department of Dermatology and Allergology, University of Szeged, Szeged, Hungary;* [5]*First Department of Medicine, University of Szeged, Szeged, Hungary;* [6]*Szentágothai Research Centre, Institute for Translational Medicine, Medical School, University of Pécs, Pécs, Hungary; and* [7]*Division of Gastroenterology, First Department of Medicine, Medical School, University of Pécs, Pécs, Hungary*

Abstract

Altered esophageal ion transport mechanisms play a key role in inflammatory and cancerous diseases of the esophagus, but epithelial ion processes have been less studied in the esophagus because of the lack of a suitable experimental model. In this study, we generated three-dimensional (3D) esophageal organoids (EOs) from two different mouse strains and characterized the ion transport processes of the EOs. EOs form a cell-filled structure with a diameter of 250–300 μm and were generated from epithelial stem cells as shown by FACS analysis. Using conventional PCR and immunostaining, the presence of Slc26a6 Cl^-/HCO_3^- anion exchanger (AE), Na^+/H^+ exchanger (NHE), Na^+/HCO_3^- cotransporter (NBC), cystic fibrosis transmembrane conductance regulator (CFTR), and anoctamin 1 Cl^- channels was detected in EOs. Microfluorimetric techniques revealed high NHE, AE, and NBC activities, whereas that of CFTR was relatively low. In addition, inhibition of CFTR led to functional interactions between the major acid-base transporters and CFTR. We conclude that EOs provide a relevant and suitable model system for studying the ion transport mechanisms of esophageal epithelial cells, and they can be also used as preclinical tools to assess the effectiveness of novel therapeutic compounds in esophageal diseases associated with altered ion transport processes.

CFTR; esophagus; ion transport

INTRODUCTION

Research in recent years has increasingly highlighted the importance of ion transport processes in inflammatory and cancerous diseases of the esophagus, as indicated by numerous clinical studies (1, 2). These studies revealed altered expression of individual acid-base transporters in Barrett's esophagus, squamous cell carcinoma, and adenocarcinoma. Conversely, the activity of these ion transporters has been less studied mainly because of the lack of a suitable experimental model. Currently, a number of esophageal cell lines ranging from normal cells to esophageal adenocarcinoma are available. Although cell lines are easy to maintain, they have also limitations. Some cell lines are genetically modified to preserve their proliferation or derived from preexisting cancerous tissue, making them unsuitable for studying physiological processes. In addition, because of their genetic instability, cells can spontaneously differentiate into other cell types. The Ussing

chamber is an old but commonly used apparatus for studying esophageal permeability, and it is also suitable for investigating transepithelial ion transport processes. However, application of this technique is often limited by the condition, permeability, and short life span of the tissue, as well as reproducibility.

Organoids are three-dimensional cell culture systems derived from progenitor or stem cells that provide a near physiological in vitro model for studying epithelial function. The discovery of organoids has greatly contributed to improved understanding of the ion transport processes of individual organs such as the pancreas, colon, and airways (3–5). Esophageal organoids (EOs) were first derived from mouse esophageal tissue by DeWard et al (6). The basal layer of the esophageal mucosa consists of a subpopulation of undifferentiated stem cells with self-renewal ability and high proliferative capacity. After proliferation, cells migrate toward the lumen while undergoing differentiation and replace the suprabasal cells (7). Under appropriate culture

http://www.ajpcell.org

Table 1. *Compositions of the solutions*

	Standard HEPES	Standard HCO_3^-	NH_4Cl HEPES	High-K^+ HEPES	NH_4Cl HCO_3^-	Na^+-Free HEPES	Na^+-Free HCO_3^-	Cl^--Free HEPES	Cl^--Free HCO_3^-
NaCl	140	115	110	5	95				
KCl	5	5	5	130	5	5	5		
$MgCl_2$	1	1	1	1	1	1	1		
$CaCl_2$	1	1	1	1	1	1	1		
HEPES acid	10		10			10		10	
Glucose	10	10	10	10	10	10	10	10	10
$NaHCO_3$		25			25				25
NH_4Cl			20		20				
Na-HEPES				10					
NMDG-Cl						140	115		
Na-gluconate								140	115
Mg-gluconate								1	1
Ca-gluconate								6	6
K_2-sulfate								2.5	2.5
Choline HCO_3^-							25		
Atropine							0.01		

Values are presented in mM.

conditions, organoids grown from stem cells develop a similar structure as the organ of origin including the presence of several cell layers, but the difference is that the outermost layer is composed of basal undifferentiated cells and the internal cell mass is formed by differentiated keratinocytes (6).

Although EOs provide a suitable model for performing functional assays, the presence and activity of ion transporters have not been investigated using EOs. In this study, we characterized the activity and presence of ion transporters in mouse EOs for the first time. We illustrated that mouse EOs express functionally active Na^+/H^+ exchanger (NHE), Na^+/HCO_3^- cotransporter (NBC), Cl^-/HCO_3^- anion exchanger (AE), and cystic fibrosis transmembrane conductance regulator (CFTR) Cl^- channels. Our results provide insights into the ion transport defects related to certain esophageal diseases and highlight a relevant experimental model system for assessing the effects of drug molecules on esophageal ion transporters.

MATERIALS AND METHODS

Mice

Mice (8 to 16 wk old of both sexes) on the C57BL/6 and CD-1 backgrounds were bred and housed in standard plastic cages under a 12-h:12-h light-dark cycle at room temperature ($23 \pm 1°C$), and they were given free access to standard laboratory chow and drinking solutions. Animal experiments were conducted in accordance with the Guide for the Care and Use of Laboratory Animals (US Department of Health and Human Services) and approved by the local Ethical Board of the University of Szeged.

Solutions and Chemicals

General laboratory chemicals were obtained from Sigma-Aldrich (Budapest, Hungary). 2,7-Bis-(2-carboxyethyl)-5(6)-carboxyfluorescein acetoxymethyl ester (BCECF-AM) and N-(ethoxycarbonylmethyl)-6-methoxyquinolinium bromide (MQAE) were purchased from Molecular Probes Inc. (Eugene, OR). BCECF-AM (2 μmol/L) and MQAE (5 μM) were prepared in dimethyl sulfoxide (DMSO) and stored at $-20°C$. 4-Isopropyl-3-methylsulfonylbenzoyl-guanidin methanesulfonate (HOE-642) was provided by Sanofi Aventis (Frankfurt, Germany) and dissolved in DMSO. Nigericin (10 mM) was prepared in ethanol and stored at $-20°C$. Forskolin was obtained from Tocris (Bristol, UK) and stored as a 250 mM stock solution in DMSO. The compositions of the solutions are presented in Table 1. Standard HEPES-buffered solutions were gassed with 100% O_2, and their pH was adjusted to 7.4 with NaOH. Standard HCO_3^-/CO_2-buffered solutions were gassed with 95% O_2-5% CO_2 to adjust their pH to 7.4. All experiments were performed at $37°C$.

Isolation of Esophageal Epithelial Cells

After removal and longitudinal opening of the esophagus, the tissue was placed into PluriSTEM dispase II solution (2 U/mL) and incubated at $37°C$ for 40 min. Then, the mucosa was peeled from the submucosa using forceps, and the mucosa was incubated at $37°C$ in 1× trypsin-EDTA solution for 15 min, during which time the tissue was vortexed in every 2 min. To inactivate trypsin, the trypsin-EDTA solution (with floating cells) was pipetted into soybean trypsin inhibitor (STI) solution. The STI solution with the undigested tissue pieces was filtered through a 40-μm cell strainer. Cells were then centrifuged for 10 min at 2,000 rpm, and the cell pellet was resuspended in 300 μL of complete organoid culture medium.

Generation of EOs

The required volume of the cell suspension (7,500 cells/well on a 24-well tissue culture plate) was mixed with

Table 2. *List of primary and secondary antibodies used in the study*

Primary Antibodies	Company	Cat. No.	Dilution
Slc9a1	Alomone	ANX-010	1:100
Slc9a2	Alomone	ANX-002	1:100
Slc26a3	Invitrogen	PA5-68530	1:600
Slc26a6	Santa Cruz Biotechnology	sc-515230	1:200
Slc4a4	Abcam	ab187511	1:100
CFTR	Alomone	ACL-006	1:200
ANO1	Alomone	ACL-011	1:200

CFTR, cystic fibrosis transmembrane conductance regulator.

Table 3. *Primer sequences used in the study*

Gene	Reverse Primer	Forward Primer	Product Size, bp
Slc9a1	TGGCTCTACTGTCCTTTGGG	GAGGAGGAAGATGAGGACGG	194
Slc9a2	GAAATCAGGCTGCCGAAGAG	CTACTTCATGCCAACTCGCC	183
Slc26a3	ACCCTTTGAGATGGTCCAGG	TTCCTTCCCACTAGCCACTG	161
Slc26a6	AGCTCCTGGTTACTGTCCAC	TCATTGGGGCCACTGGTATT	235
Slc4a4	CAGCCACATACCAGGGAAGA	CGGCTTTGCTAGTCACCATC	171
CFTR	TCTGCATGGGTTCTGGGAAT	GAGCAATGTCTGGCAGTACG	249
ANO1	GGGGCTGTGGTTGTTACAAG	ATCCCCAAAGACATCAGCCA	150

CFTR, cystic fibrosis transmembrane conductance regulator.

Matrigel extracellular matrix at a 40:60 ratio and portioned in the wells, followed by incubation at 37°C for 15 min to allow solidification of the gel. Complete organoid culture medium was added to cover the Matrigel and incubated at 37°C. After 3–4 days, organoid formation was visible. They reach their maximum size on *days 8–12*. The growth medium consisted of Advanced Dulbecco's modified Eagle's medium/F12, 1× N2 and 1× B27 Supplements, 1× Glutamax (Gibco), 10 mM HEPES (Biosera), 2% penicillin/streptomycin (Gibco), 1 mM N-acetyl-L-cysteine (Sigma), 100 ng/mL R-spondin 1, 100 ng/mL Noggin (both from Peprotech), 50 ng/mL mouse epidermal growth factor (R&D), 10 μM Y27632 ROCK-kinase inhibitor (ChemCruz), and 5% WNT3A-conditioned medium. Wnt3A-conditioned medium was prepared by collecting the supernatant from L-Wnt3A cells (ATCC, Cat. No. CRL-2647) according to the manufacturer's protocol.

Flow Cytometry

The expression of leucine-rich repeat-containing G-protein-coupled receptor 5 (LGR5) and cytokeratin 14 (CK14) was measured by flow cytometry on a FACSCalibur flow cytometer (BD Biosciences Immunocytometry Systems, Franklin Lakes, NJ) after staining the cells on ice for 30 min with LGR5-PE (Origene, Cat. No. TA400001) and CK14-FITC (Novusbio, Cat. No. NBP2-47720F) fluorochrome-conjugated antibodies and their matching isotype controls (PE Mouse IgG1, κ Isotype Ctrl Antibody, Cat. No. 400111 and FITC Mouse IgG3, κ Isotype Ctrl Antibody, Cat. No. 401317, both from Biolegend). The data were analyzed using Flowing Software (Cell Imaging Core,
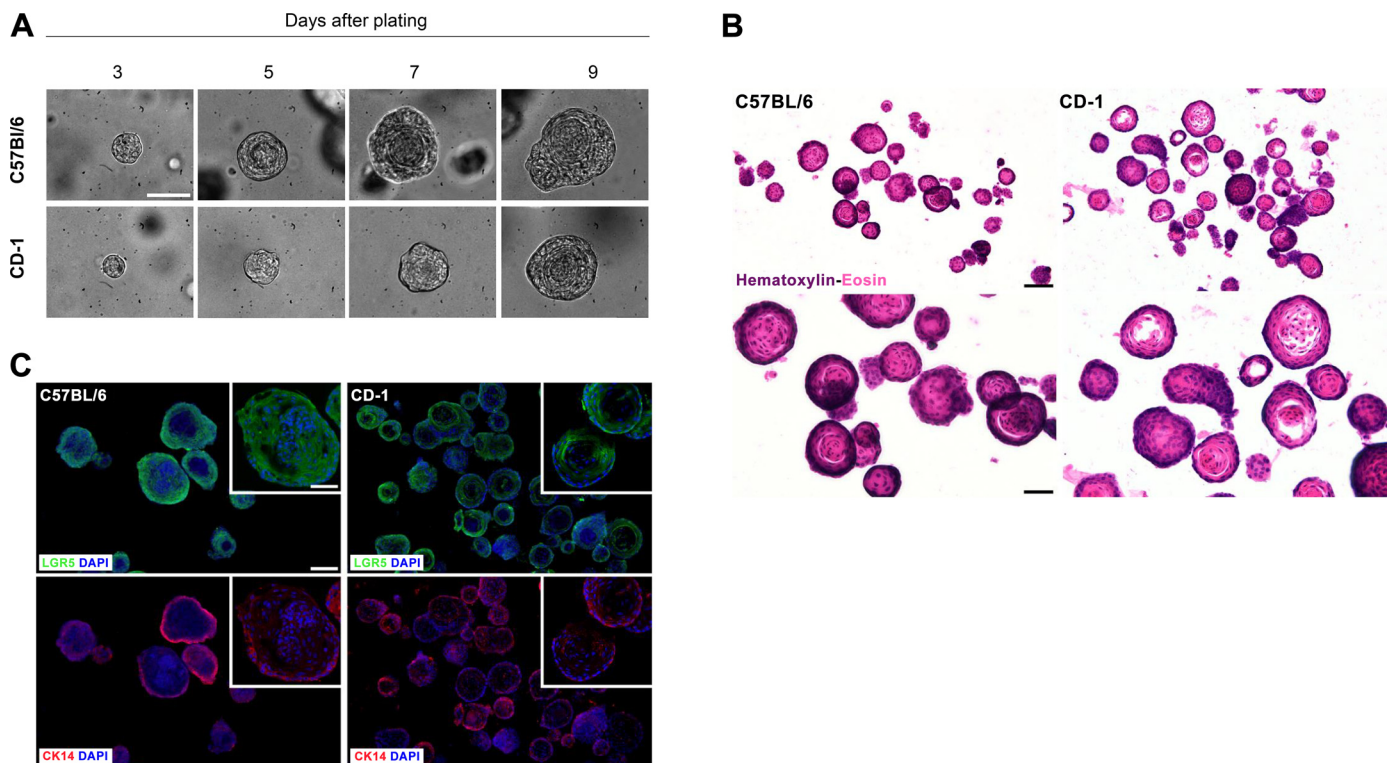

Figure 1. Characterization of esophageal organoids (EOs). *A*: representative bright field images of EOs grown for 9 days from freshly isolated esophageal mucosa. Images were taken using an Olympus IX71 inverted microscope. The scale bar represents 100 μm. *B*: hematoxylin and eosin staining of EOs developed from C57BL/6 and CD-1 mouse esophageal tissue. The scale bar represents 100 μm (upper line) and 50 μm (bottom line), respectively. *C*: confocal images of EOs stained for leucine-rich repeat-containing G-protein-coupled receptor 5 (LGR5, green), cytokeratin 14 (CK14, red), and DAPI (blue). The scale bar represents 100 μm (main photo) and 50 μm (*inset* photo), respectively.

Turku Center for Biotechnology, Finland), and the percentage of positive cells was expressed as the means ± SD.

Immunofluorescence Staining and Histology

Organoid cultures were fixed with 4% PFA in 0.1 mol/L phosphate buffer for 1 h at room temperature and washed three times with PBS. The fixed samples were cryoprotected in 30% sucrose solution (in PBS) containing 0.01% sodium azide at 4°C until embedding in Tissue-Tek O.C.T. compound (Sakura). The 16-μm parallel sections were sectioned using a cryostat (Leica CM 1850, Leica), mounted to gelatin-coated slides, and stored at −20°C until use. After air-drying for 10 min, the sections were permeabilized with 0.1% Triton X-100 in PBS and blocked for 1 h at 24°C with 3% BSA in PBS. The sections were then incubated with primary antibodies (overnight, 4°C). On the next day, sections were washed in PBS three times, and isotype-specific secondary antibodies were diluted in blocking buffer and applied for 1 h at room temperature. The sections were washed three times with PBS and covered using Vectashield mounting medium containing DAPI (1.5 μg/mL, Vector Laboratories), which labeled the nuclei of the cells. Immunoreactive sections were analyzed using a BX-41 epifluorescence microscope (Olympus) equipped with a DP-74 digital camera and CellSens software (V1.18, Olympus) or using an Olympus Fv-10i-W compact confocal microscope system (Olympus) with Fluoview Fv10i
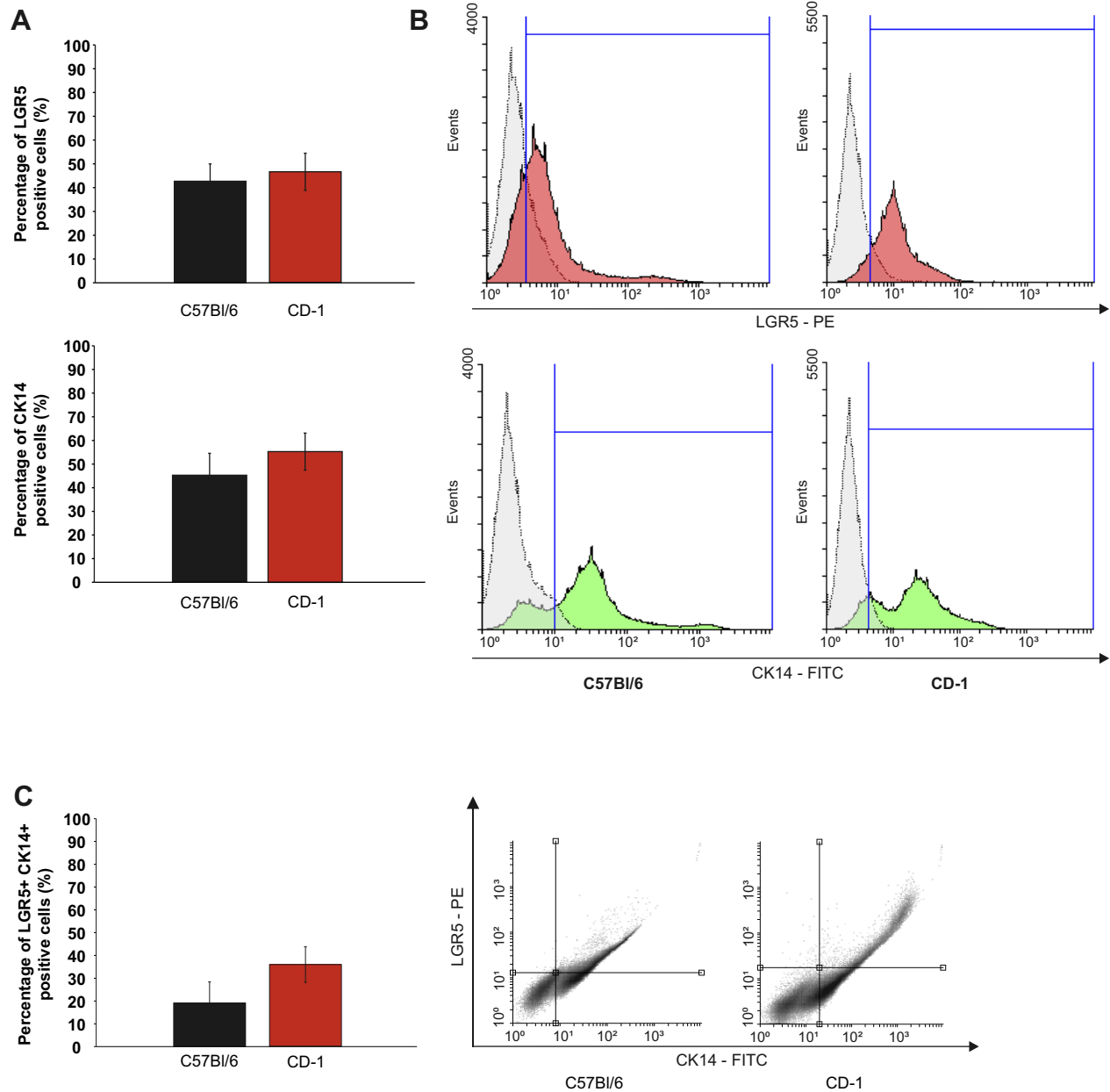
Figure 2. Flow cytometry analysis of leucine-rich repeat-containing G-protein-coupled receptor 5 (LGR5) and cytokeratin 14 (CK14) expression. *A*: percentage of LGR5- and CK14-positive cells in the cell suspension of esophageal mucosa obtained from CD-1 and C57BL/6 mice. *B*: representative histograms of the FACS analysis with the respective isotype controls (gray). *C*: representative dot plots present CK14 and LGR5 double-positive cells. $n = 3$ mice, unpaired Student's t test.

software (V2.1, Olympus). For hematoxylin and eosin (HE) staining, sections were incubated with Mayer's Hematoxylin solution (Sigma) for 5 min. Sections were washed with tap water and incubated into distilled water twice for 3 min each. Sections were then incubated in 1% eosin solution in distilled water (Sigma) for 2 min. Stained sections were dehydrating through 96% and 100% alcohol, cleared in xylene, and mounted in DPX (Sigma). Microphotographs were taken using a DP-74 digital camera using a light microscope (BX-41) and CellSens software (V1.18). All images were further processed using the GNU Image Manipulation Program (GIMP 2.10.0) and NIH ImageJ analysis software (imagej.nih.gov/ij). Details of the primary and secondary antibodies are presented in Table 2.

Gene Expression Analysis Using RT-PCR

Total RNA was isolated from the organoids using a NucleoSpin RNA Kit (Macherey–Nagel, Düren, Germany). Two micrograms of RNA were reverse-transcribed using a High-Capacity cDNA Reverse Transcription Kit (Applied Biosystems, Foster City, CA). PCR was performed using DreamTaq DNA polymerase in a final volume of 20 μL. All reactions were performed under the following conditions: 94°C for 5 min; 30 cycles of 94°C for 30 s, 60°C for 30 s, and 72°C for 1 min; and final elongation at 72°C for 10 min. The PCR products (18 μL) were separated by electrophoresis on a 2% agarose gel and visualized using an AlphaImager EC Gel Documentation System. As a positive control, kidney cDNA was used in the case of Slc9a1, Slc9a2, Slc26a6, Slc4a4, and CFTR, and pancreas cDNA was used in the case of Slc26a3

and anoctamine-1 (ANO-1). Primer sequences are presented in Table 3.

Measurement of the Intracellular Cl⁻ Concentration ([Cl⁻]ᵢ) and pH Microfluorimetry

EOs were attached to a poly-L-lysine-coated coverslip (24 mm) forming the base of a perfusion chamber and mounted on the stage of an inverted fluorescence microscope linked to the Xcellence imaging system (Olympus). Organoids were then bathed with different solutions at 37°C at a perfusion rate of 5–6 mL/min. Then, 6–12 regions of interests (ROIs) were examined in each experiments, and one measurement was obtained per second. $[Cl^-]_i$ was estimated using the fluorescent dye MQAE. Specifically, organoids were incubated with MQAE (5 μM) for 2–3 h at 37°C, and changes in $[Cl^-]_i$ were determined by exciting the cells at 340 nm with emitted light monitored at 380 nm. Fluorescence signals were normalized to the initial fluorescence intensity (F/F0) and expressed as relative fluorescence. To determine intracellular pH (pH_i), cells were loaded with the pH-sensitive fluorescent dye BCECF-AM (2 μM, 1 h, 37°C) and excited at 490 and 440 nm. The 490/440 fluorescence emission ratio was measured at 535 nm. The calibration of the fluorescence emission ratio to pH_i was performed using the high-K^+/nigericin technique, as previously described (8, 9).

Measurement of the Activity of the Acid-Base Transporters

To estimate the activity of NHE and NBC, the NH₄Cl prepulse technique was used. Briefly, exposure of EOs to 20 mM
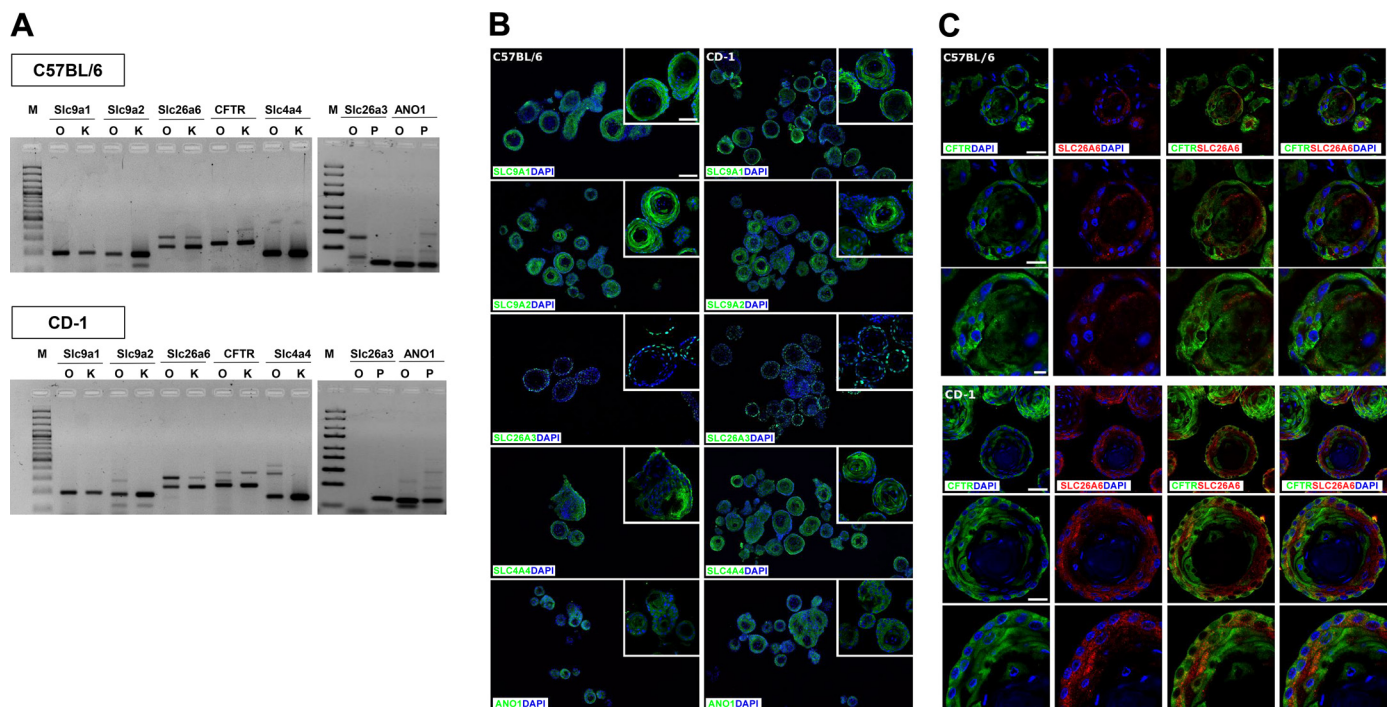

Figure 3. Expression of ion transporters in esophageal organoids (EOs). *A*: mature EOs were collected 9 days after plating, and RNA was prepared from the organoids. Gene expression of ion transporters was investigated with traditional RT-PCR analysis. *B*: immunostaining of EOs for Slc9a1 (first line), Slc9a2 (second line), Slc26a3 (third line), Slc4a4 (fourth line), and ANO1 (fifth line). The scale bar represents 100 μm (main photo) and 50 μm (*inset* photo), respectively. *C*: costaining of Slc26a6 (red) and cftr (green). The scale bar represents 50 μm (upper line), 25 μm (middle line), and 10 μm (bottom line), for both mice strains. CFTR, cystic fibrosis transmembrane conductance regulator.

NH_4Cl for 3 min induced an immediate rise in pH_i because of the rapid entry of lipophilic basic NH_3 into the cells. After the removal of NH_4Cl, pH_i rapidly decreased. This acidification is caused by the dissociation of intracellular NH_4^+ to H^+ and NH_3, followed by the diffusion of NH_3 from the cells. In standard HEPES-buffered solution, the initial rate of pH_i ($\Delta pH/\Delta t$) recovery from the acid load (over the first 60 s) reflects the activities of NHEs, whereas in HCO_3^-/CO_2-buffered solutions, the rate represents the activities of both NHE and NBC (10).

Two independent methods were used to estimate AE activity. Using the NH_4Cl prepulse technique, the initial rate of pH_i recovery from alkalosis in HCO_3^-/CO_2-buffered solutions was analyzed (10). Previous data indicated that under these conditions, the recovery over the first 30 s reflects the activity of AE (10). The Cl^- withdrawal technique was also applied, in which removal of Cl^- from the external solution causes immediate and reversible alkalization of the pH_i because of the reverse operation of AE under these conditions. Previous data illustrated that the initial rate of alkalization over the first 60 s reflects the activity of AE (11).

Statistical Analysis

Results are expressed as the means ± SD. Statistical analyses were performed using analysis of variance followed by Bonferroni multiple comparison post hoc test. $P \leq 0.05$ was accepted as significant.

RESULTS

Characterization of EO Cultures

Isolated esophageal epithelial cells (EECs) were plated in Matrigel supplemented with organoid culture medium at a final concentration of 40%. On the 3rd day after plating, organoid formation was observed, and therefore, we assessed organoid growth starting from *day 3* (Fig. 1A). The size of the organoids increased steadily in the following days, peaking between *days 7* and *9*. Organoids between 50 and 150 μm in size were used for our experiments. HE staining of the organoids illustrated that cells are located in several layers inside the organoids, matching the structure of normal esophageal tissue (Fig. 1B). The inner cell mass consisted of differentiated cells that move from the periphery to the inside of the organoids during their maturation. In addition, the centers of some organoids were empty, or they contained keratinized materials produced by the cells. To verify that organoids are generated from stem cells, we used the stem cell marker LGR5. Immunofluorescence staining revealed strong LGR5 expression in both C57BL/6 and CD-1 organoids (Fig. 1C), and FACS analysis demonstrated that 42.70 ± 7.27% of the isolated C57BL/6 EECs and 46.46 ± 7.81% of the isolated CD-1 EECs were LGR5-positive (Fig. 2, A and B). In the next step, we verified that the organoids were derived from single EECs. CK14 is a cytoplasmic keratin expressed in the basal SECs (12, 13).
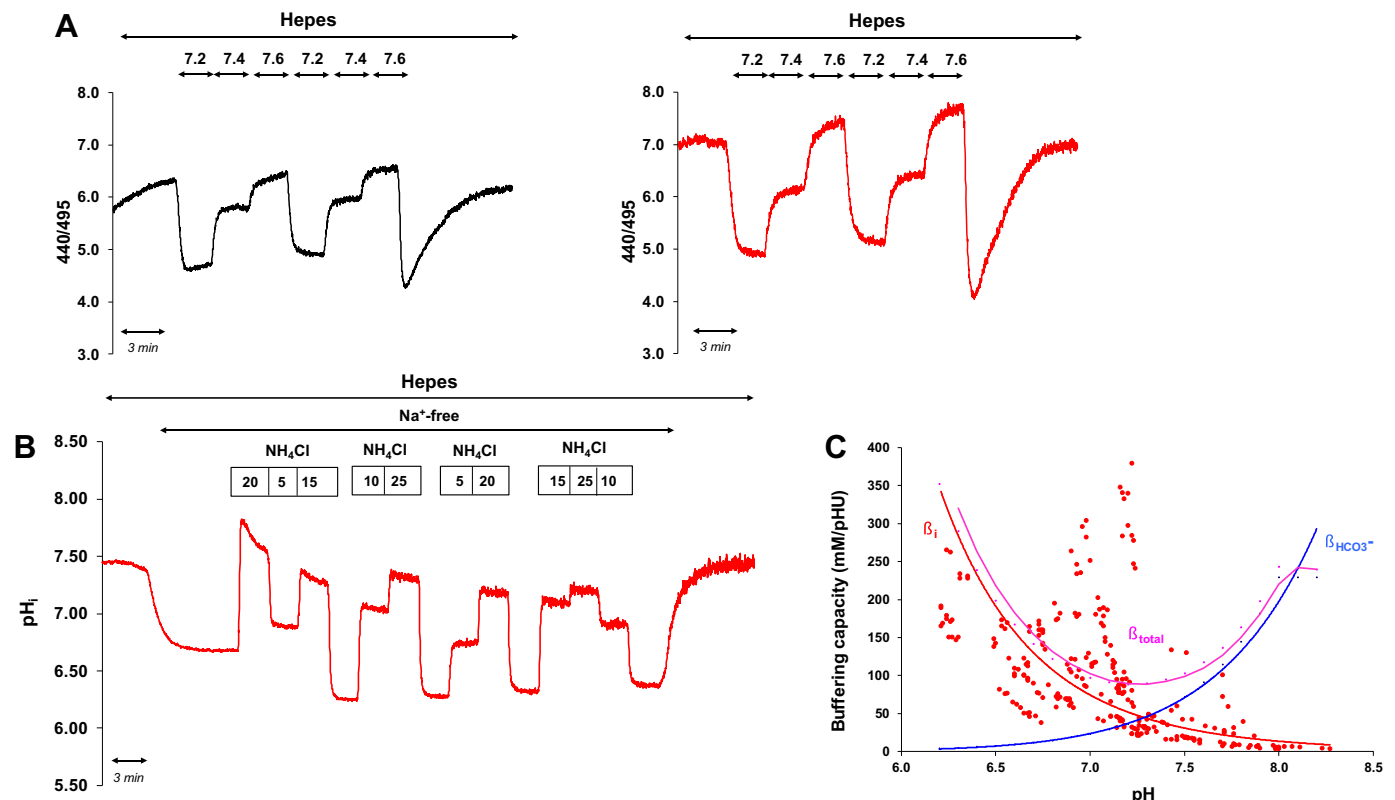

Figure 4. Initial pH and buffering capacity of esophageal organoids. A: organoids were exposed to nigericin/high-K^+–HEPES solution at pH 7.2, 7.4, and 7.6. The resting intracellular pH (pH_i) was calculated from this three-point calibration using the classic linear model. B: organoids were exposed to various concentrations of NH_4Cl in nominally Na^+- and HCO_3^--free solutions, and the total buffering capacity (β_{total}; C) of the cells was calculated using the following equation: $\beta_{total} = \beta_i + \beta_{HCO3-} = \beta_i + 2.3 \times [HCO_3^-]_i$, where β_i refers to the ability of intrinsic cellular components to buffer changes of pH_i and β_{HCO3}^- is the buffering capacity of the HCO_3^-/CO_2 system. The black line shows the organoid response isolated from C57BL/6 mice, whereas the red line shows the organoid response isolated from CD-1 mice. $n = 6$–7 organoids/17–19 ROIs.

As presented on Fig. 1C, the outer cell layer of the organoids was CK14-positive, indicating that the organoids originate from the mucosa and display a morphologically similar structure as normal esophageal tissue. FACS analysis indicated that $45.29 \pm 9.25\%$ of the isolated C57BL/6 EECs and $55.32 \pm 7.80\%$ of the isolated CD-1 EECs were CK14-positive (Fig. 2, A and B). Interestingly, there was a slight difference in the double-positive (LGR5 and CK14) fraction. The proportion of double-positive cells was higher in CD-1 mouse organoids ($35.37 \pm 1.24\%$) than in C57BL/6 mouse organoids ($19.34 \pm 2.03\%$, Fig. 2C).

mRNA and Protein Expression of Ion Transporters in EOs

The mRNA expression of ion transporters was investigated using conventional RT-PCR. We revealed the presence of *Slc9A1* (NHE-1), *Slc9A2* (NHE-2), *Slc26a6* (PAT1), *CFTR*, *Scl4a4* (NBCe1B), and *ANO1* in both the C57BL/6 and CD-1 organoids (Fig. 3A). The presence of these transporters was also confirmed at the protein level using immunohistochemistry (Fig. 3, B and C). By contrast, the *Slc26a3* (DRA) transporter could not be detected at either the mRNA or protein level. Because the CFTR Cl^- channel and Slc26a6 interact with each other in several secretory epithelia (14), we examined the colocalization of these two transporters on the organoids. CFTR and Slc26a6 exhibited diffuse staining throughout cells without special localization to the apical or basal membrane. Interestingly, Slc26a6 staining was more detectable in cells on the periphery, whereas in the case of CFTR, central cells also displayed positive staining.

Resting pH_i of EOs and Determination of Buffering Capacity

To investigate the pH regulatory mechanisms of EO cultures, we initially determined the resting pH_i of the cells. EOs were exposed to standard HEPES solution (pH 7.4), followed by a 5-min exposure to a high-K^+/nigericin-HEPES solution at pH 7.2, 7.4, and 7.6 (Fig. 4A). The resting pH_i of the organoids was determined using the classical linear model (8, 9). The resting pH_i of C57BL/6 organoids was 7.61 ± 0.03, whereas that of CD-1 organoids was 7.58 ± 0.03. The total buffering capacity (β_{total}) of EOs was estimated using the NH_4^+ prepulse technique, as previously described (Fig. 4B) (10, 15). Briefly, organoids were exposed to various concentrations of NH_4Cl in nominally Na^+- and HCO_3^--free solutions, and β_{total} of the cells was calculated using the following equation: $\beta_{total} = \beta_i + \beta_{HCO3}^- = \beta_i + 2.3 \times [HCO_3^-]_i$, where β_i describes the ability of intrinsic cellular components to respond to buffer changes of pH_i (calculated by the Henderson–Hasselbach equation) and β_{HCO3}^- is the buffering capacity of the HCO_3^-/CO_2 system. The measured rates of pH_i change ($\Delta pH/\Delta t$) were converted to transmembrane base flux $J(B^-)$ using the following equation: $J(B^-) = \Delta pH/\Delta t \times \beta_{total}$. β_{total} at the initial pH_i was used to calculate $J(B^-)$. We denoted base influx as $J(B)$ and base efflux (secretion) as $-J(B^-)$.
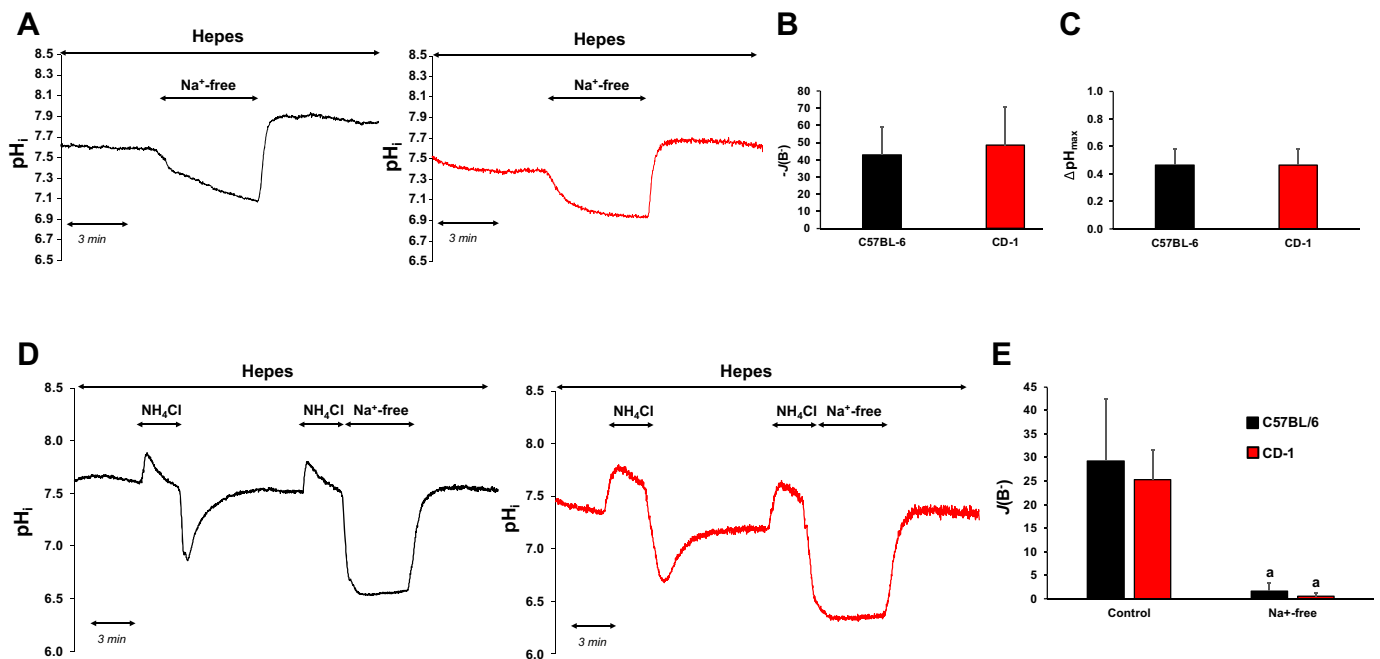

Figure 5. Investigation of Na^+/H^+ exchanger (NHE) activity in esophageal organoids (EOs). *A*: removal of Na^+ from standard HEPES solution caused rapid intracellular acidosis in organoids isolated from C57BL/6 (black line) and CD-1 (red line) mice confirmed the presence of a Na^+-dependent H^+ efflux mechanism. Summary data for the maximal intracellular pH (pH_i) change (ΔpH_{max}) (*B*) and the calculated base flux [$J(B^-)$] (*C*) induced by Na^+ removal. *D*: recovery from acid load reflects the activity of NHE in standard HEPES-buffered solution. After the second NH_4Cl pulse, Na^+ was removed from the external solution to investigate the activity of NHE. *E*: summary bar chart presents the initial rate of pH_i recovery ($J(B^-)$) from an acid load. $J(B^-)$ was calculated from the dpH/dt obtained by linear regression analysis of pH_i measurements made over the first 60 s after Na^+ removal (one pH_i measurement was made per second; ANOVA followed by Bonferroni multiple comparison post hoc test). The buffering capacity at the initial pH_i was used for the calculation of $J(B^-)$ (see METHODS). Data are presented as the mean $\pm$ SD. $^aP \leq 0.05$ vs. Control. $n = 4$–8 organoids/19–23 ROIs.

Activity of NHE

NHE is an integral plasma membrane protein that mediates the electroneutral exchange of extracellular Na^+ and intracellular H^+, thereby playing an important role in the alkalization of cells. NHE activity was investigated by removing extracellular Na^+ from the external solution. As presented in Fig. 5A, Na^+ removal induced a sharp decrease in pH_i, suggesting that EOs express functionally active NHE. There was no significant difference in the rate $[-J(B^-)]$, and extent (ΔpH_{max}) of the pH_i decreases between the two mouse strains (Fig. 5, B and C). The presence of NHE was also confirmed using the ammonium prepulse technique (Fig. 5D). Organoids were exposed to 20 mM NH_4Cl (3 min) in standard HEPES-buffered solution, which induced a high degree of intracellular alkalization because of the rapid influx of NH_3 into cells. After removing NH_4Cl from the bath, pH_i dramatically decreased and then returned to baseline. Under these conditions, recovery from acidosis reflects the activity of NHE. In the absence of Na^+, recovery from acidosis was negligible, indicating that in the absence of HCO_3^-, NHE is mainly responsible for the alkalization of cells (Fig. 5, D and E). The NHE gene family contains several isoforms (NHE-1–9) with different functions and expression patterns (16). To identify the most active isoform on organoids, the NHE isoform-specific inhibitor HOE-642 was used. This inhibitor blocks NHE-1 and NHE-2 isoforms in a concentration-dependent manner. At a concentration of 1 μM, only the NHE-1 isoform is inhibited, whereas 50 μM HOE-642 inhibits both isoforms (2, 17). We chose this inhibitor because our previous studies on human esophageal cell lines indicated that these two isoforms are responsible for the majority of NHE activity (2). Organoids were acid-loaded with 20 mM NH_4Cl followed by a 3-min incubation in Na^+-free HEPES solution. In the absence of Na^+, the NHE is blocked, and thus, pH_i is not regenerated. On the readministration of extracellular Na^+, NHE regained its function and its activity could be estimated from the initial rate of pH_i recovery over the first 60 s. As presented in Fig. 6A, 1 μM HOE-642 decreased pH_i recovery by $87.81 \pm 1.17\%$ in C57BL/6 organoids and $82.37 \pm 7.32\%$ in CD-1 organoids, whereas the administration of 50 μM HOE-642 resulted in further decreases ($97.54 \pm 0.52\%$ in C57BL/6 organoids and $92.91 \pm 3.76\%$ in CD-1 organoids; Fig. 6B). These data indicate that although NHE-1 has higher activity, NHE-2 is also active on organoids. The fact that some activity remained even in the presence of 50 μM HOE-642 suggests the presence of other Na^+-dependent acid-extruding mechanisms.

Activity of NBC

NBC is an electrogenic transporter that mainly localizes to the basolateral membrane in most epithelia, in which it mediates the cotransport of Na^+ and HCO_3^- into cells.
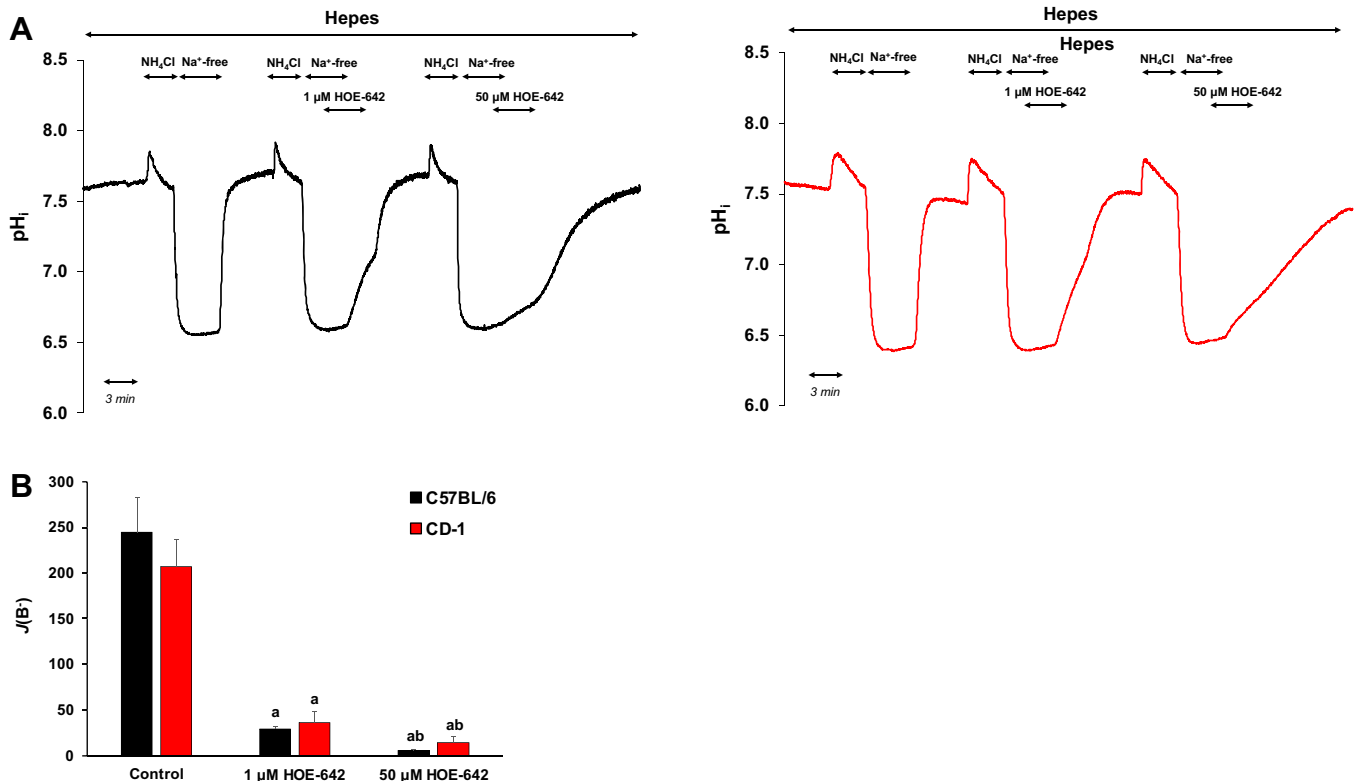

Figure 6. Investigation of Na^+/H^+ exchanger (NHE) isoforms on esophageal organoids (EOs). A: representative intracellular pH (pH_i) curves (black line, C57BL/6; red line, CD-1) present the recovery from acidosis in the presence of 1 and 50 μM HOE-642. B: summary data of the calculated activities of the different NHE isoforms in the presence of the isoform-selective NHE inhibitor HOE-642. The rate of pH recovery [$J(B^-)$] was calculated from the $\Delta pH/\Delta t$ obtained via linear regression analysis of the pH_i measurement performed over the first 60 s of recovery from the lowest pH_i level (initial pH_i). The buffering capacity at the initial pH_i was used to calculate $J(B^-)$. Data are presented as the mean ± SD. [a]$P \leq 0.05$ vs. Control. [b]$P \leq 0.05$ vs. 1 μM HOE-642. ANOVA followed by Bonferroni multiple comparison post hoc test. $n = 5$–6 organoids/5–11 ROIs.

Inside cells, HCO_3^- binds H^+ and causes intracellular alkalization. Therefore, in standard HCO_3^-/CO_2-buffered external solution, both NHE and NBC fight against cellular acidosis. NBC activity was investigated by the NH_4Cl prepulse technique (Fig. 7A). Administration of HCO_3^-/CO_2 rapidly and greatly decreased pH_i because of the quick diffusion of CO_2 into the cytoplasm. Significant pH_i recovery was observed after acidification, suggesting the important role of HCO_3^- efflux into EOs through NBC (Fig. 7A). After the NH_4Cl pulse, recovery from alkalosis was more rapid than observed in the presence of standard HEPES-buffered solution, indicating that in addition to NHE, NBC is also active in the presence of HCO_3^-. Removal of Na^+ from the external solution almost completely abolished the recovery from acidosis. To determine NBC activity, NHE function was blocked by the nonspecific NHE inhibitor amiloride, which was added 1 min before and during the readministration of Na^+. As presented in Fig. 7, A and B, the recovery from acidosis was decreased by $61.88 \pm 5.3\%$ in C57BL/6 organoids and $62.18 \pm 7.3\%$ in CD-1 organoids in the presence of amiloride, indicating that NHE is responsible for much of the recovery from acidosis, but there is also functionally active NBC on the cells. Interestingly, we found a significant difference in recovery following Na^+ deprivation between the C57BL/6 and CD-1 organoids, suggesting greater NBC activity in C57BL/6 mice.

Activity of the Cl^-/HCO_3^- Exchanger

The HCO_3^- transporter family includes several transport proteins, of which Slc26 proteins functions as an electroneutral Cl^-/HCO_3^- exchanger. Among the Slc26 exchangers, the presence of Slc26a6 (PAT1) was detected at both the mRNA and protein level in the C57BL/6 and CD-1 organoids. Slc26a6 mediates Cl^- and HCO_3^- exchange with a $1Cl^-/2HCO_3^-$ stoichiometry. To determine whether this Cl^-/HCO_3^- exchanger is functionally active on the organoids, the Cl^- removal technique was used (Fig. 8, A–C). In the presence of external Cl^-, Slc26a6 mediates the efflux of HCO_3^- and the uptake of Cl^-, therefore playing role in the acidification of cells. Removal of Cl^- from standard HCO_3^-/CO_2-buffered solution induced strong alkalization because of the reverse mode of the exchanger (Fig. 8A). By contrast, in the absence of HCO_3^-, Cl^- removal caused minimal, reversible alkalization (Fig. 8B). The presence of functionally active AE has been also confirmed by the NH_4Cl prepulse technique (Fig. 8, D and E). We previously illustrated that in the presence of HCO_3^-, the initial rate of recovery (30 s) from alkalosis reflects the activity of Cl^-/HCO_3^- exchangers (11, 18). As presented in Fig. 8E, there was no significant difference in AE activity between the two mouse organoids.
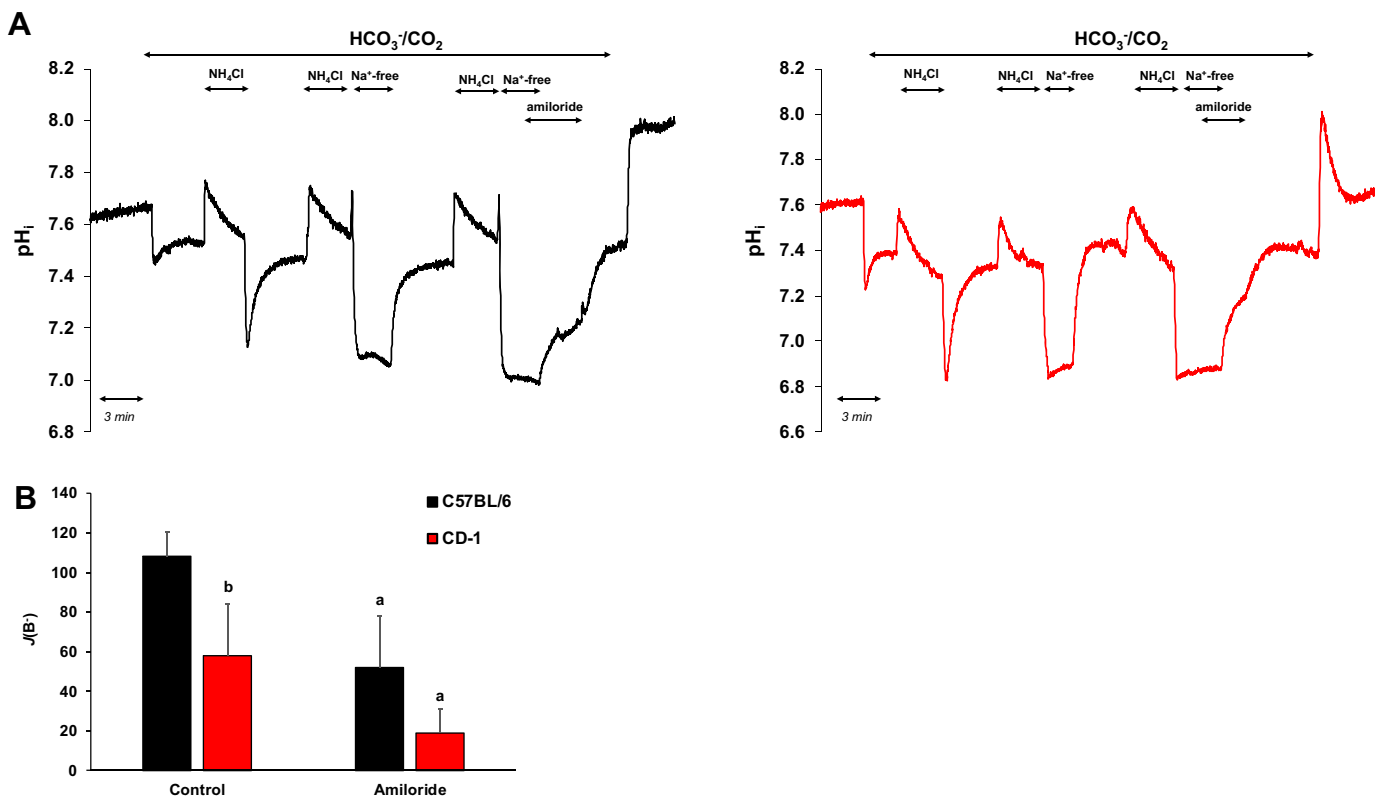

Figure 7. Investigation of Na^+/HCO_3^- cotransporter (NBC) activity in esophageal organoids (EOs). A: representative intracellular pH (pH_i) curves (black line, C57BL/6; red line, CD-1) present the recovery from acidosis in the presence of 0.2 mM amiloride. B: summary data present the calculated activity of NBC in the presence of the Na^+/H^+ exchanger (NHE) inhibitor amiloride. The rate of acid recovery [$J(B^-)$] was calculated from the $\Delta pH/\Delta t$ obtained via linear regression analysis of the pH_i measurement performed over the first 60 s of recovery from the lowest pH_i (initial pH_i). The buffering capacity at the initial pH_i was used to calculate $J(B^-)$. Data are presented as the mean $\pm$ SD. [a]$P \leq 0.05$ vs. Control. [b]$P \leq 0.05$ vs. C57BL/6. ANOVA followed by Bonferroni multiple comparison post hoc test. n = 9–11 organoids/15–17 ROIs.

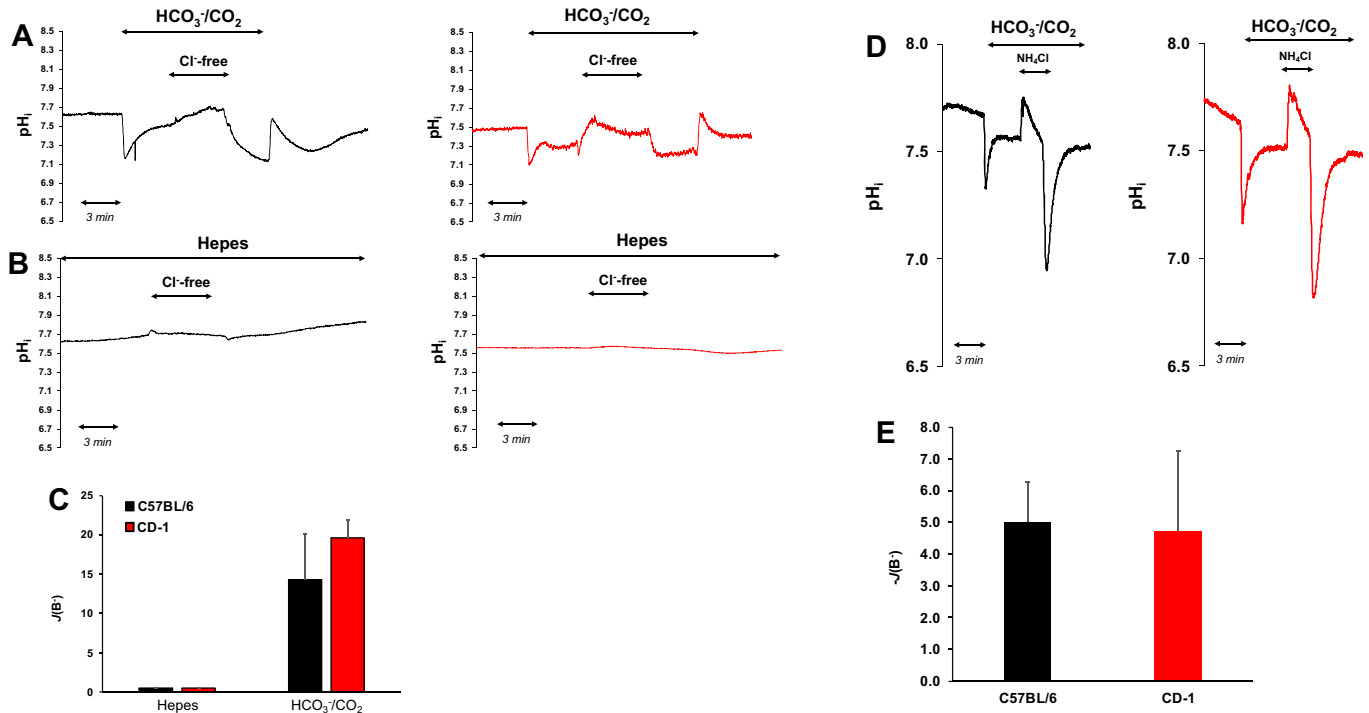**Figure 8.** Investigation of Cl^-/HCO_3^- exchanger activity in esophageal organoids. Cl^-/HCO_3^- exchanger activity was investigated by the Cl^- removal technique in the presence (*A*) and absence (*B*) of HCO_3^-/CO_2 (black line, C57BL/6; red line, CD-1). *C*: the rate of acid recovery $J(B^-)$ was calculated from the dpH/dt obtained via linear regression analysis of intracellular pH (pH$_i$) measurements performed over the first 60 s after exposure to the Cl^--free solution. The buffering capacity at the initial pH$_i$ was used to calculate $J(B^-)$. $n = 4$–15. *D*: the activity of the Cl^-/HCO_3^- exchanger was also measured using the alkali loading method and expressed (*E*) as calculated $J(B^-)$, which was calculated from the dpH/dt obtained via linear regression analysis of pH$_i$ measurements performed over the first 30 s of recovery from the highest pH$_i$ level (initial pH$_i$) achieved in the presence of NH_4Cl. The buffering capacity at the start point pH$_i$ was used for the calculation of $J(B^-)$. Data are presented as the mean ± SD. ANOVA followed by Bonferroni multiple comparison post hoc test. $n = 7$–20 organoids/25–37 ROIs.

Activity of CFTR

The CFTR Cl^- channel, which is present on most epithelial cells, mediates the efflux of Cl^- from cells. The presence of this ion channel has been detected at both the mRNA and protein level in organoids; therefore, we also investigated its activity using the Cl^--sensitive fluorescent dye MQAE and CFTR activator forskolin. As presented in Fig. 9, *A* and *B*, the administration of 10 μM forskolin caused a small increase in initial rate of Cl^- efflux (19.61 ± 4.52% in C57BL/6 organoids and 21.83 ± 9.72% in CD-1 organoids), and Cl^- loss reached steady state after ∼10 min. The effect of 5 μM forskolin was negligible. To investigate whether there is a functional relationship between CFTR and the acid-base transporters, the activity of the transporters was examined in the presence of the CFTR inhibitor CFTRinh-172 (10 μM; Fig. 9, *C–E*). Using the NH_4Cl prepulse technique, we found that the activity of AE was significantly decreased by CFTR inhibition (18.60 ± 3.34% in C57BL/6 organoids and 35.71 ± 11.77% in CD-1 organoids; Fig. 9*D*), whereas recovery from acidosis was only inhibited in C57BL/6 organoids (Fig. 9*E*).

Conclusions

The present study is the first to describe and functionally characterize the most common ion transport processes on EOs using two frequently used laboratory mouse strains (C57BL/6 and CD-1). Regulation of pH$_i$ in epithelial cells is

crucial, as most biological processes are affected by changes in pH. Ion transporters are involved in the regulation of pH$_i$ and extracellular pH. Specifically, the transporters are polarized on epithelial cells, ensuring the unidirectional movement of substances. Esophageal ion transport processes were most intensively studied in the 1990s, mostly using primary tissue. These studies investigated the basic acid-base transporters and characterized the effect of acid and bile on the function of these transporters (1). Although extremely important information was obtained from these investigations, the primary tissues used in these studies did not permit the specific investigation of a given transporter. The development of organoid cultures was a significant breakthrough in the examination of individual organs and tissues. Their biggest advantages include their easy maintenance, suitability for longer studies, and recapitulation of physiological conditions. In addition, organoids can be frozen and passaged, allowing the function of different transporters to be compared even on the same genetic background.

To investigate the ion transport mechanisms of EOs, we initially determined the resting pH and total buffering capacity of the cells. We found that the starting pH of the organoids was nearly 7.6 in CD-1 organoids and slightly higher than 7.6 in C57BL/6 organoids. This unusually high initial pH has also been detected in human and rabbit esophageal cells (19, 20). The cause of the high resting pH$_i$ is not fully known.
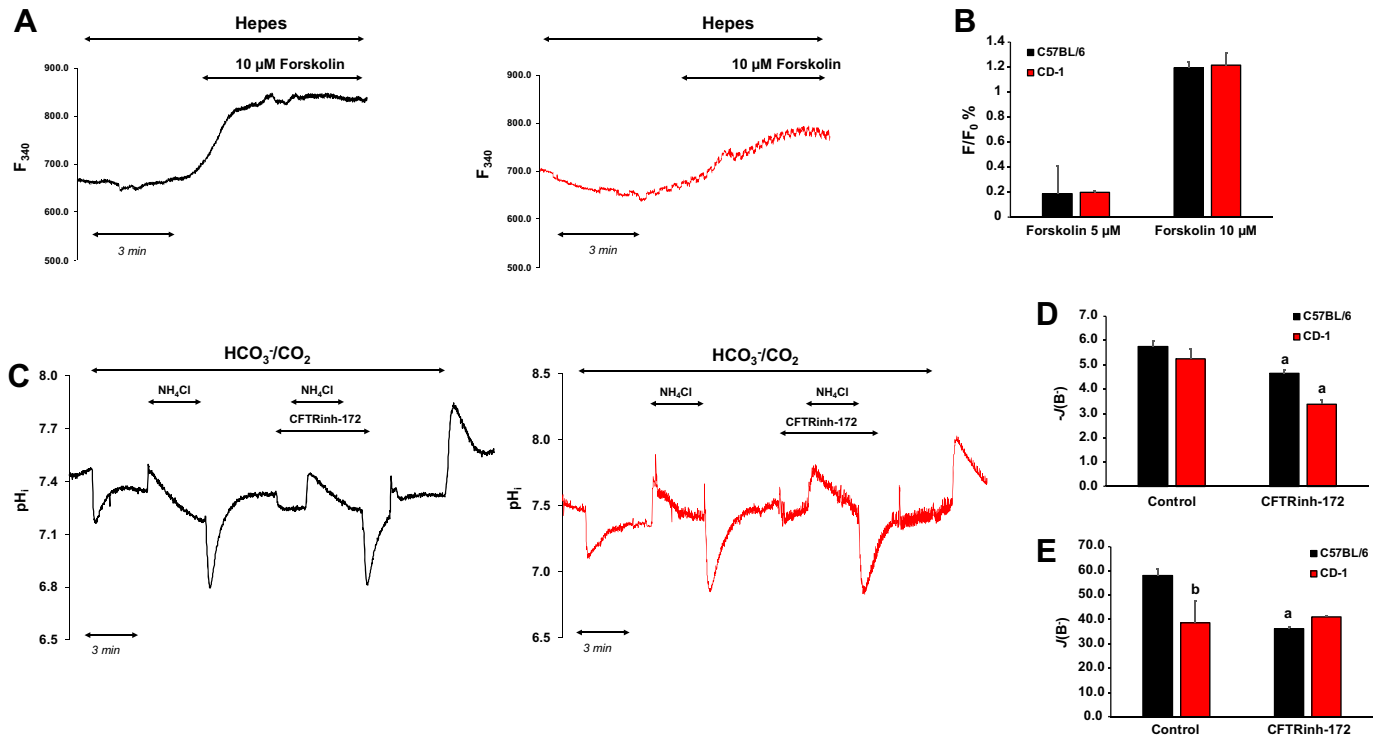
Figure 9. Investigation of cystic fibrosis transmembrane conductance regulator (cftr) activity in esophageal organoids (EOs). *A*: representative intracellular pH (pH$_i$) curves (black line, C57BL/6; red line, CD-1) present the effect of forskolin on Cl$^-$ efflux. *B*: summary data for the maximal fluorescence intensity changes, n = 19–22. *C*: representative pH$_i$ curves present the recovery from acid and alkali loading in the presence of 10 μM CFTRinh-172. The rates of alkali recovery [$-J$(B$^-$)] (*D*) and acid recovery [J(B$^-$)] (*E*) were calculated from the ΔpH/Δt obtained via linear regression analysis of pH$_i$ measurements performed over the first 30 and 60 s of recovery from the highest and lowest pH$_i$ (initial pH$_i$), respectively. The buffering capacity at the initial pH$_i$ was used to calculate J(B$^-$) and $-J$(B$^-$). Data are presented as the mean ± SD. [a]$P \leq 0.05$ vs. Control. [b]$P \leq 0.05$ vs. C57BL/6. ANOVA followed by Bonferroni multiple comparison post hoc test. n = 3–4 organoids/3–6 ROIs.

Presumably, this finding can be explained by the excessive activity of the alkalizing transporters that act against acidosis. Our results demonstrated the presence of a Na$^+$-dependent H$^+$ efflux mechanism on EOs, probably NHE, which was
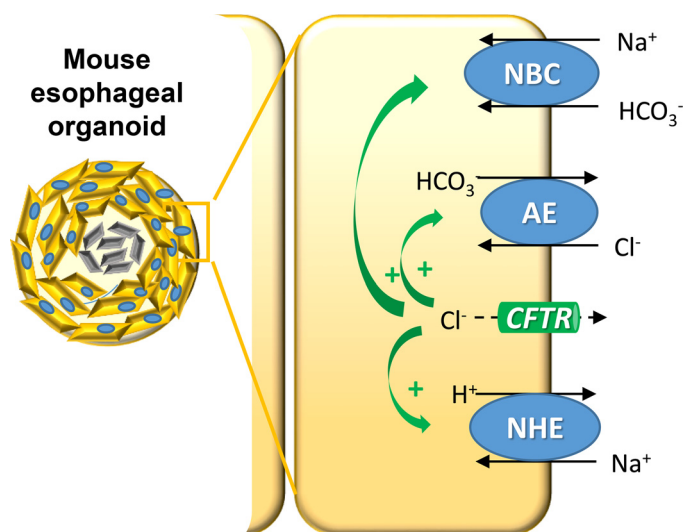

Figure 10. Ion transporters on the mouse esophageal organoids (EOs). Schematic figure shows the major, functionally active acid-base transporters on mouse OEs.

functionally active. The presence of NHE-1 on rat and rabbit EECs was previously demonstrated (21). By contrast, NHE-1 and NHE-2 expression is extremely low in normal human esophagus but strong in Barrett's and esophageal cancer (2, 22, 23). HOE-642 largely inhibited NHE function, suggesting that more than 90% of functionally active NHEs in EOs are NHE-1 and NHE-2. Concerning the residual activity, other NHE isoforms or a proton pump is presumably responsible. One possible candidate is NHE3, which was previously detected on human esophageal cells, in which it participate in the formation of dilated intercellular spaces, and the expression of this isoform increases with the severity of GERD (24, 25). Immunolocalization of NHE-1 and NHE-2 demonstrated that NHE-1 expression was mostly observed in the periphery, whereas NHE-2 staining was more pronounced in the inner cell layers. The different localization of NHE-1 and NHE-2 can be explained by the fact that organoids are composed of different types of cells. The outermost cell layer of the organoids consists of basal cells, whereas the inner cell layers are composed of differentiated keratinocytes. This indicates that NHE-1 is mainly expressed in basal cells, whereas NHE-2 is expressed in keratinocytes. Our finding that NHE-1 is mainly located in basal cells is consistent with the observation that NHE-1 is highly expressed in human SECs (2, 22, 23).

NBC is another transporter that can protect cells from acidosis. We revealed the presence of NBC in EOs, and it plays an important role in pH$_i$ regulation. CO$_2$-induced acidosis

was almost completely reversed, which can be explained by the influx of HCO_3^- through NBC. Furthermore, we found a significant difference in recovery from acidosis in the presence and absence of HCO_3^-, and fairly significant recovery was observed in the presence of amiloride. Taken together, these data strongly indicate that EOs express functionally active NBC. The presence of NBC has to date been identified in submucosal glands, in which it plays role in HCO_3^- secretion (26, 27). The presence of NBC has also been demonstrated in human EECs, and similarly as NHE, its expression is increased in Barrett's carcinoma (2). The role of NBC in SECs is not entirely clear, but presumably, it might play a central role in the regulation of pH_i and transcellular transport of HCO_3^-. Because NBC mediates HCO_3^- uptake, its presence also presupposes the presence of AE on these cells. Using a microfluorimetric technique, we detected a Cl^--dependent HCO_3^- efflux mechanism on EOs. Removal of Cl^- from the external solution in the presence of HCO_3^- induced strong alkalosis via the reverse mode of the Cl^-/HCO_3^- exchanger. In addition, the presence of HCO_3^- significantly increased the rate of recovery from alkalosis. Previous studies by our laboratory demonstrated that recovery from alkalosis in the presence of HCO_3^- is the result of HCO_3^- efflux through the Cl^-/HCO_3^- exchanger (11, 18). Among the Cl^-/HCO_3^- exchangers, the presence of Na^+-dependent and Na^+-independent transporters was demonstrated on rabbit SECs (28). In addition, the presence of Slc26a6 was detected on SMGs, thereby mediating HCO_3^- secretion together with NBC and CFTR (26, 27). In EOs, strong Slc26a6 expression was found at both the mRNA and protein level, whereas Slc26a3 expression was weak and nonspecific. The Slc26a6 transporter is primarily located on the apical membrane of secretory epithelial cells, in which it plays an essential role in HCO_3^- secretion (29). Because the esophageal epithelium is not a typical secretory epithelium, the presence of this transporter on EOs is unusual. In addition, Slc26a6 expression was more pronounced at the periphery, indicating that basal cells have some HCO_3^--secreting capacity. In many secretory epithelia, Slc26 AEs interact with the CFTR Cl^- channel in the regulation of HCO_3^- secretion (30, 31). To investigate the presence of CFTR and its coexpression with the Slc26a6 transporter, we investigated the colocalization of these transporters using immunostaining. As an interesting finding of our study, the CFTR Cl^- channel is expressed on EOs. Immunolocalization illustrated that both peripheral and central cells highly express CFTR. Costaining of CFTR and Slc26a6 revealed some colocalization, mainly in cells on the periphery, indicating that the two transporters interact with each other. To investigate the functional interaction between CFTR and Slc26a6, the microfluorimetric technique was used. The CFTR activator forskolin concentration-dependently increased the activity of CFTR, although the response to forskolin was relatively low even in the presence of supramaximal concentrations, indicating that CFTR channel activity is lower than usually observed for secretory epithelia, such as those in the pancreas or lungs (32). The presence of the CFTR inhibitor CFTRinh-172 decreased the rate of recovery from alkalosis in both C57BL/6 and CD-1 organoids, CFTR probably regulates the activity of AE. Interestingly, we found that CFTR inhibition also significantly reduced recovery from acidosis in C57BL/6 organoids.

Because both NBC and NHE are involved in recovery from acidosis in the presence of HCO_3^-, CFTR may interact with one of these transporters, but this type of interaction was not previously described. CFTR has been detected in the ductal cells of porcine submucosal glands, in which it localizes primarily to the apical membrane and plays an important role in ductal HCO_3^- secretion (26). It has also been detected in SECs, in which its presence is restricted to the basal cell layer (33). In SECs, CFTR mediates Cl^- transport together with the voltage-gated Cl^- channel ClC-2, which plays a pivotal role in protection against acid-induced injury, as demonstrated with the ClC-2 agonist lubiprostone (33). Because lubiprostone has been illustrated to activate CFTR (34, 35), the role of CFTR in this process has been postulated. The protective role of CFTR was also demonstrated in BE and esophageal cancer (36–40). These experiments demonstrated that CFTR plays a protective role against esophageal cancer, and overexpression of this channel is associated with good prognosis in squamous cell carcinoma. We also revealed the presence of the Ca^{2+}-activated Cl^- channel ANO1 or TMEM16A in EOs. One study examined the presence of ANO1 in the esophageal epithelium and indicated that its expression is increased in eosinophilic esophagitis and correlated with the severity of the disease. Furthermore, ANO1 has been reported to play central roles in the proliferation of basal zone hyperplasia via an IL-13-mediated pathway (41).

In this study, we uncovered for the first time the presence of the major epithelial ion transporters in Eos (Fig. 10). We demonstrated that NHE, NBC, AE, and the CFTR Cl^- channel are active in EOs, and there was no significant difference in the expression and activity of NHE, AE, and CFTR between the two mouse strains. However, it should be mentioned that organoids are heterogeneous structures, therefore the identified ion transporter activities cannot be applied to all cells within the organoid. Further studies are needed to determine the transport mechanisms in each individual cell type. We can conclude that the EOs comprise a suitable experimental system to investigate ion transport processes, and therefore, they can be used to study the role of ion transporters in different esophageal diseases or test drug molecules that affect the function of ion transporters.

GRANTS

DISCLOSURES

No conflicts of interest, financial or otherwise, are declared by the authors.

AUTHOR CONTRIBUTIONS

V.V. conceived and designed research; M.M.K., T.B., E.B., E.G., and Z.V. performed experiments; M.M.K., T.B., Z.V., and V.V. analyzed data; V.V. interpreted results of experiments; M.M.K. and V.V. prepared figures; V.V. drafted manuscript; M.M.K., T.B., P.H., and V.V. edited and revised manuscript; M.M.K., T.B., E.B., E.G., Z.V., P.H., and V.V. approved final version of manuscript.

REFERENCES

1. **Becskeházi E**, **Korsós MM**, **Erőss B**, **Hegyi P**, **Venglovecz V**. Oesophageal ion transport mechanisms and significance under pathological conditions. *Front Physiol* 11: 855, 2020. doi:10.3389/fphys.2020.00855.

2. **Laczkó D**, **Rosztóczy A**, **Birkás K**, **Katona M**, **Rakonczay Z Jr**, **Tiszlavicz L**, **Róka R**, **Wittmann T**, **Hegyi P**, **Venglovecz V**. Role of ion transporters in the bile acid-induced esophageal injury. *Am J Physiol Gastrointest Liver Physiol* 311: G16–G31, 2016. doi:10.1152/ajpgi.00159.2015.

3. **de Jonge HR**, **Bijvelds MJC**, **Strubberg AM**, **Liu J**, **Clarke LL**. Organoids as a model for intestinal ion transport physiology. In: *Ion Transport Across Epithelial Tissues and Disease*, edited by Hamilton KL, Devor DC. Cham: Springer, 2020. doi:10.1007/978-3-030-55310-4_1.

4. **Molnár R**, **Madácsy T**, **Varga A**, **Németh M**, **Katona X**, **Görög M**, **Molnár B**, **Fanczal J**, **Rakonczay Z Jr**, **Hegyi P**, **Pallagi P**, **Maléth J**. Mouse pancreatic ductal organoid culture as a relevant model to study exocrine pancreatic ion secretion. *Lab Invest* 100: 84–97, 2020. doi:10.1038/s41374-019-0300-3.

5. **Sachs N**, **Papaspyropoulos A**, **Zomer-van Ommen DD**, **Heo I**, **Böttinger L**, **Klay D**, et al. Long-term expanding human airway organoids for disease modeling. *EMBO J* 38: e100300, 2019. doi:10.15252/embj.2018100300.

6. **DeWard AD**, **Cramer J**, **Lagasse E**. Cellular heterogeneity in the mouse esophagus implicates the presence of a nonquiescent epithelial stem cell population. *Cell Rep* 9: 701–711, 2014. doi:10.1016/j.celrep.2014.09.027.

7. **Kalabis J**, **Oyama K**, **Okawa T**, **Nakagawa H**, **Michaylira CZ**, **Stairs DB**, **Figueiredo JL**, **Mahmood U**, **Diehl JA**, **Herlyn M**, **Rustgi AK**. A subpopulation of mouse esophageal basal cells has properties of stem cells with the capacity for self-renewal and lineage specification. *J Clin Invest* 118: 3860–3869, 2008. doi:10.1172/JCI35012.

8. **Thomas JA**, **Buchsbaum RN**, **Zimniak A**, **Racker E**. Intracellular pH measurements in Ehrlich ascites tumor cells utilizing spectroscopic probes generated in situ. *Biochemistry* 18: 2210–2218, 1979. doi:10.1021/bi00578a012.

9. **Hegyi P**, **Rakonczay Z**, **Gray MA**, **Argent BE**. Measurement of intracellular pH in pancreatic duct cells: a new method for calibrating the fluorescence data. *Pancreas* 28: 427–434, 2004. doi:10.1097/00006676-200405000-00012.

10. **Hegyi P**, **Gray MA**, **Argent BE**. Substance P inhibits bicarbonate secretion from guinea pig pancreatic ducts by modulating an anion exchanger. *Am J Physiol Cell Physiol* 285: C268–C276, 2003. doi:10.1152/ajpcell.00574.2002.

11. **Venglovecz V**, **Rakonczay Z Jr**, **Ozsvári B**, **Takács T**, **Lonovics J**, **Varró A**, **Gray MA**, **Argent BE**, **Hegyi P**. Effects of bile acids on pancreatic ductal bicarbonate secretion in guinea pig. *Gut* 57: 1102–1112, 2008. doi:10.1136/gut.2007.134361.

12. **Harnden P**, **Southgate J**. Cytokeratin 14 as a marker of squamous differentiation in transitional cell carcinomas. *J Clin Pathol* 50: 1032–1033, 1997. doi:10.1136/jcp.50.12.1032.

13. **Reis-Filho JS**, **Simpson PT**, **Martins A**, **Preto A**, **Gärtner F**, **Schmitt FC**. Distribution of p63, cytokeratins 5/6 and cytokeratin 14 in 51 normal and 400 neoplastic human tissue samples using TARP-4 multitumor tissue microarray. *Virchows Arch* 443: 122–132, 2003. doi:10.1007/s00428-003-0859-2.

14. **Fong P**. CFTR-SLC26 transporter interactions in epithelia. *Biophys Rev* 4: 107–116, 2012. doi:10.1007/s12551-012-0068-9.

15. **Weintraub WH**, **Machen TE**. pH regulation in hepatoma cells: roles for Na-H exchange, Cl-HCO3 exchange, and Na-HCO3 cotransport. *Am J Physiol Gastrointest Liver Physiol* 257: G317–G327, 1989. doi:10.1152/ajpgi.1989.257.3.G317.

16. **Slepkov ER**, **Rainey JK**, **Sykes BD**, **Fliegel L**. Structural and functional analysis of the Na$+$/H$+$ exchanger. *Biochem J* 401: 623–633, 2007. doi:10.1042/BJ20061062.

17. **Pallagi-Kunstár É**, **Farkas K**, **Maléth J**, **Rakonczay Z Jr**, **Nagy F**, **Molnár T**, **Szepes Z**, **Venglovecz V**, **Lonovics J**, **Rázga Z**, **Wittmann T**, **Hegyi P**. Bile acids inhibit Na$^+$/H$^+$ exchanger and Cl$^-$/HCO$_3^-$ exchanger activities via cellular energy breakdown and Ca^{2+})overload in human colonic crypts. *Pflugers Arch* 467: 1277–1290, 2015. doi:10.1007/s00424-014-1560-9.

18. **Venglovecz V**, **Hegyi P**, **Rakonczay Z Jr**, **Tiszlavicz L**, **Nardi A**, **Grunnet M**, **Gray MA**. Pathophysiological relevance of apical large-conductance Ca^{2+}-activated potassium channels in pancreatic duct epithelial cells. *Gut* 60: 361–369, 2011. doi:10.1136/gut.2010.214213.

19. **Tobey NA**, **Koves G**, **Orlando RC**. Human esophageal epithelial cells possess an Na$+$/H$+$ exchanger for H$+$ extrusion. *Am J Gastroenterol* 93: 2075–2081, 1998. doi:10.1111/j.1572-0241.1998.00596.x.

20. **Tobey NA**, **Reddy SP**, **Keku TO**, **Cragoe EJ Jr**, **Orlando RC**. Studies of pHi in rabbit esophageal basal and squamous epithelial cells in culture. *Gastroenterology* 103: 830–839, 1992. doi:10.1016/0016-5085(92)90014-P.

21. **Shallat S**, **Schmidt L**, **Reaka A**, **Rao D**, **Chang EB**, **Rao MC**, **Ramaswamy K**, **Layden TJ**. NHE-1 isoform of the Na$+$/H$+$ antiport is expressed in the rat and rabbit esophagus. *Gastroenterology* 109: 1421–1428, 1995. doi:10.1016/0016-5085(95)90626-6.

22. **Ariyoshi Y**, **Shiozaki A**, **Ichikawa D**, **Shimizu H**, **Kosuga T**, **Konishi H**, **Komatsu S**, **Fujiwara H**, **Okamoto K**, **Kishimoto M**, **Marunaka Y**, **Otsuji E**. Na$+$/H$+$ exchanger 1 has tumor suppressive activity and prognostic value in esophageal squamous cell carcinoma. *Oncotarget* 8: 2209–2223, 2017. doi:10.18632/oncotarget.13645.

23. **Guan B**, **Hoque A**, **Xu X**. Amiloride and guggulsterone suppression of esophageal cancer cell growth in vitro and in nude mouse xenografts. *Front Biol (Beijing)* 9: 75–81, 2014. doi:10.1007/s11515-014-1289-z.

24. **Yang SC**, **Chen CL**, **Yi CH**, **Liu TT**, **Shieh KR**. Changes in gene expression patterns of circadian-clock, transient receptor potential vanilloid-1 and nerve growth factor in inflamed human esophagus. *Sci Rep* 5: 13602, 2015. doi:10.1038/srep13602.

25. **Zeng C**, **Vanoni S**, **Wu D**, **Caldwell JM**, **Wheeler JC**, **Arora K**, **Noah TK**, **Waggoner L**, **Besse JA**, **Yamani AN**, **Uddin J**, **Rochman M**, **Wen T**, **Chehade M**, **Collins MH**, **Mukkada VA**, **Putnam PE**, **Naren AP**, **Rothenberg ME**, **Hogan SP**. Solute carrier family 9, subfamily A, member 3 (SLC9A3)/sodium-hydrogen exchanger member 3 (NHE3) dysregulation and dilated intercellular spaces in patients with eosinophilic esophagitis. *J Allergy Clin Immunol* 142: 1843–1855, 2018. doi:10.1016/j.jaci.2018.03.017.

26. **Abdulnour-Nakhoul S**, **Nakhoul HN**, **Kalliny MI**, **Gyftopoulos A**, **Rabon E**, **Doetjes R**, **Brown K**, **Nakhoul NL**. Ion transport mechanisms linked to bicarbonate secretion in the esophageal submucosal glands. *Am J Physiol Regul Integr Comp Physiol* 301: R83–R96, 2011. doi:10.1152/ajpregu.00648.2010.

27. **Abdulnour-Nakhoul S**, **Nakhoul NL**, **Wheeler SA**, **Wang P**, **Swenson ER**, **Orlando RC**. HCO3- secretion in the esophageal submucosal glands. *Am J Physiol Gastrointest Liver Physiol* 288: G736–G744, 2005. doi:10.1152/ajpgi.00055.2004.

28. **Tobey NA**, **Reddy SP**, **Khalbuss WE**, **Silvers SM**, **Cragoe EJ Jr**, **Orlando RC**. Na($+$)-dependent and -independent Cl$^-$/HCO$_3^-$ exchangers in cultured rabbit esophageal epithelial cells. *Gastroenterology* 104: 185–195, 1993 [Erratum in *Gastroenterology* 105: 649, 1993]. doi:10.1016/0016-5085(93)90851-3.

29. **Wang J**, **Wang W**, **Wang H**, **Tuo B**. Physiological and pathological functions of SLC26A6. *Front Med (Lausanne)* 7: 618256, 2020. doi:10.3389/fmed.2020.618256.

30. **Ko SB**, **Zeng W**, **Dorwart MR**, **Luo X**, **Kim KH**, **Millen L**, **Goto H**, **Naruse S**, **Soyombo A**, **Thomas PJ**, **Muallem S**. Gating of CFTR by the STAS domain of SLC26 transporters. *Nat Cell Biol* 6: 343–350, 2004. doi:10.1038/ncb1115.

31. **Stewart AK**, **Yamamoto A**, **Nakakuki M**, **Kondo T**, **Alper SL**, **Ishiguro H**. Functional coupling of apical Cl-/HCO3- exchange with CFTR in stimulated HCO3- secretion by guinea pig interlobular pancreatic duct. *Am J Physiol Gastrointest Liver Physiol* 296: G1307–G1317, 2009. doi:10.1152/ajpgi.90697.2008.

32. **Saint-Criq V**, **Gray MA**. Role of CFTR in epithelial physiology. *Cell Mol Life Sci* 74: 93–115, 2017. doi:10.1007/s00018-016-2391-y.

33. **Krüger J**, **Pridgen TA**, **Taylor ER**, **Garman KS**, **Blikslager AT**. Lubiprostone protects esophageal mucosa from acid injury in porcine esophagus. *Am J Physiol Gastrointest Liver Physiol* 318: G613–G623, 2020. doi:10.1152/ajpgi.00086.2019.

34. **Ao M**, **Venkatasubramanian J**, **Boonkaewwan C**, **Ganesan N**, **Syed A**, **Benya RV**, **Rao MC**. Lubiprostone activates Cl- secretion via cAMP signaling and increases membrane CFTR in the human colon carcinoma cell line, T84. *Dig Dis Sci* 56: 339–351, 2011. doi:10.1007/s10620-010-1495-8.

35. **Norimatsu Y**, **Moran AR**, **MacDonald KD.** Lubiprostone activates CFTR, but not ClC-2, via the prostaglandin receptor (EP(4)). *Biochem Biophys Res Commun* 426: 374–379, 2012. doi:10.1016/j.bbrc.2012.08.097.

36. **Gharahkhani P**, **Fitzgerald RC**, **Vaughan TL**, **Palles C**, **Gockel I**, **Tomlinson I**, et al**.** Genome-wide association studies in oesophageal adenocarcinoma and Barrett's oesophagus: a large-scale meta-analysis. *Lancet Oncol* 17: 1363–1373, 2016. doi:10.1016/S1470-2045(16)30240-6.

37. **Hassall E**, **Israel DM**, **Davidson AG**, **Wong LT.** Barrett's esophagus in children with cystic fibrosis: not a coincidental association. *Am J Gastroenterol* 88: 1934–1938, 1993.

38. **Holt EW**, **Yimam KK**, **Liberman MS.** Esophageal adenocarcinoma in a 40-year-old man with cystic fibrosis: coincidence or not? *Ochsner J* 13: 252–255, 2013.

39. **Li W**, **Wang C**, **Peng X**, **Zhang H**, **Huang H**, **Liu H.** CFTR inhibits the invasion and growth of esophageal cancer cells by inhibiting the expression of NF-κB. *Cell Biol Int* 42: 1680–1687, 2018. doi:10.1002/cbin.11069.

40. **Matsumoto Y**, **Shiozaki A**, **Kosuga T**, **Kudou M**, **Shimizu H**, **Arita T**, **Konishi H**, **Komatsu S**, **Kubota T**, **Fujiwara H**, **Okamoto K**, **Kishimoto M**, **Konishi E**, **Otsuji E.** Expression and role of CFTR in human esophageal squamous cell carcinoma. *Ann Surg Oncol*, 2021. doi:10.1245/s10434-021-09752-y.

41. **Vanoni S**, **Zeng C**, **Marella S**, **Uddin J**, **Wu D**, **Arora K**, **Ptaschinski C**, **Que J**, **Noah T**, **Waggoner L**, **Barski A**, **Kartashov A**, **Rochman M**, **Wen T**, **Martin L**, **Spence J**, **Collins M**, **Mukkada V**, **Putnam P**, **Naren A**, **Chehade M**, **Rothenberg ME**, **Hogan SP.** Identification of anoctamin 1 (ANO1) as a key driver of esophageal epithelial proliferation in eosinophilic esophagitis. *J Allergy Clin Immunol* 145: 239–254.e2, 2020. doi:10.1016/j.jaci.2019.07.049.

PUBLICATION No.2.

Article

Inhibition of NHE-1 Increases Smoke-Induced Proliferative Activity of Barrett's Esophageal Cell Line

Eszter Becskeházi [1], Marietta Margaréta Korsós [1], Eleonóra Gál [1], László Tiszlavicz [2], Zsófia Hoyk [3], Mária A. Deli [3], Zoltán Márton Köhler [4], Anikó Keller-Pintér [4], Attila Horváth [5], Kata Csekő [6,7], Zsuzsanna Helyes [6,7], Péter Hegyi [8,9,10] and Viktória Venglovecz [1,*]

1   Department of Pharmacology and Pharmacotherapy, University of Szeged, H-6721 Szeged, Hungary; eszter.becskehazi@gmail.com (E.B.); margaretakorsos@gmail.com (M.M.K.); galeleonora@gmail.com (E.G.)
2   Department of Pathology, University of Szeged, H-6725 Szeged, Hungary; tiszlavicz.laszlo@med.u-szeged.hu
3   Biological Research Centre, Institute of Biophysics, H-6726 Szeged, Hungary; hoyk.zsofia@brc.hu (Z.H.); deli.maria@brc.hu (M.A.D.)
4   Department of Biochemistry, University of Szeged, H-6720 Szeged, Hungary; kohler.zoltan.marton@gmail.com (Z.M.K.); keller.aniko@med.u-szeged.hu (A.K.-P.)
5   Department of Pharmacognosy, University of Szeged, H-6720 Szeged, Hungary; horvath.attila@pharmacognosy.hu
6   Department of Pharmacology and Pharmacotherapy, Medical School & Szentágothai Research Centre, University of Pécs, H-7624 Pécs, Hungary; csekoe.kata@gmail.com (K.C.); zsuzsanna.helyes@aok.pte.hu (Z.H.)
7   PharmInVivo Ltd., H-7629 Pécs, Hungary
8   First Department of Medicine, University of Szeged, H-6720 Szeged, Hungary; hegyi.peter@pte.hu
9   Medical School & Szentágothai Research Centre, Institute for Translational Medicine, University of Pécs, H-7624 Pécs, Hungary
10 Division of Gastroenterology, First Department of Medicine, Medical School, University of Pécs, H-7624 Pécs, Hungary
*   Correspondence: venglovecz.viktoria@med.u-szeged.hu; Tel.: +36-62-545-677

Abstract: Several clinical studies indicate that smoking predisposes its consumers to esophageal inflammatory and malignant diseases, but the cellular mechanism is not clear. Ion transporters protect esophageal epithelial cells by maintaining intracellular pH at normal levels. In this study, we hypothesized that smoking affects the function of ion transporters, thus playing a role in the development of smoking-induced esophageal diseases. Esophageal cell lines were treated with cigarette smoke extract (CSE), and the viability and proliferation of the cells, as well as the activity, mRNA and protein expression of the Na^+/H^+ exchanger-1 (NHE-1), were studied. NHE-1 expression was also investigated in human samples. For chronic treatment, guinea pigs were exposed to tobacco smoke, and NHE-1 activity was measured. Silencing of NHE-1 was performed by using specific siRNA. CSE treatment increased the activity and protein expression of NHE-1 in the metaplastic cells and decreased the rate of proliferation in a NHE-1-dependent manner. In contrast, CSE increased the proliferation of dysplastic cells independently of NHE-1. In the normal cells, the expression and activity of NHE-1 decreased due to in vitro and in vivo smoke exposure. Smoking enhances the function of NHE-1 in Barrett's esophagus, and this is presumably a compensatory mechanism against this toxic agent.

Keywords: esophagus; ion transport; smoking; NHE-1; Barrett's esophagus

1. Introduction

Cigarette smoking is responsible for the development of many diseases, especially different types of cancers. Since smoking primarily affects the lungs, the effects of smo-king have been most intensively studied on this organ. However, other organs may also be affected, such as the esophagus, which is directly exposed to cigarette smoke. For this rea-son, a number of clinical studies have been conducted to examine the connection bet-ween

smoking and esophageal diseases. These studies have shown that smoking strongly correlates with the development of esophageal adenocarcinoma (EAC) and Barrett's esophagus (BE) and also increases the risk of progression from BE to EAC [1–5]. In contrast, only a few data are available regarding the cellular mechanism of smoking-induced lesions. In an older study, Orlando et al. showed that the esophageal potential difference is reduced by cigarette smoke extract (CSE), in which inhibition of Na^+ transport plays an important role [6]. This study suggests that smoking alters the ion transport processes in esophageal epithelial cells (EECs); however, it is not known whether this takes part in the development of BE or EAC.

Ion transport processes through the esophageal mucosa play an important protective role, as they greatly contribute to the maintenance of normal intracellular pH (pH_i). Several ion transporters have been identified on EECs in recent years, and their role has been characterized both under physiological and pathophysiological conditions [7,8]. Our workgroup showed that acid and/or bile acids alters the activity and expression of ion transporters, which may be important in the development and progression of esophageal diseases [8]. Among the acid–base transporters, the Na^+/H^+ exchanger (NHE) is one of the most important transmembrane protein that mediates the exchange of Na^+ and H^+. In addition to playing an important role in the alkalization of the pH_i, it also regulates cell vo-lume, proliferation, migration, and invasion [9–11]. Several members of the NHE family are known, of which NHE-1 is the most common, ubiquitously expressed isoform. The presence of NHE-1 has been shown in the esophagus of several species, such as rat and rabbit, where it is essentially involved in the regulation of pH_i [12]. In contrast, the expression of this isoform in the normal human esophagus is controversial, and its importance is more highlighted under pathological conditions [8,13–17]. Increased NHE-1 expression has been shown in BE, which probably plays a protective role against the acid- or bile-induced injury by enhancing the cellular resistance of the cells [8,15,18]. The role of NHE-1 in EAC is controversial. Some studies suggest that NHE-1 enhances the growth of eso-phageal cancer cells, while other studies have shown that NHE-1 expression is associated with longer postoperative survival [13,16].

There is no information on how smoking affects NHE-1 activity or expression in the esophagus. Since Na^+ transport is inhibited by smoking [6], it is conceivable that NHE-1 plays a role in the pathogenesis of cigarette-smoke-induced esophageal diseases. Therefore, the objective of the present study was to investigate the effect of tobacco smoke on normal, metaplastic and dysplastic cells and to investigate the role of NHE-1 in it.

2. Results

2.1. Effect of CSE on Esophageal Epithelial Cell Proliferation

To examine the effect of CSE on cell proliferation, first we determined the concentrations of CSE at which the cells retained their viability. CSE concentrations were chosen based on the literature data [19,20]. Cytotoxicity studies showed that both CP-A and CP-D cells mostly tolerated CSE at 1 and 10 μg/mL concentrations, at each incubation time (6, 24 and 72 h). In contrast, 100 μg/mL CSE induced a high degree of cell death, especially during longer incubation (Figure 1a). Therefore, in the proliferation assays, the effect of 1 and 10 μg/mL CSE was examined for 6, 24 and 72 h (Figure 1b). In the metaplastic, CP-A cells, CSE treatment dose-dependently reduced cell proliferation in the 24 and 72 h treatment groups. In contrast, in the dysplastic, CP-D cells 72 h CSE treatment significantly increased the proliferation.
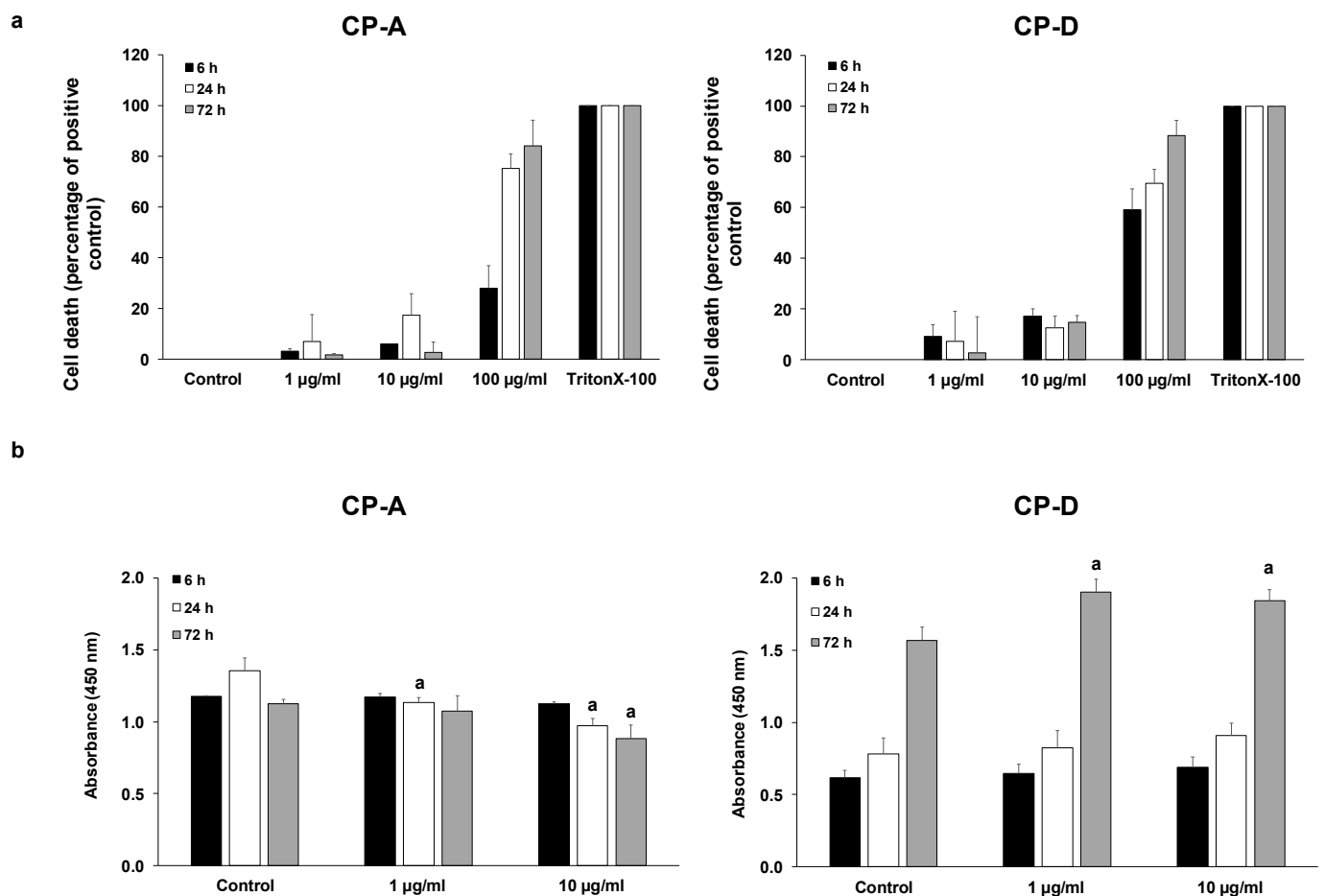
Figure 1. Effects of cigarette smoke extract (CSE) treatment on cell viability and proliferation. Metaplastic (CP-A) and dysplastic (CP-D) esophageal cell lines were exposed to different concentrations of CSE for 6, 24 and 72 h and the effects on cellular viability (**a**) and proliferation (**b**) were studied, using LDH and CCK8 assays, respectively. In the case of viability assay, 0.1% Triton X-100 was used as a positive control. Data represent mean $\pm$ SEM of three independent experiments; a = $p \leq 0.05$ vs. control.

2.2. Activity and Expression of NHE-1 in the Metaplastic and Dysplastic Cells

Next, we examined the rate of NHE activity in the CP-A and CP-D cell lines, using the NH_4Cl pre-pulse technique (Figure 2a,b). As shown in Figure 2a, in the absence of HCO_3^- the initial rate of regeneration from acidosis reflects the activity of NHE. Currently, nine NHE isoforms are known, and among them the presence of NHE-1 and NHE-2 was confirmed in the esophageal mucosa [8,12,21]. Our previous studies showed that NHE-1 displays greater activity and is better expressed than NHE-2 both in the metaplastic and dysplastic cells [8], indicating that NHE-1 is primarily responsible for the regeneration from acidosis. As shown in Figure 2a,b, regeneration from acidosis was higher in CP-A (BF: 5.47 $\pm$ 0.52) than in CP-D cells (BF: 3.36 $\pm$ 0.24), indicating that CP-A cells have higher NHE-1 activity. We have also compared the mRNA and protein expressions of NHE-1 between the metaplastic and dysplastic cells at different time points (6, 24 and 72 h). In addition, mRNA expression of NHE-1 (*SLC9A1*) was investigated by RT-PCR 24 h after plating the cells. As an internal gene, human beta actin (*ACTB*) was used. RT-PCR analysis revealed that there was no significant difference in NHE-1 expression among CP-A and CP-D cells, and no difference was observed between the different incubation times (Figure 2c). Similar to RT-PCR, the Western blot analysis showed no difference in the protein expression of NHE-1 between the CP-A and CP-D cells (Figure 2d).
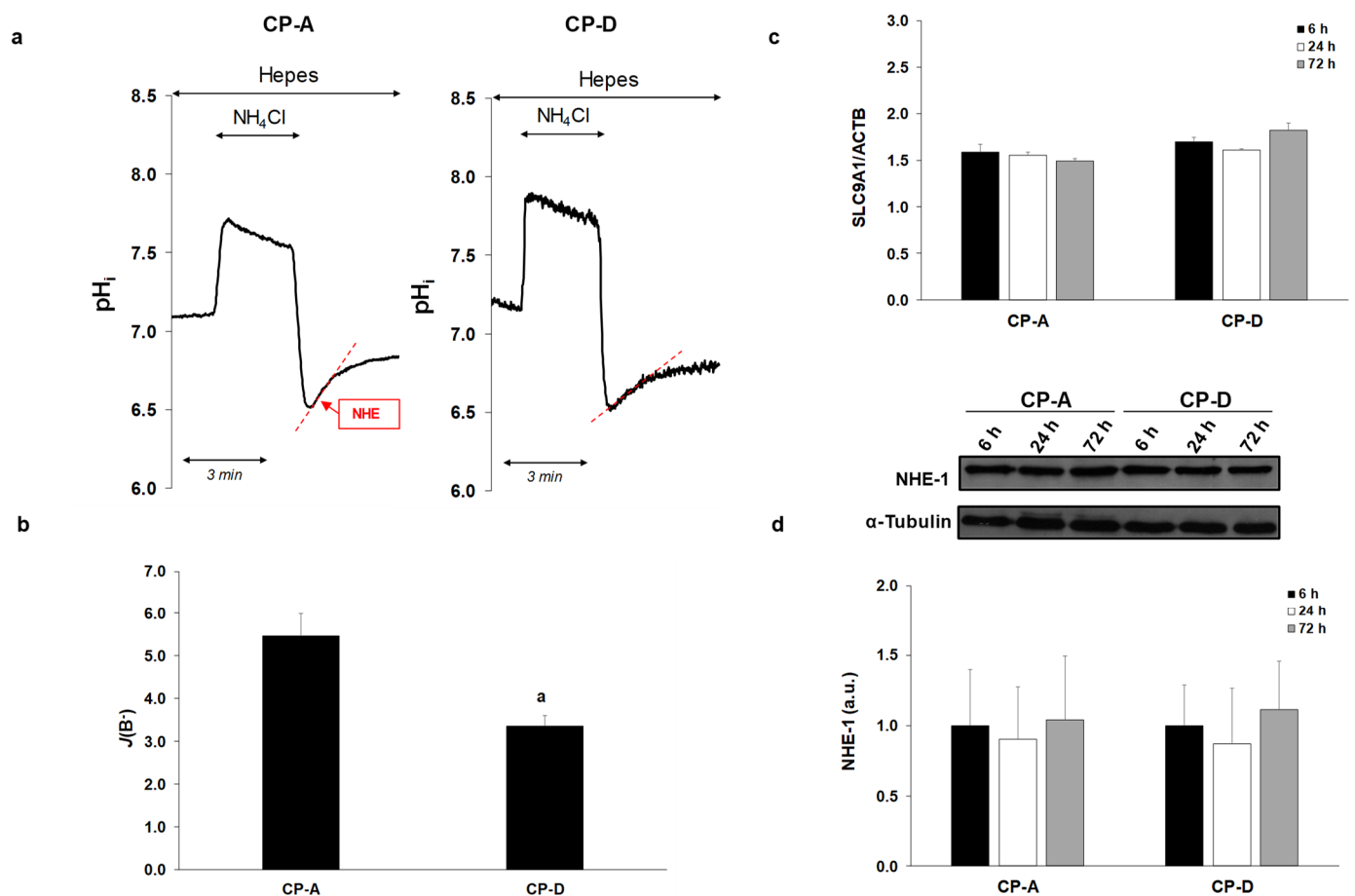
Figure 2. Activity, mRNA and protein expression of Na$^+$/H$^+$ exchanger-1 (NHE-1) in esophageal cell lines. (**a**) Representative intracellular pH (pH$_i$) curves present the recovery from acidosis in CP-A and CP-D cells. (**b**) Summary data of the calculated activity of NHE-1 in the different cell lines. The rate of pH recovery (J(B$^-$)) was calculated from the ΔpH/Δt obtained via linear regression analysis of the pH$_i$ measurement performed over the first 60 s of recovery from the lowest pH$_i$ level (initial pH$_i$). The buffering capacity at the initial pH$_i$ was used to calculate J(B$^-$). Data are presented as the mean $\pm$ SEM. a: $p \leq 0.05$ vs. CP-A; n = 5–11 exp./26–91 region of interests (ROIs). (**c**) mRNA and (**d**) protein expression of NHE-1 in the CP-A and CP-D cells. α-Tubulin was used as a protein-loading control. Data represent mean $\pm$ SEM of three independent experiments.

2.3. Effect of CSE on The Activity and Expression of NHE-1

In order to investigate the effect of CSE on the activity of NHE-1, the previously mentioned NH$_4$Cl pre-pulse technique was used. Since CSE alone can affect the fluorescence signals, cells were pretreated with 1, 10 or 100 µg/mL CSE for 1 h, and then NHE activity was measured (Figure 3a,b). Control cells were incubated in HEPES solution without CSE. In the case of CP-A cells, pretreatment with 1 µg/mL CSE decreased NHE activity from 5.47 $\pm$ 0.52 to 3.08 $\pm$ 0.55. In contrast, at higher concentrations (10 and 100 µg/mL, respectively) the activity of the exchanger increased (8.18 $\pm$ 1.3 at 10 µg/mL CSE and 12.28 $\pm$ 0.73 at 100 µg/mL CSE). In CP-D cells, CSE strongly reduced NHE-1 activity at all three concentrations (from 3.36 $\pm$ 0.24 to 1.25 $\pm$ 0.26 at 1 µg/mL CSE, 1.62 $\pm$ 0.23 at 10 µg/mL CSE and 1.46 $\pm$ 0.29 at 100 µg/mL CSE, respectively).
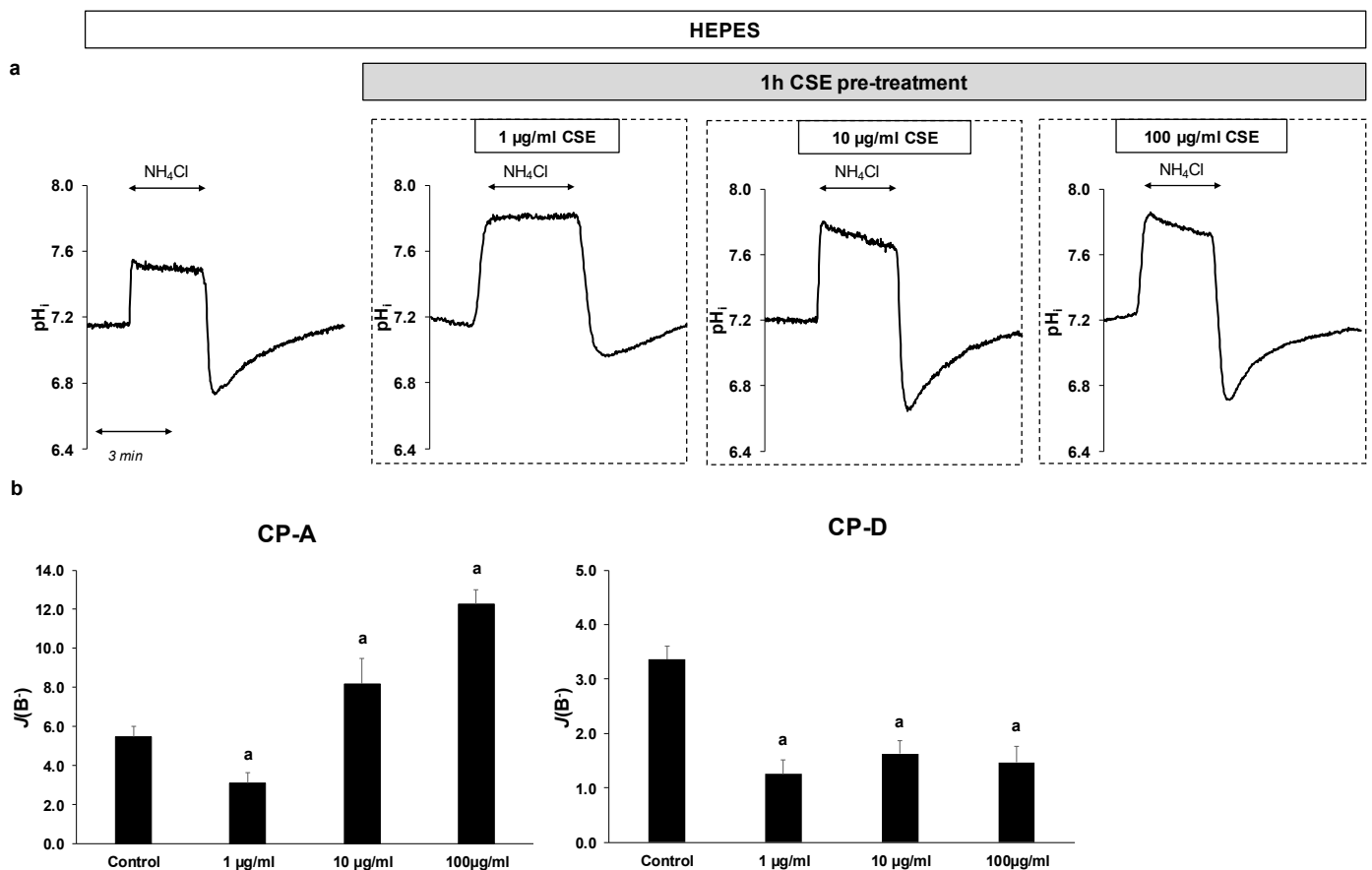
Figure 3. Effects of cigarette smoke extract (CSE) treatment on the activity of Na$^+$/H$^+$ exchanger-1 (NHE-1) in esophageal cell lines. Metaplastic (CP-A) and dysplastic (CP-D) esophageal cell lines were pretreated with different concentrations of CSE (1, 10 and 100 μg/mL) for 1 h, and the activity of NHE-1 was measured. (**a**) Representative intracellular pH (pH$_i$) curves present the recovery from acidosis in CP-A cells. (**b**) Summary data of the calculated activity of NHE-1 in the different cell lines. The rate of pH recovery (J(B$^-$)) was calculated as described in Figure 2b. Data are presented as the mean $\pm$ SEM; a = $p \leq 0.05$ vs. control; n = 12–14 exp./66–68 ROIs.

The CSE treatment did not cause significant differences in mRNA expression of NHE-1 in any of the cell lines (Figure 4a). In contrast, the protein expression was increased in the CP-A cells upon CSE treatment, almost in all treated groups (Figure 4b). In the CP-D cells, CSE treatment caused a robust increase at 1 μg/mL concentration in the 6 h treatment group, while no significant change was detected in the other groups.

2.4. Smoking Decreases NHE-1 Activity on Normal Esophageal Epithelial Cells

In order to investigate how CSE affects NHE activity under physiological conditions, we studied the effect of CSE on normal EECs isolated from guinea pigs. The same concentrations were used as for the cell lines, and the cells were pretreated with CSE in the same manner. As shown in Figure 5a,b, NHE activity was significantly reduced by CSE treatment (from 12.19 ± 0.46 to 4.64 ± 0.94 at 1 μg/mL CSE, to 3.96 ± 0.43 at 10 μg/mL CSE and to 4.49 ± 0.4 at 100 μg/mL CSE, respectively). In order to investigate the chronic effects of smoking, guinea pigs were exposed to cigarette smoke for one, two and four months, respectively, and then NHE activity was examined (Figure 5c). Guinea pigs of the same age were used as controls. Similar to acute CSE treatment, chronic treatment decreased NHE activity from 15.81 ± 0.91 to 7.98 ± 0.52 in the 1-month group, from 9.92 ± 0.78 to 7.9 ± 0.33 in the 2-month group and from 10.86 ± 0.54 to 5.46 ± 0.19 in the 4-month group (Figure 5d). These data indicate that smoking decreases the activity of NHE-1 in the normal eso-phageal mucosa.
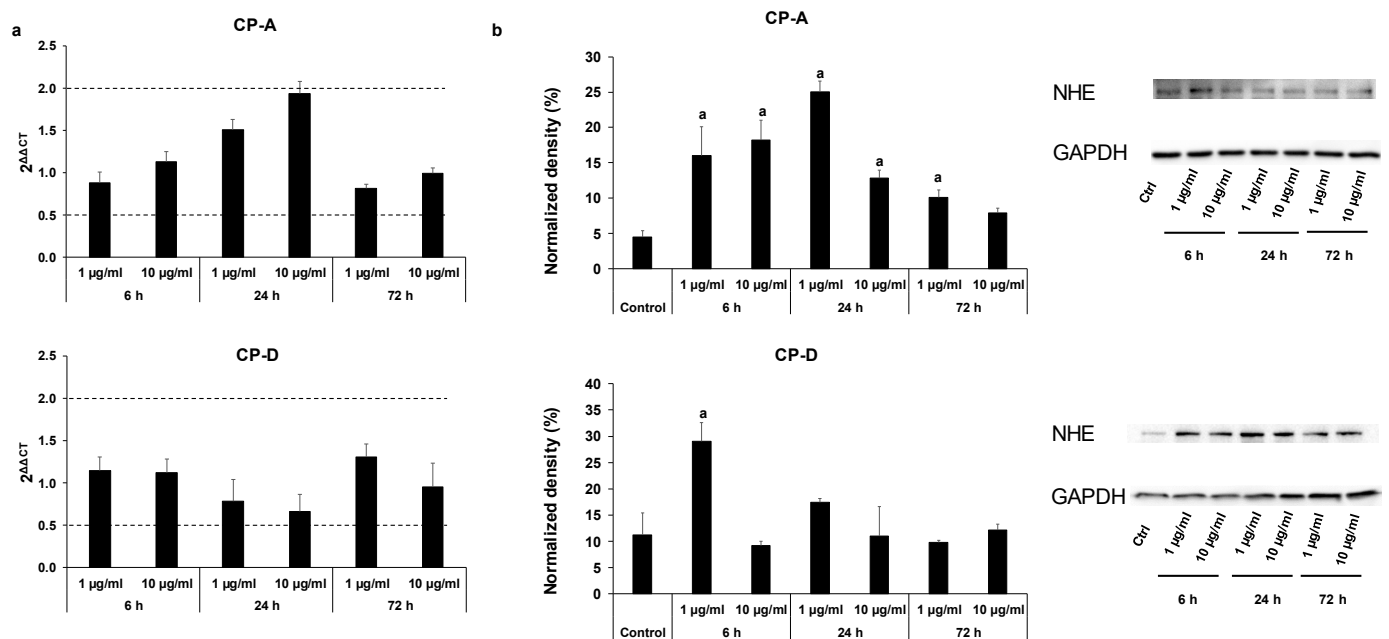
Figure 4. Effects of cigarette smoke extract (CSE) treatment on the mRNA and protein expression of Na^+/H^+ exchanger-1 (NHE-1) in esophageal cell lines. Metaplastic (CP-A) and dysplastic (CP-D) esophageal cell lines were treated with dif-ferent concentrations of CSE (1 and 10 µg/mL) for 6, 24 and 72 h, and the relative gene (**a**) and protein (**b**) expressions of NHE-1 were investigated by real-time PCR and Western blot, respectively. GAPDH was used as a protein-loading control. Data represent mean $\pm$ SEM of three independent experiments; a = $p \leq 0.05$ vs. control.

2.5. Effect of Smoking on NHE-1 Protein Expression in Human Esophageal Samples

Protein expression of NHE-1 was investigated in normal squamous epithelium and in BE samples obtained from patients with smoking and non-smoking history (Figure 6a,b). Patients who had never smoked or not smoked for more than a year were classified as non-smokers, while patients who had been smokers for at least 20 years were classified as smokers. Only patients with known smoking status were included in the analysis. As controls, normal esophageal biopsy samples and the intact tumor-free margin of surgically resected esophageal cancer were used. Weak NHE-1 expression was detected in the normal esophageal epithelium, and it was further reduced by smoking. In BE, strong NHE-1 expression was observed, mainly at the basolateral membrane of the columnar cells. In smokers, NHE-1 expression increased, and staining was detected not only in the plasma membrane but in the cytoplasm as well. Interestingly, strong NHE-1 staining was also observed in the glands. There was no significant difference between the intestinal and non-intestinal metaplasia, neither in the smoker nor in the non-smoker group.

2.6. Role of NHE-1 in The CSE-Induced Proliferation

In order to investigate whether the altered expression or activity of NHE-1 has any role in the effect of CSE on proliferation, we silenced the *SLC9A1* gene, using specific siRNA (Figure 7a–d). The efficiency of silencing was investigated at both mRNA and protein levels (Figure 7a,b). In CP-A cells, NHE-1 knockdown reduced the rate of proliferation at each incubation time, suggesting that NHE-1 is essential for the normal function of the cells (Figure 7c). In the CP-D cells, the lack of NHE-1 protein initially increased the rate of proliferation, whereas no significant difference was observed with additional incubation times (Figure 7c). In the absence of NHE-1, CSE treatment increased the rate of proliferation in the CP-A cells in almost all treated groups. For CP-D cells, proliferation increased alone in the 72h treatment group (Figure 7d).
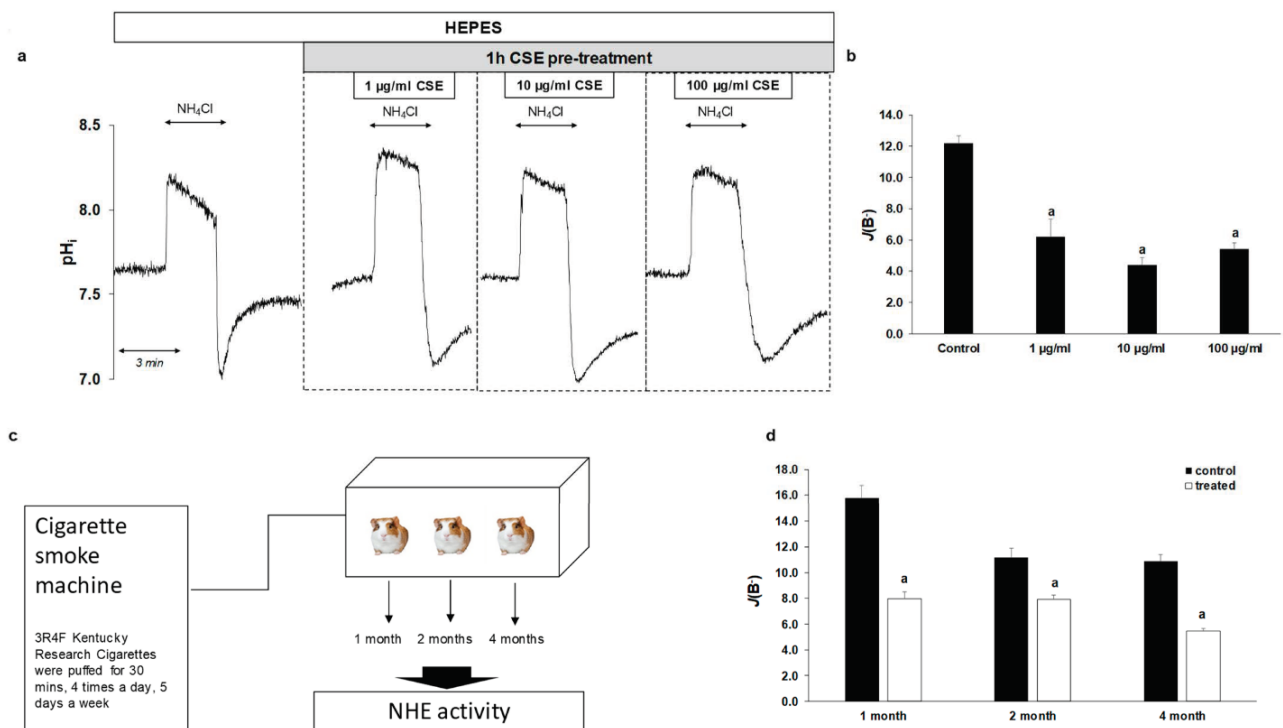
Figure 5. Effects of cigarette smoke extract (CSE) treatment and smoking on the activity of Na$^+$/H$^+$ exchanger-1 (NHE-1) in guinea pig esophageal epithelial cells (EECs). (**a**) Normal guinea pig EECs were pretreated with different concentrations of CSE (1, 10 and 100 μg/mL) for 1 h and the activity of NHE-1 was measured. Representative intracellular pH (pH$_i$) curves show the recovery from acidosis. (**b**) Summary data of the calculated activity of NHE-1 in guinea pig EECs. The rate of pH recovery ($J(B^-)$) was calculated as described in Figure 2b. Data are presented as the mean ± SEM; a: $p \leq 0.05$ vs. control; n = 13–18 exp./86–99 ROIs. (**c**) Chronic effect of cigarette smoking was investigated, using smoking chamber. Guinea pigs were exposed to whole body cigarette smoke 4 times a day, 5 days a week, 30 min each time, using a TE2 closed-chamber manual smoking system. After 1, 2, or 4 months of smoking, the animals were sacrificed and NHE-1 activity was measured. (**d**) Summary data of the calculated activity of NHE-1 in guinea pig EECs. The rate of pH recovery ($J(B^-)$) was calculated as described in Figure 2b. Data are presented as the mean ± SEM; a: $p \leq 0.05$ vs. control; n = 8–16exp./81–210 ROIs.
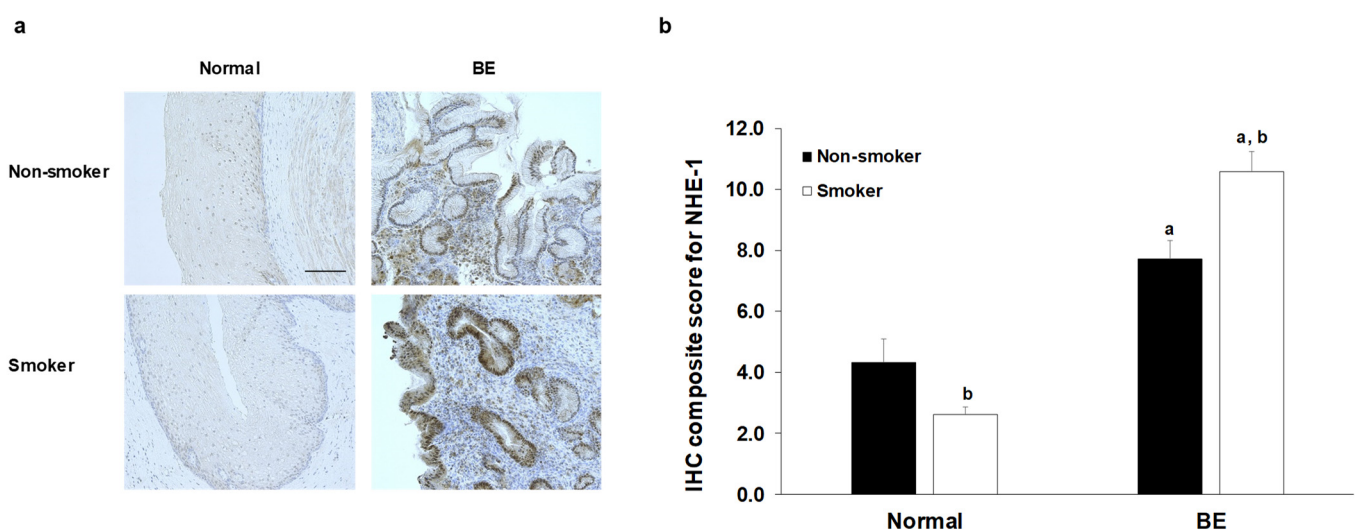

Figure 6. Expression of Na$^+$/H$^+$ exchanger-1 (NHE-1) in human esophageal samples. (**a**) Representative immunohistochemical stainings show the presence of NHE-1 in human esophageal samples. Scale bar represents 100 μm. (**b**) Quantification of DAB intensities were calculated, using a semi-quantitative scoring system. Data represent mean ± SEM of 23–25 specimens/3–6 patients each group; a = $p \leq 0.05$ vs. normal; b = $p \leq 0.05$ vs. non-smoker. BE: Barrett's esophagus.
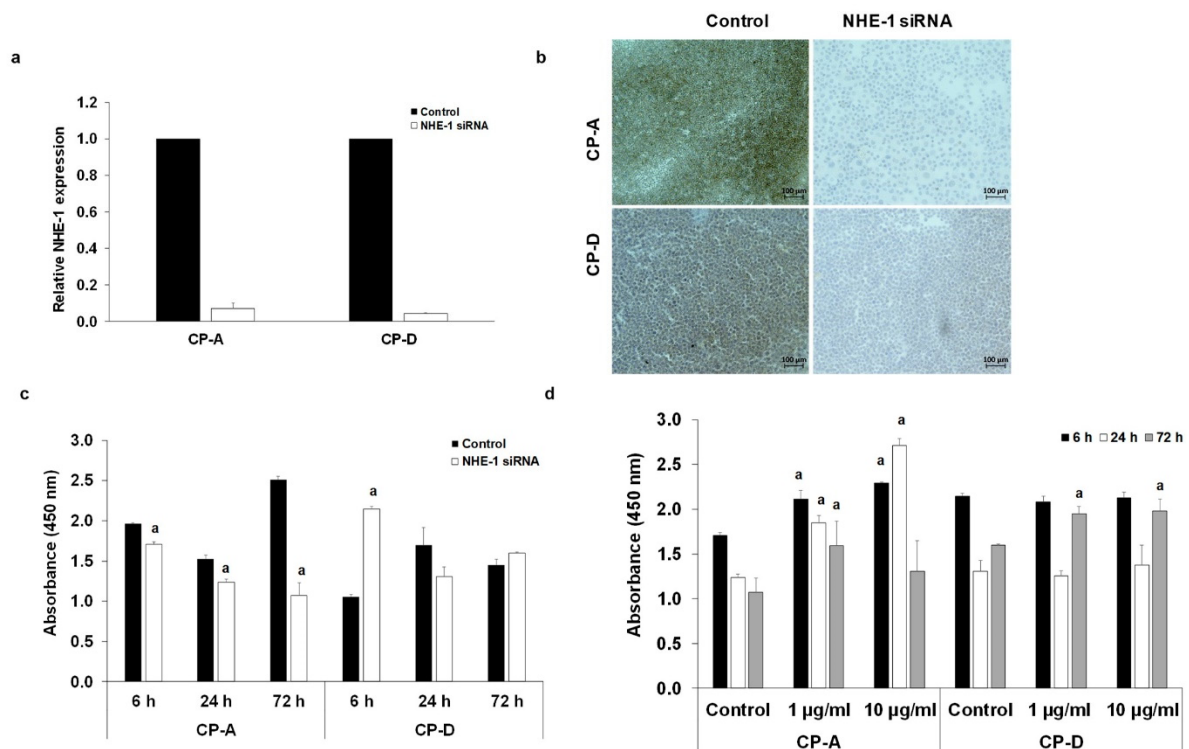
Figure 7. Knockdown of Na^+/H^+ exchanger-1 (NHE-1) in human esophageal cell lines. The expression levels of NHE-1 were investigated by RT-PCR (**a**) and immunohistochemistry (**b**) in control cells and in cells treated with specific siRNA for *SLC9A1*. The rate of proliferation was determined in the non-treated (**c**) and cigarette smoke extract-treated (**d**) CP-A and CP-D cells. Data represent mean ± SEM of three independent experiments; a = $p \leq 0.05$ vs. control.

3. Discussion

Recent studies have described that altered expression or activity of ion transporters play an important role in the development or progression of different types of cancer [22–26]. For this reason, many ion transporters emerged as potential targets for cancer therapy [27,28]. Our study demonstrates, for the first time, that smoking affects cell proliferation in BE in which the ubiquitously expressed transmembrane transporter, NHE-1, plays a central role. In the presence of NHE-1, CSE decreased the proliferation of metaplastic cells, whereas, in the absence of the exchanger, cell proliferation increased due to the CSE treatment. This result may be significant from the point of view that NHE-1 plays a protective role in BE, and decreased NHE-1 expression may contribute to the neoplastic progression of BE in smoking patients.

An interesting observation of our study is that CSE treatment slightly reduced the proliferation of metaplastic cells, while it increased the proliferation of dysplastic cells. The decreased proliferation in the metaplastic cells is presumably due to the decreased cell viability at higher concentrations of CSE. In contrast, dysplastic cells were much more resistant to CSE, and despite the low degree of cell death, cell proliferation increased with treatment. In order to study the underlying mechanisms, we investigated the effect of smoking on ion transport processes. Esophageal ion transporters play an important protective role in EECs by preventing acidic or basic shift in pH_i. Therefore, disruption of pH regulatory processes leads to an upset of extra- and intracellular pH, which can result in changes in cellular function and also causes genetic instability. It is well-known that the pH of tumor is dysregulated and typically an acidic microenvironment develops within the tumor that promotes cell division and migration [29–32]. Among the ion transporters NHE-1 is an ubiquitously expressed plasma membrane protein that plays an essential role in maintaining physiological pH_i. Inadequate function of this transporter has been described in several cancer types, including esophageal cancer [13,16,33–37]; therefore,

NHE-1 emerged as a potential target in anti-cancer therapy [37,38]. We showed that, in the case of acute CSE exposure, higher concentrations of CSE increased NHE-1 activity in the metaplastic cells; this is presumably a defense mechanism by which the cells try to maintain the normal pH homeostasis. In contrast, decreased activity of NHE-1 in CP-D cells indicates damaged compensatory pH regulatory mechanisms. We have previously shown that bile, which is an important etiological factor in the development of GERD and BE, had the opposite effect that is decreased the activity of NHE-1 in the metaplastic cells and increased it in the dysplastic cells [8]. In order to get a more complete picture of the effect of CSE, we treated the cells with CSE for 6, 24 and 72 h and the mRNA, and the protein expressions of NHE-1 were investigated. In CP-A cells, CSE treatment induced an increase in mRNA expression, but this did not reach a significant level. However, a clear elevation was found at the protein level that is thought to be associated with the increased NHE-1 activity by CSE. Examination of human esophageal samples also showed that smoking increases NHE-1 expression in both intestinal and non-intestinal metaplasia, consistent with the results obtained on the CP-A cells. In the case of CP-D cells, no significant change in either mRNA or protein expressions was observed after long-term or higher-dose CSE administration, indicating that only the activity of the protein changes due to the CSE treatment. In order to investigate how smoking affects NHE activity under normal conditions, we examined the effect of acute and chronic tobacco exposure on guinea pig EECs. We chose guinea pigs because we have previously shown that ion-transport processes in the secretory gland of the guinea pig is similar to humans; in addition, more cells can be obtained from the esophagus of guinea pig than from the esophagus of mice or rat [39]. The duration of chronic in vivo smoking was determined based on the literature data [40–42]. Our results showed that both acute and chronic tobacco smoke exposures significantly reduce NHE-1 function. In the case of acute CSE exposure no dose-dependent effect was observed. This can be explained by the fact, that the composition of each CSE preparation may slightly differ from each other as it contains thousands of components, most of which are unstable molecules. Since the CSE extract was not analyzed and only the concentration of the whole extract was calculated minor or larger differences in the preparations may be responsible for the lack of a dose-response effect. In the case of chronic smoking, smoking did not cause as much a decrease in the 2-month-old guinea pigs as in the 1- and 4-month-old animals. One explanation for this is that the effects of smoking and/or the activity of NHE-1 differs in each age group. The effect of chronic smoking in humans was only studied at expression level because human EECs are not suitable for functional measurements due to the high sensitivity and low viability of the human primary cells. Consistent with the result obtained in guinea pig EECs, smoking reduced the expression of NHE-1 in humans. Although NHE-1 is expressed in a very low level in the normal human esophageal mucosa [8,13,15,16], the decreased expression of NHE-1 associates with cellular acidosis, which may increase the risk of cancer development, as a greater number of DNA damage and thus mutations develop in an acidic environment [15]. In order to clarify the role of NHE-1 in the CSE-induced proliferation, we downregulated NHE-1 by specific siRNA transfection. In the absence of NHE-1, the CSE-induced proliferation increased in the metaplastic cell line, suggesting that NHE-1, in addition to being essential in maintaining the normal pH of cells, also performs an important protective function and regulates cell proliferation against toxic agents. The protective role of NHE-1 against the carcinogenic processes has been also demonstrated in esophageal squamous cell carcinoma (ESCC), where suppression of NHE-1 increased the malignant potential and associated with poor prognosis in ESCC patients [13]. In contrast, Guan et al. have found that inhibition of NHE-1 suppressed esophageal cancer cell growth in EAC and ESCC cell lines and in nude mouse xenografts [16]. It has also been demonstrated in other cancer types that NHE-1 promotes tumor malignancy by providing appropriate pH conditions for tumor growth and invasion [11,43]. These data suggest that NHE-1 acts as a tumor oncogene rather than a suppressor in cancer. In BE, most studies agree that increased NHE activity and/or expression is more likely part of a defense or adaptive mechanism

which protects cells against toxic-agent-induced cellular acidification [8,14,15,18,44]. In the more advanced dysplastic state, inhibition of NHE-1 had no effect on the CSE-induced proliferation, indicating that, in dysplasia, the proliferative effect of CSE is independent from NHE-1.

Taken together, smoking affects NHE-1 function in normal, metaplastic and dysplastic cells differently. Under normal conditions, smoking reduces the activity and expression of NHE-1, resulting in the acidosis of pH_i. Disturbance of the pH homeostasis can lead to cell deaths or to the malignant transformation of the cells. In the metaplastic state, smoking increases the function of NHE-1, which is presumably a compensatory mechanism that prevents the onset of cancerous processes by keeping the intracellular pH in the normal range. As the expression of NHE-1 decreases, this protective mechanism disappears and the proliferative potential of the cells increases. In contrast to BE, decreased activity or expression of NHE-1 had no effect on smoking-induced proliferation in the dysplastic state indicating the involvement of other mechanisms.

We propose that upregulation of NHE-1 is the part of a protective mechanism against the harmful effects of smoking; however, further investigation would be needed to support this hypothesis. Direct increase in NHE-1 expression by using NHE-1 agonists or the use of transgenic mice models in which the *SLC9A1* gene is modified would give a more complete picture of the role of NHE-1. Nevertheless, the present results indicate that direct augmentation of NHE-1 function may provide new avenues for decreasing the damaging effect of smoking.

4. Materials and Methods

4.1. Chemicals and Solutions

All general laboratory chemicals and Trypan Blue solution (Catalogue No. T8154) were purchased from Sigma-Aldrich (Budapest, Hungary). We obtained 2,7-bis-(2-carboxyethyl)-5 (6)-carboxyfluorescein acetoxymethyl ester (BCECF-AM) from Invitrogen (Watham, MA, USA), prepared (2 μmol/L) in dimethyl sulfoxide and stored at −20 °C. Nigericin (10 μM) was dissolved in ethanol and stored at −20 °C. High-Capacity Reverse Transcription Kit, TaqMan gene expression Master Mix, lipofectamine 2000 transfection reagent were purchased from Thermo Fisher Scientifc (Watham, MA, USA). Cell Counting Kit-8 was from Dojindo Molecular Technologies (Rockville, MD, USA). Citotoxicity detection kit (LDH) was obtained from Roche (Catalogue No. 11644793001, Roche). *SLC9A1* siRNAs (siRNA ID: 119643) was from Life Technologies. The standard Na^+-HEPES solution contained (in mM): 130 NaCl, 5 KCl, 1 $CaCl_2$, 1 $MgCl_2$, 10 D-glucose and 10 Na-HEPES. NH_4Cl-HEPES solution was supplemented with 20 mM NH_4Cl, while NaCl concentration was lowered to 110 mM. HEPES-buffered solutions were gassed with 100% O_2, and their pH was set to 7.5 with HCl.

4.2. Animals

Guinea pigs (4–12 weeks old, male) were kept in standard plastic cages on 12:12 h light–dark cycle at room temperature (23 ± 1 °C) and had free access to standard laboratory chow and drinking solutions. Animal experiments were conducted in accordance with the *Guide for the Care and Use of Laboratory Animals* (United States, Department of Health and Human Services). In addition, the experimental protocol performed on non-smoking animals was approved by the local Ethical Board of the University of Szeged, Hungary.

4.3. Patients

Formalin-fixed paraffin-embedded esophageal tissue samples were retrieved from the archives of the Department of Pathology, University of Szeged (Szeged, Hungary), from January 2018 to May 2021. Retrospective data collection of patients was performed by the approval of the Ethics Committee of the University of Szeged (No. 4658), according to Helsinki Declaration and GDPR. We collected data based on diagnosis, histopathological features of the esophageal lesion, state of the disease and smoking history of the

patients from patient database used in Hungarian healthcare system (eMedSolution). Each esophageal biopsy and surgical resection sample was analyzed by pathologists earlier. Patients were basically classified into two groups: smoking group with a smoking history of more than 20 years and non-smoking group who had never smoked or had not smoked for at least a year. As a control, tumor-free resection margins and normal esophageal biopsy samples were used. The average age of BE patients was 55.1 ± 4.6 years in the smoking group ($n = 7$), and 57.3 ± 3.8 years in the non-smoking group ($n = 20$). The average age in the control group was 38.5 ± 11.5 years in the smoking group ($n = 3$), and 59.7 ± 3.8 years in the non-smoking group ($n = 7$).

4.4. Cell Cultures

CP-A (human metaplastic esophageal epithelial cell line) and CP-D (human dysplastic esophageal epithelial cell line) cells were purchased from American Type Culture Collection (Manassas, VA, USA). The complete growth medium consists of MCDB-153 basal medium, 5% fetal bovine serum, 4 mM L-glutamine, $1\times$ ITS supplement (Sigma I1884; 5 µg/mL Insulin, 5 µg/mL Transferrin and 5 ng/mL Sodium Selenite), 140 µg/mL Bovine Pituitary Extract (Sigma P1476), 20 mg/L adenine, 0,4 µg/mL hydrocortisone, 8,4 µg/L cholera toxin (Sigma C8052), 20 ng/mL recombinant human EGF (Epidermal Growth Factor) and 1% (*v/v*) penicillin/streptomycin. The cells were cultured at 37 °C and gassed with a mixture of 5% CO_2–95% air. Cells were seeded at 100% confluency and were used between 3 and 19 passage numbers.

4.5. Preparation of Cigarette-Smoke Extract

CSE was prepared at the Department of Pharmacognosy, University of Szeged. Briefly, mainstream smoke from 15 Kentucky Research Cigarettes (3R4F; 12 mg tar and 1.0 mg nicotine/cigarette), was continuously bubbled through 10 mL of distilled water. Dry weight was measured after evaporation of the crude extract with N_2. CSE solution was then diluted to the appropriate concentration, using HEPES or culture media. CSE was freshly prepared for each experiments or used within 2 days of preparation.

4.6. Cigarette-Smoke Exposure

The chronic effect of cigarette smoking was investigated by using a smoking chamber at the Department of Pharmacology and Pharmacotherapy, University of Pécs. Male guinea pigs were divided into three groups, according to the period of cigarette-smoke exposure (1-, 2- and 4-month exposure, $n = 3$/group). In order to avoid large age differrences at the time of sacrifice, animals were selected for each group based on their age, so all animals were 5 months old at the time of sacrifice. Guinea pigs were maintained under 12:12 h light/dark cycle, with free access to food and water. Animals were exposed to whole body cigarette-smoke exposure 4 times a day, 5 days a week, for 30 min each time, using a TE2 whole body smoke exposure chamber (Teague Enterprises, Woodland, CA, USA). During the experiment, 3R4F Kentucky Research Cigarettes (Kentucky Tobacco Research and Development Center, Lexington, KY, USA) were smoked and ventilated inside the chamber. The animals were sacrificed 24–48 h after the last CSE exposure, and EECs were isolated. Intact age- and sex-matched animals served as controls. All experimental procedures were in accordance with the institutional guidelines under approved protocols (No. XII./2222/2018, University of Pécs).

4.7. Isolation of Guinea Pig Esophageal Epithelial Cells

Animals were sacrificed by cervical dislocation, the esophagus was removed and EECs were isolated as described previously [45]. Briefly, the organ was cut longitudinally, rinsed in Hank's Balanced Salt Solution (HBSS, Sigma H9269) and digested in dispase solution (2 U/mL, Sigma D4818) for 40 min. After digestion, the inner, epithelial layer of the esophagus was detached from the submucosa and rinsed in HBSS. Then the epithelial layer was incubated in 0.5% Trypsin–EDTA solution supplemented with 1% (*v/v*) antimy-

coticum/antibioticum for 2 × 15 min. The trypsin was inhibited by a filtered Soybean trypsin inhibitor (Gibco, 10684033) solution, and the whole lysate was centrifuged for 5 min, at 1000 rpm. The cell pellet was diluted in keratinocyte serum free media (KSFM, Gibco, Catalogue No. 17005042) supplemented with 1% (*v/v*) antimycoticum/antibioticum and seeded onto cover glasses and incubated until use. Viability of guinea pig EECs was investigated by using Trypan Blue reagent. After the incubation, bright field images were taken under 40× magnification, and stained cells were counted and considered not viable.

4.8. Immunohistochemistry

Immunohistochemical analysis of NHE-1 expressions was performed on 4% buffered formalin-fixed sections of human esophageal samples embedded in paraffin. The 5 μm–thick sections were stained in an automated system (Autostain, Dako, Glostrup, Denmark). Briefly, the slides were deparaffinized, and endogenous peroxidase activity was blocked by incubation with 3% H_2O_2 (10 min). Antigenic sites were disclosed by applying citrate buffer in a pressure cooker (120 °C, 3 min). To minimize non-specific background staining, the sections were then pre-incubated with milk (30 min). Subsequently, the sections were incubated with a human anti-NHE-1 (1:100 dilution, 30 min, Alomone Laboratories) primary polyclonal antibody and exposed to LSAB2 labeling (Dako, Glostrup, Denmark) for 2 × 10 min. The immunoreactivity was visualized with 3,3′-diaminobenzidine (10 min); then the sections were dehydrated, mounted and examined. NHE-1 expressing cells were identified by the presence of a dark red/brown chromogen. A semi-quantitative scoring system was used to evaluate the expression of NHE-1. The intensity of staining (0 = negative, 1 = weak, 2 = moderate and 3 = strong) and the percentage of positive cells (1–0–25% of the cells are positive, 2–25–50% of the cells are positive, 3–50–75% of the cells are positive and 75–100% of the cells are positive) were scored and then the composite score was obtained by multiplying the intensity of staining and the percen-tage of immunoreactive cells.

4.9. Quantitative Real-Time PCR Analysis

Total mRNA was isolated by using an RNA isolation kit of Macherey-Nagel (Nucleospin RNA Plus kit, Macherey-Nagel, Germany) according to manufacturer's instructions. The concentration of RNA was determined by spectrophotometry (NanoDrop 3.1.0, Rockland, DE, USA). Two micrograms of total RNA were reverse-transcribed, using High-Capacity cDNA Archive Kit (Applied Biosystems) according to manufacturer's instructions. Quantitative real-time PCR was carried out on a Roche LightCycler 96 SW (Roche, Basel, Switzerland). TaqMan probe sets of *SLC9A1* were used to check gene expression. Target gene expression levels were normalized to a human housekeeping gene, β-actin (*ACTB*), and then, using the $\Delta\Delta C_T$ method, relative gene expression was calculated. Fold changes were represented ($2^{-\Delta\Delta CT}$). Values below 0.5 and above 2.00 were considered significant.

4.10. Western Blot

Cells were lysed in Cell Lysis Buffer (Catalogue No. 9803, Cell Signaling Technology, Danvers, MA, USA) supplemented with complete EDTA-free protease inhibitor (Roche, Catalogue No. 11873580001). Then samples were centrifuged at 2500 rpm for 20 min at 4 °C, and the supernatants were used. Protein concentration in the samples was determined by using a BCA assay (Pierce Chemical, Rockford, IL, USA) or Bradford reagent (Bio-Rad Laboratories, Hercules, CA, USA), and equal amounts of proteins (20 or 30 μg) were resolved on polyacrylamide gel and transferred onto Protran (GE Healthcare Amersham™) or PVDF (Invitrogen, Watham, MA, USA) membranes. Membranes were incubated overnight with rabbit polyclonal anti-NHE-1 (Catalogue No. ANX-010, Alomone Labs, Jerusalem, Israel), mouse monoclonal anti-GAPDH (Catalogue No. MAB 374, Sigma Aldrich, Hungary) or mouse monoclonal anti-α-Tubulin antibody (Catalogue No. T9026, Merck, Darmstadt, Germany) followed by the incubation with the appropriate HRP-conjugated secondary antibody (Catalogue No. P0448 goat anti-rabbit and P0161 rabbit anti-mouse, DAKO, Glostrup,

Denmark or G-21040 goat anti-mouse, Invitrogen, Watham, MA, USA). The peroxidase activity was visualized by using the enhanced chemi-luminescence assay (Advansta, Menlo Park, CA, USA) or with Clarity Chemiluminescence Substrate (Bio-Rad Laboratories, Hercules, CA, USA). Signal intensities were quantified by using the QuantityOne software (Bio-Rad, Hercules, CA, USA) or Image Lab Software, version 5.2 (Bio-Rad Laboratories, Hercules, CA, USA). The results from each membrane were normalized to the GAPDH or α-Tubulin values and compared to the 6 h control.

4.11. Measurement of Intracellular pH

Cells were seeded onto 24 mm cover glasses which were placed on the stage of an inverted microscope connected with an Xcellence imaging system (Olympus, Budapest, Hungary). Cells were incubated with a pH-sensitive fluorescence dye, BCECF-AM for 30–60 min according to cell type. Cells were perfused with solutions at 37 °C at a 5 to 6 mL/min perfusion rate. Average 5–12 regions of interest (ROIs) were marked in each measurement, and one image was taken per second. The cells were excited with 440 and 495 nm wavelength, and a 440/495 ratio was detected at 535 nm. One pH_i measurement was obtained per second. In situ calibration of the fluorescence signal was performed by using the high K^+-nigericin technique. Since CSE alone influences fluorescence signals, cells were pretreated with freshly prepared CSE (1, 10 and 100 μg/mL) for 1 h before microfluorometric measurements.

4.12. Determination of Buffering Capacity

The total buffering capacity (β_{total}) of cells was estimated according to the NH_4Cl pre-pulse technique, as previously described [46,47]. Briefly, EECs were exposed to various concentrations of NH_4Cl in Na^+- and HCO_3^--free solutions. The total buffering capacity of the cells was calculated by using the following equation: $\beta_{total} = \beta_i + \beta_{HCO3-} = \beta_i + 2.3 \times [HCO_3^-]_i$, where β_i refers to the ability of intrinsic cellular components to buffer changes of pH_i and was estimated by the Henderson–Hasselbach equation. The measured rates of pH_i change ($\Delta pH/\Delta t$) were converted to transmembrane base flux $J(B^-)$, using the following equation: $J(B^-) = \Delta pH/\Delta t \times \beta_i$. The β_i value at the start point pH_i was used for the calculation of $J(B^-)$.

4.13. Measurement of Na^+/H^+ Exchanger Activity

For evaluating the activity of NHE-1, NH_4Cl pre-pulse technique was used. EECs were exposed to NH_4Cl (20 mM) for 3 min, which resulted in a sudden pH_i elevation through NH_3 diffusion into the cells. NH_4Cl withdrawal caused a remarkable decrease in pH_i as the intracellular NH_4^+ and H^+ dissociating and basic NH_3 exiting the cells. The regeneration from acidosis (the first 60 s) reflects the activity of NHEs in standard HEPES-buffered solutions. The following equation was used for estimating the transmembrane base flux: $J(B^-) = \Delta pH/\Delta t \times \beta_i$, where $\Delta pH/\Delta t$ was calculated by linear regression analysis, whereas the intrinsic buffering capacity (β_i) was determined by the Henderson–Hasselbach equation.

4.14. SLC9A1 Gene Silencing

Cells were seeded on a 6-well plate in antibiotic-free complete growth medium and incubated overnight. *SLC9A1* gene silencing was performed at 40–50% confluency. Then 100 pmol *SLC9A1* siRNA was dissolved in 250 μL Opti-MEM (Gibco, Catalogue No. 31985070) reduced serum medium. Then 5 or 7.5 μL Lipofectamine 2000 was added to 250 μL Opti-MEM and incubated for 5 min at room temperature. Then the prepared siRNA solution and Lipofectamine 2000 were mixed and incubated for 20 min to form complexes. The complexes were added to the wells, mixed gently by rocking the plate back and forth and then incubated for 72 h. After transfection, RT-qPCR and immunocytochemistry was performed to estimate mRNA and protein levels.

4.15. Proliferation

Cells were seeded at 10^3 cells per well into a 96-well plate (100 μL/well) in complete growth medium and allowed to attach for 24 h. Cells were then treated with CSE (1 and 10 μg/mL) for 6, 24 and 72 h. After the treatments, 10 μL of CCK8 solution was added to each well and the cells were incubated for further 3 h. Absorbance was detected at 450 nm, using a FLUOstar OPTIMA Spectrophotometer (BMG Labtech, Ortenberg, Germany).

4.16. Cytotoxicity Assay

For cytotoxicity assay, 100 μL of cell suspension was seeded into a 96-well plate (2.5×10^4 cells/well) and allowed to adhere overnight. On the following day, the cells were incubated with CSE (1, 10 and 100 μg/mL) for 6, 24 and 72 h. Then 100 μL of supernatant from each of the wells was carefully transferred into a new 96-well plate containing 100 μL reaction mixture. We then measured lactate dehydrogenase (LDH) activity at 490 nm using a FLUOstar OPTIMA Spectrophotometer (BMG Labtech, Ortenberg, Germany). For background controls, we measured 200 μL assay medium, without cells. For low controls, we used 100 μL cell suspension and 100 μL assay medium. In the case of high controls, the mixture of 100 μL cell suspension and 100 μL Triton-X 100 (0.1%) solution was measured. The LDH release induced by Triton-X 100 was assigned to 100%. The average absorbance values of each of the triplicates were calculated, and the average value of the background control (LDH activity contained in the assay medium) was subtracted from each of the samples to reduce background noises. We then calculated the percentage of cytotoxicity by using the following formula: Cytotoxicity (%) = (exp. value–low control/high control–low control) × 100. Low control determines the LDH activity released from the untreated normal cells (spontaneous LDH release), whereas high control determines the maximum releasable LDH activity in the cells (maximum LDH release).

4.17. Statistical Analysis

Results were described as means ± SE. For statistical analysis, one-way ANOVA and Student's *t*-test were used, $p \leq 0.05$ were considered significant.

References

1. Cook, M.B.; Kamangar, F.; Whiteman, D.C.; Freedman, N.D.; Gammon, M.D.; Bernstein, L.; Brown, L.M.; Risch, H.A.; Ye, W.; Sharp, L.; et al. Cigarette smoking and adenocarcinomas of the esophagus and esophagogastric junction: A pooled analysis from the international BEACON consortium. *J. Natl. Cancer Inst.* **2010**, *102*, 1344–1353. [CrossRef] [PubMed]
2. Cook, M.B.; Shaheen, N.J.; Anderson, L.A.; Giffen, C.; Chow, W.H.; Vaughan, T.L.; Whiteman, D.C.; Corley, D.A. Cigarette smoking increases risk of Barrett's esophagus: An analysis of the Barrett's and Esophageal Adenocarcinoma Consortium. *Gastroenterology* **2012**, *142*, 744–753. [CrossRef] [PubMed]

3. Kuang, J.J.; Jiang, Z.M.; Chen, Y.X.; Ye, W.P.; Yang, Q.; Wang, H.Z.; Xie, D.R. Smoking Exposure and Survival of Patients with Esophagus Cancer: A Systematic Review and Meta-Analysis. *Gastroenterol. Res. Pract.* **2016**, *2016*, 7682387. [CrossRef] [PubMed]

4. Wang, Q.L.; Xie, S.H.; Li, W.T.; Lagergren, J. Smoking Cessation and Risk of Esophageal Cancer by Histological Type: Systematic Review and Meta-analysis. *J. Natl. Cancer Inst.* **2017**, *109*, djx115. [CrossRef] [PubMed]

5. Coleman, H.G.; Bhat, S.; Johnston, B.T.; McManus, D.; Gavin, A.T.; Murray, L.J. Tobacco smoking increases the risk of high-grade dysplasia and cancer among patients with Barrett's esophagus. *Gastroenterology* **2012**, *142*, 233–240. [CrossRef] [PubMed]

6. Orlando, R.C.; Bryson, J.C.; Powell, D.W. Effect of cigarette smoke on esophageal epithelium of the rabbit. *Gastroenterology* **1986**, *91*, 1536–1542. [CrossRef]

7. Becskehazi, E.; Korsos, M.M.; Eross, B.; Hegyi, P.; Venglovecz, V. OEsophageal Ion Transport Mechanisms and Significance Under Pathological Conditions. *Front. Physiol.* **2020**, *11*, 855. [CrossRef]

8. Laczko, D.; Rosztoczy, A.; Birkas, K.; Katona, M.; Rakonczay, Z., Jr.; Tiszlavicz, L.; Roka, R.; Wittmann, T.; Hegyi, P.; Venglovecz, V. Role of ion transporters in the bile acid-induced esophageal injury. *Am. J. Physiol. Gastrointest. Liver Physiol.* **2016**, *311*, G16–G31. [CrossRef]

9. Demaurex, N.; Grinstein, S. Na$^+$/H$^+$ antiport: Modulation by ATP and role in cell volume regulation. *J. Exp. Biol.* **1994**, *196*, 389–404. [CrossRef]

10. Grinstein, S.; Rotin, D.; Mason, M.J. Na$^+$/H$^+$ exchange and growth factor-induced cytosolic pH changes. Role in cellular proliferation. *Biochim. Biophys. Acta* **1989**, *988*, 73–97. [CrossRef]

11. Stock, C.; Schwab, A. Role of the Na/H exchanger NHE1 in cell migration. *Acta Physiol.* **2006**, *187*, 149–157. [CrossRef] [PubMed]

12. Shallat, S.; Schmidt, L.; Reaka, A.; Rao, D.; Chang, E.B.; Rao, M.C.; Ramaswamy, K.; Layden, T.J. NHE-1 isoform of the Na$^+$/H$^+$ antiport is expressed in the rat and rabbit esophagus. *Gastroenterology* **1995**, *109*, 1421–1428. [CrossRef]

13. Ariyoshi, Y.; Shiozaki, A.; Ichikawa, D.; Shimizu, H.; Kosuga, T.; Konishi, H.; Komatsu, S.; Fujiwara, H.; Okamoto, K.; Kishimoto, M.; et al. Na$^+$/H$^+$ exchanger 1 has tumor suppressive activity and prognostic value in esophageal squamous cell carcinoma. *Oncotarget* **2017**, *8*, 2209–2223. [CrossRef]

14. Fujiwara, Y.; Higuchi, K.; Tominaga, K.; Watanabe, T.; Oshitani, N.; Arakawa, T. Functional oesophageal epithelial defense against acid. *Inflammopharmacology* **2005**, *13*, 1–13. [CrossRef]

15. Goldman, A.; Shahidullah, M.; Goldman, D.; Khailova, L.; Watts, G.; Delamere, N.; Dvorak, K. A novel mechanism of acid and bile acid-induced DNA damage involving Na$^+$/H$^+$ exchanger: Implication for Barrett's oesophagus. *Gut* **2010**, *59*, 1606–1616. [CrossRef]

16. Guan, B.; Hoque, A.; Xu, X. Amiloride and guggulsterone suppression of esophageal cancer cell growth in vitro and in nude mouse xenografts. *Front. Biol.* **2014**, *9*, 75–81. [CrossRef]

17. Tobey, N.A.; Koves, G.; Orlando, R.C. Human esophageal epithelial cells possess an Na$^+$/H$^+$ exchanger for H$^+$ extrusion. *Am. J. Gastroenterol.* **1998**, *93*, 2075–2081. [CrossRef]

18. Goldman, A.; Chen, H.; Khan, M.R.; Roesly, H.; Hill, K.A.; Shahidullah, M.; Mandal, A.; Delamere, N.A.; Dvorak, K. The Na$^+$/H$^+$ exchanger controls deoxycholic acid-induced apoptosis by a H$^+$-activated, Na$^+$-dependent ionic shift in esophageal cells. *PLoS ONE* **2011**, *6*, e23835. [CrossRef]

19. Liu, Y.; Wang, B.; Liu, X.; Lu, L.; Luo, F.; Lu, X.; Shi, L.; Xu, W.; Liu, Q. Epigenetic silencing of p21 by long non-coding RNA HOTAIR is involved in the cell cycle disorder induced by cigarette smoke extract. *Toxicol. Lett.* **2016**, *240*, 60–67. [CrossRef] [PubMed]

20. Zhao, Y.; Xu, Y.; Li, Y.; Xu, W.; Luo, F.; Wang, B.; Pang, Y.; Xiang, Q.; Zhou, J.; Wang, X.; et al. NF-kappaB-mediated inflammation leading to EMT via miR-200c is involved in cell transformation induced by cigarette smoke extract. *Toxicol. Sci.* **2013**, *135*, 265–276. [CrossRef] [PubMed]

21. Kong, J.; Nakagawa, H.; Isariyawongse, B.K.; Funakoshi, S.; Silberg, D.G.; Rustgi, A.K.; Lynch, J.P. Induction of intestinalization in human esophageal keratinocytes is a multistep process. *Carcinogenesis* **2009**, *30*, 122–130. [CrossRef]

22. Boedtkjer, E. Ion Channels, Transporters, and Sensors Interact with the Acidic Tumor Microenvironment to Modify Cancer Progression. *Rev. Physiol. Biochem. Pharmacol.* **2021**, 1–46. [CrossRef]

23. Chen, J.; Zhang, M.; Ma, Z.; Yuan, D.; Zhu, J.; Tuo, B.; Li, T.; Liu, X. Alteration and dysfunction of ion channels/transporters in a hypoxic microenvironment results in the development and progression of gastric cancer. *Cell Oncol.* **2021**, *44*, 739–749. [CrossRef]

24. Lu, C.; Ma, Z.; Cheng, X.; Wu, H.; Tuo, B.; Liu, X.; Li, T. Pathological role of ion channels and transporters in the development and progression of triple-negative breast cancer. *Cancer Cell Int.* **2020**, *20*, 377. [CrossRef]

25. Stock, C. How Dysregulated Ion Channels and Transporters Take a Hand in Esophageal, Liver, and Colorectal Cancer. *Rev. Physiol. Biochem. Pharmacol.* **2020**. [CrossRef]

26. Zhang, M.; Li, T.; Zhu, J.; Tuo, B.; Liu, X. Physiological and pathophysiological role of ion channels and transporters in the colorectum and colorectal cancer. *J. Cell Mol. Med.* **2020**, *24*, 9486–9494. [CrossRef] [PubMed]

27. Arcangeli, A.; Becchetti, A. New Trends in Cancer Therapy: Targeting Ion Channels and Transporters. *Pharmaceuticals* **2010**, *3*, 1202–1224. [CrossRef] [PubMed]

28. Ramirez, A.; Garcia-Quiroz, J.; Aguilar-Eslava, L.; Sanchez-Perez, Y.; Camacho, J. Novel Therapeutic Approaches of Ion Channels and Transporters in Cancer. *Rev. Physiol. Biochem. Pharmacol.* **2020**, 1–57. [CrossRef]

29. Corbet, C.; Feron, O. Tumour acidosis: From the passenger to the driver's seat. *Nat. Rev. Cancer* **2017**, *17*, 577–593. [CrossRef] [PubMed]

30. Estrella, V.; Chen, T.; Lloyd, M.; Wojtkowiak, J.; Cornnell, H.H.; Ibrahim-Hashim, A.; Bailey, K.; Balagurunathan, Y.; Rothberg, J.M.; Sloane, B.F.; et al. Acidity generated by the tumor microenvironment drives local invasion. *Cancer Res.* **2013**, *73*, 1524–1535. [CrossRef]

31. Kato, Y.; Ozawa, S.; Miyamoto, C.; Maehata, Y.; Suzuki, A.; Maeda, T.; Baba, Y. Acidic extracellular microenvironment and cancer. *Cancer Cell Int.* **2013**, *13*, 89. [CrossRef] [PubMed]

32. Swietach, P.; Vaughan-Jones, R.D.; Harris, A.L.; Hulikova, A. The chemistry, physiology and pathology of pH in cancer. *Philos Trans. R Soc. Lond B Biol. Sci.* **2014**, *369*, 20130099. [CrossRef] [PubMed]

33. Brisson, L.; Driffort, V.; Benoist, L.; Poet, M.; Counillon, L.; Antelmi, E.; Rubino, R.; Besson, P.; Labbal, F.; Chevalier, S.; et al. NaV1.5 Na(+) channels allosterically regulate the NHE-1 exchanger and promote the activity of breast cancer cell invadopodia. *J. Cell Sci.* **2013**, *126*, 4835–4842. [CrossRef]

34. Li, S.; Bao, P.; Li, Z.; Ouyang, H.; Wu, C.; Qian, G. Inhibition of proliferation and apoptosis induced by a Na$^+$/H$^+$ exchanger-1 (NHE-1) antisense gene on drug-resistant human small cell lung cancer cells. *Oncol. Rep.* **2009**, *21*, 1243–1249. [CrossRef]

35. Serafino, A.; Moroni, N.; Psaila, R.; Zonfrillo, M.; Andreola, F.; Wannenes, F.; Mercuri, L.; Rasi, G.; Pierimarchi, P. Anti-proliferative effect of atrial natriuretic peptide on colorectal cancer cells: Evidence for an Akt-mediated cross-talk between NHE-1 activity and Wnt/beta-catenin signaling. *Biochim. Biophys. Acta* **2012**, *1822*, 1004–1018. [CrossRef]

36. Vaish, V.; Sanyal, S.N. Role of Sulindac and Celecoxib in chemoprevention of colorectal cancer via intrinsic pathway of apoptosis: Exploring NHE-1, intracellular calcium homeostasis and Calpain 9. *Biomed. Pharm.* **2012**, *66*, 116–130. [CrossRef]

37. Reshkin, S.J.; Cardone, R.A.; Harguindey, S. Na$^+$-H$^+$ exchanger, pH regulation and cancer. *Recent Pat. Anticancer Drug Discov.* **2013**, *8*, 85–99. [CrossRef]

38. Loo, S.Y.; Chang, M.K.; Chua, C.S.; Kumar, A.P.; Pervaiz, S.; Clement, M.V. NHE-1: A promising target for novel anti-cancer therapeutics. *Curr. Pharm. Des.* **2012**, *18*, 1372–1382. [CrossRef]

39. Venglovecz, V.; Rakonczay, Z., Jr.; Ozsvari, B.; Takacs, T.; Lonovics, J.; Varro, A.; Gray, M.A.; Argent, B.E.; Hegyi, P. Effects of bile acids on pancreatic ductal bicarbonate secretion in guinea pig. *Gut* **2008**, *57*, 1102–1112. [CrossRef] [PubMed]

40. Bracke, K.R.; D'Hulst, A.I.; Maes, T.; Demedts, I.K.; Moerloose, K.B.; Kuziel, W.A.; Joos, G.F.; Brusselle, G.G. Cigarette smoke-induced pulmonary inflammation, but not airway remodelling, is attenuated in chemokine receptor 5-deficient mice. *Clin. Exp. Allergy* **2007**, *37*, 1467–1479. [CrossRef] [PubMed]

41. D'Hulst, A.I.; Vermaelen, K.Y.; Brusselle, G.G.; Joos, G.F.; Pauwels, R.A. Time course of cigarette smoke-induced pulmonary inflammation in mice. *Eur. Respir. J.* **2005**, *26*, 204–213. [CrossRef]

42. Stevenson, C.S.; Docx, C.; Webster, R.; Battram, C.; Hynx, D.; Giddings, J.; Cooper, P.R.; Chakravarty, P.; Rahman, I.; Marwick, J.A.; et al. Comprehensive gene expression profiling of rat lung reveals distinct acute and chronic responses to cigarette smoke inhalation. *Am. J. Physiol. Lung Cell Mol. Physiol.* **2007**, *293*, L1183–L1193. [CrossRef]

43. Stock, C.; Pedersen, S.F. Roles of pH and the Na(+)/H(+) exchanger NHE1 in cancer: From cell biology and animal models to an emerging translational perspective? *Semin. Cancer Biol.* **2017**, *43*, 5–16. [CrossRef] [PubMed]

44. Fujiwara, Y.; Higuchi, K.; Takashima, T.; Hamaguchi, M.; Hayakawa, T.; Tominaga, K.; Watanabe, T.; Oshitani, N.; Shimada, Y.; Arakawa, T. Roles of epidermal growth factor and Na$^+$/H$^+$ exchanger-1 in esophageal epithelial defense against acid-induced injury. *Am. J. Physiol. Gastrointest Liver Physiol.* **2006**, *290*, G665–G673. [CrossRef] [PubMed]

45. Kalabis, J.; Wong, G.S.; Vega, M.E.; Natsuizaka, M.; Robertson, E.S.; Herlyn, M.; Nakagawa, H.; Rustgi, A.K. Isolation and characterization of mouse and human esophageal epithelial cells in 3D organotypic culture. *Nat. Protoc.* **2012**, *7*, 235–246. [CrossRef] [PubMed]

46. Hegyi, P.; Gray, M.A.; Argent, B.E. Substance P inhibits bicarbonate secretion from guinea pig pancreatic ducts by modulating an anion exchanger. *Am. J. Physiol. Cell Physiol.* **2003**, *285*, C268–C276. [CrossRef]

47. Weintraub, W.H.; Machen, T.E. pH regulation in hepatoma cells: Roles for Na-H exchange, Cl-HCO3 exchange, and Na-HCO3 cotransport. *Am. J. Physiol.* **1989**, *257*, G317–G327. [CrossRef]

Co-author certification

I, myself as a corresponding author of the following publication(s) declare that the authors have no conflict of interest, and Marietta Margaréta Korsós Ph.D. candidate had significant contribution to the jointly published research(es). The results discussed in her thesis were not used and not intended to be used in any other qualification process for obtaining a PhD degree.

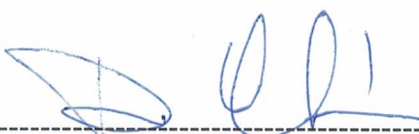The publication(s) relevant to the applicant's thesis:

Publication No.1.:

Marietta Margaréta Korsós, Tamás Bellák, Eszter Becskeházi, Eleonóra Gál, Zoltán Veréb, Péter Hegyi, Viktória Venglovecz. Mouse organoid culture is a suitable model to study esophageal ion transport mechanisms. AMERICAN JOURNAL OF PHYSIOLOGY – CELL PHYSIOLOGY; 321(5):C798-C811. doi: 10.1152/ajpcell.00295.2021. PMID: 34524930. (2021)

Publication No.2.:

Eszter Becskeházi, Marietta Margaréta Korsós, Eleonóra Gál, Tiszlavicz L, Hoyk Z, Deli MA, Zoltán Márton Köhler, Anikó Keller-Pintér, Attila Horváth, Kata Csekő, Zsuzsanna Helyes, Péter Hegyi, Viktória Venglovecz. Inhibition of NHE-1 Increases Smoke-Induced Proliferative Activity of Barrett's Esophageal Cell Line. INTERNATIONAL JOURNAL OF MOLECULAR SCIENCES; 22(19):10581. doi: 10.3390/ijms221910581. PMID: 34638919; PMCID: PMC8509038. (2021)

Szeged, 2023.08.04.

Dr. Viktória Venglovecz
corresponding author, supervisor